

Functional Analysis
of Heat Shock Protein HSPA4

Dissertation
zur Erlangung des Doktorgrades
der Mathematisch-Naturwissenschaftlichen Fakultäten
der Georg-August-Universität zu Göttingen



vorgelegt von
Amal Zohir Abo-Zeid Barakat
aus Kairo, Ägypten

Göttingen, 2010

D 7

Referent:

Korreferentin:

Tag der mündlichen Prüfung:

Prof. Dr. med. Dr. h.c. W. Engel

Prof. Dr. S. Hoyer-Fender

To my husband Mahmoud, for her patience and love

To my family for their moral support

To my friends for their support

To my supervisors for their valuable advices

TABLE OF CONTENTS

CONTENTS	
ABBREVIATIONS	
1. INTRODUCTION	1
1.1 The heat shock protein family: the very short overview.....	1
1.2 The heat shock protein family 110 (HSP110).....	1
1.3 Expression and function of <i>Hspa4</i>	4
1.4 Aims of the study.....	6
2. MATERIAL AND METHODS	7
2.1 Materials.....	7
2.1.1 Chemicals.....	7
2.1.2 Solutions, buffers and media.....	9
2.1.3 Laboratory materials.....	10
2.1.4 Sterilisation of solutions and equipments.....	11
2.1.5 Media, antibiotics and agar-plates.....	11
2.1.5.1 Media for bacteria.....	11
2.1.5.2 Antibiotics.....	12
2.1.5.3 IPTG/X-Gal plate.....	12
2.1.6 Bacterial strains.....	12
2.1.7 Plasmids.....	12
2.1.8 Synthetic oligonucleotides.....	12
2.1.8.1 Primers used for generation of cDNA probes.....	13
2.1.8.2 Genotyping primers.....	13
2.1.8.3 Real time PCR primers.....	14
2.1.9 Mouse strains.....	15
2.1.10 Antibodies.....	15
2.1.11 Enzymes.....	16
2.1.12 Kits.....	17
2.1.13 Equipment.....	17

2.2 Methods.....	18
2.2.1 Isolation of nucleic acids.....	18
2.2.1.1 Small-scale isolation of plasmid DNA.....	18
2.2.1.2 Isolation of genomic DNA from tissue samples.....	18
2.2.1.3 Isolation of total RNA from tissue samples	18
2.2.2 Determination of nucleic acid concentration.....	19
2.2.3 Gel electrophoresis.....	19
2.2.3.1 Agarose gel electrophoresis of DNA.....	19
2.2.3.2 Agarose gel electrophoresis of RNA.....	20
2.2.4 Purification of DNA fragments from agarose gel.....	20
2.2.5 Enzymatic modifications of DNA.....	21
2.2.5.1 Digestion of DNA using restriction enzymes.....	21
2.2.5.2 Ligation of DNA fragments.....	21
2.2.6 Transformation of competent bacteria.....	21
2.2.7 Polymerase chain reaction (PCR).....	22
2.2.7.1 PCR amplification of DNA fragments.....	22
2.2.7.2 Genotyping of knockout mice by using PCR.....	22
2.2.7.3 Reverse transcription PCR (RT-PCR).....	23
2.2.7.3.1 DNase I digestion.....	23
2.2.7.3.2 Reverse transcription technique.....	24
2.2.7.4 Quantitive Real-Time PCR	24
2.2.8 Protein and biochemical methods.....	25
2.2.8.1 Isolation of total protein from mouse tissues.....	25
2.2.8.2 Isolation of total protein from cell culture.....	25
2.2.8.3 Determination of protein concentration.....	25
2.2.8.4 SDS-PAGE gel for separation of proteins.....	25
2.2.9 Blotting techniques.....	26
2.2.9.1 Northern blotting of RNA.....	26
2.2.9.2 Western blotting of protein.....	26
2.2.9.3 Incubation of protein –bound membranes with antibodies.....	27
2.2.10 “Random Prime” method for generation of ³² P labeled DNA.....	27

2.2.11 Hybridisation of nucleic acids.....	28
2.2.12 DNA sequencing.....	28
2.2.13 Histological techniques.....	29
2.2.13.1 Tissue preparation for paraffin-embedding.....	29
2.2.13.2 Sections of the paraffin block.....	29
2.2.13.3 Immunofluorescence staining	29
2.2.13.4 Immunocytochemical staining of germ cell suspension.....	30
2.2.13.5 Hematoxylin-eosin (H&E) staining of histological sections.....	30
2.2.13.6 Apoptosis detection.....	30
2.2.14 Masson's Trichrome staining.....	31
2.2.15 Tissue preparation for electron microscopy.....	31
2.2.16 Echocardiogram.....	32
2.2.17 Microarray analysis.....	32
2.2.18 Computer analysis.....	33
3. RESULTS.....	34
3.1 Analysis of <i>Hspa4</i> - deficient mice on the hybrid C57BL/6J x 129/SV genetic background.....	34
3.1.1 Impaired progression of the first wave of spermatogenesis in juvenile <i>Hspa4</i> -deficient mice.....	34
3.1.2 Immunohistochemical analysis of <i>Hspa4</i> ^{-/-} testes.....	35
3.1.3 Increase of apoptotic germ cells in <i>Hspa4</i> ^{-/-} testes.....	40
3.1.4 Expression analysis of germ cell marker genes in <i>Hspa4</i> -deficient testes.....	41
3.1.5 Expression analysis of other members of HSP110 family in <i>Hspa4</i> ^{-/-} testis.....	41
3.2 <i>Hspa4</i> -deficient mice with the inbred 129/Sv genetic background display postnatal growth retardation.....	45
3.2.1 Metabolic state in <i>Hspa4</i> -deficient mice.....	45
3.2.1.1 Measurement of glucose levels in sera of <i>Hspa4</i> -deficient mice...	45
3.2.1.2 Expression of <i>Pepck</i> in liver of fasted <i>Hspa4</i> ^{-/-} mice.....	46
3.2.2 Is growth retardation due to malabsorbtion of lipids in intestine?.	47

3.2.3 Expression analysis of apolipoprotein B and AIV in intestine and liver during postnatal development of <i>Hspa4</i> ^{-/-} mice.....	48
3.2.4 Growth hormone (GH) signaling is not affected in <i>Hspa4</i> ^{-/-} mice	48
3.2.5 Analysis of skeletal muscles of <i>Hspa4</i> - deficient mice.....	51
3.2.5.1 <i>Hspa4</i> -deficient mice display skeletal muscle myopathy.....	51
3.2.5.2 Skeletal muscle myopathy develops during early postnatal development.....	51
3.2.6 Analysis of the heart in <i>Hspa4</i> -deficient mice	55
3.2.6.1 Development of cardiac hypertrophy in <i>Hspa4</i> -deficient mice.....	55
3.2.6.2 Echocardiographic measurements in wild type and mutant mice.....	60
3.2.6.3 Ultrastructural analysis of sections <i>Hspa4</i> ^{-/-} heart.....	60
3.2.6.4 Analyses of molecular markers of cardiac hypertrophy.....	62
3.2.6.5 Upregulation of fibrosis marker genes in heart of <i>Hspa4</i> ^{-/-} mice.....	62
3.2.6.6 Molecular pathways in the regulation of cardiac hypertrophy.....	66
3.2.6.6.1 Analysis of STAT3 and MAPK signaling in heart of <i>Hspa4</i> ^{-/-} mice.	66
3.2.6.6.2 Genes involved in calcineurin/NFAT pathway are upregulated in heart of <i>Hspa4</i> ^{-/-} mice.....	69
3.2.6.7 Microarray analysis of cardiac gene expression.....	71
3.2.6.8 Quantitative real-time PCR analysis.....	80
3.2.7 Expression analysis of HSPA4L and HSPH1 in <i>Hspa4</i> -deficiency.....	84
3.2.8 The effect of aging and oxidative stress on expression of HSPA4	85
4. DISCUSSION	88
4.1 Overview of results of this study.....	88
4.2 The role of HSPA4 for germ cell development.....	91
4.3 Potential role of <i>Hspa4</i> in regulation of cell cycle.....	94
4.4 The cause of growth retardation in <i>Hspa4</i> -deficient mice.....	96
4.5 Role of <i>Hspa4</i> in skeletal muscle development.....	97
4.6 Development of cardiac hypertrophy in <i>Hspa4</i> -deficient mice.....	99
4.6.1 MAPK/ERK signaling pathway.....	101
4.6.2 IL-6-gp130-STAT3 signalling pathway.....	103
4.6.3 Calcineurin/NFAT signaling pathway.....	103

Table of contents

4.6.4 Cardiac fibrosis in <i>Hspa4</i> ^{-/-} mice.....	108
4.6.5 Role of heat shock in heart protection.....	110
4.6.6 Expression profiles of <i>Hspa4</i> ^{-/-} heart.....	110
5. SUMMARY.....	114
6. REFERENCES.....	116
ACKNOWLEDGEMENTS.....	
<i>Curriculum vitae</i>	

Abbreviations

Abbreviations

ABI	Applied Biosystem Instrument
ATP	Adenosintriphosphate
BLAST	Basic Local Alignment Tools
bp	base pair
BSA	Bovine serum albumin
°C	Degree Celsius
cDNA	complementary DNA
Cy3	indocarbocyanine
dATP	Desoxyriboadenosintnphosphate
dH ₂ O	distil Water
DAPI	Diamidino-2-phenylindoledihydrochloride
dCTP	Desoxyribocytosintriphosphate
DMSO	Dimethyl sulfoxide
DEPC	Diethylpyrocarbonate
DNA	Deoxyribonucleic acid
DNase	deoxyribonuclease
dNTP	deoxynucleotidetriphosphate
dpc	day post coitus
dT	deoxythymidinate
DTT	Dithiothreitol
EDTA	Ethylene diamine tetraacetic acid
FCS	Fetal calf serum
g	gravity
gm	gram
HEPS	N-(-hydroxymethyl)piperazin,N'-3-propansulfoneacid
HPLC	High performance liquid chromatograpy
hr(s)	hour(s)IGL
IgG	Immunoglobulin G
IPTG	Isopropyl-B-thiogalactopyranoside

Abbreviations

JL	Jackson Laboratory
kb	kilobase
LB	Luria-Bertrani
M	molarity
ML	Molecular layer
MoCo	Molybdenum cofactor
MOCS	Molybdenum cofactor synthesis step
MOPS	3 - [N-Morpholino] -Propanesulfate
mRNA	messenger Ribonucleic acid
mg	milligram
MHZ	Megahertz
ml	milliliter
μ l	microliter
min	minute
NaAc	Sodium acetate
NCBI	National Center for Biotechnology Information
ng	nanogram
nm	nanometer
NTP	Nucleotidetriphosphate
OD	Optimal density
PAGE	Polyacrylamide Gel Electrophoresis
PCR	Polymerase chain reaction
pH	Preponderance of hydrogen ions
pmol	picomol
PBS	Phosphatebuffered saline
PBT	Phosphatebuffered saline + Tween 20
PMSF	Phenylmethylsulfonyl fluoride
RNA	Ribonucleic acid
Rnase	Ribonuclease
rpm	revolution per minute
RT	Room temperature

Abbreviations

RT-PCR	Reverse transcriptase-PCR
SDS	Sodium Dodecylsulfate
SDS-PAGE	SDS-Polyacrylamide Gel Electrophoresis
sec	second
Tag	Thermus aquaticus
TBE	Tris-Borate-EDTA-Electrophoresis buffer
TE	Tris-EDTA buffer
TEMED	Tetramethylethylene diamine
Tris	Trihydroxymethylaminomethane
U	Unit
UV	Ultra violet
V	Voltage
w/v	weight/volume
X-Gal	5-brom-4-chlor-3-indolyl- β -Dgalactopyranoside

1. Introduction

1.1 The heat shock protein family: the very short overview

In both prokaryotes and eukaryotes, transcription of most genes for heat shock proteins (HSPs) is induced by environmental stress conditions and various agents, including heat shock, anoxia, heavy metals, and certain inhibitors of mitochondrial respiration (Lindquist and Craig, 1988 ; Welch, 1992). HSPs in mammalian cells are classified into several families based on their apparent molecular mass and degrees of structural homology. HSPs are subdivided into small HSPs (25-28 kDa), HSP40 (40kDa), HSP60, HSP70 (68-80 kDa), HSP90 (83-99 kDa), and high-molecular-weight HSPs (110 kDa). Many members of these subfamilies are in fact not heat inducible, but their expression is induced in a tissue-specific manner or during development. The number of genes encoding the different HSP members varies between organisms. The number of genes encoding the diverse HSP family members largely varies per organism. For HSP70, the number of genes varies from three in *Escherichia coli*, 14 in *Arabidopsis thaliana*, 12 in *Drosophila melanogaster* and 13 in *Homo sapiens*. For small HSP (sHSP), the number of genes is relatively high in plants and the same holds true for HSP40 (Table 1.1) (Vos *et al.*, 2008). HSPs act as molecular chaperones that recognize unfolded or newly translated proteins and promote acquisition of the functional native state (Frydman, 2001). Therefore, molecular chaperones prevent the aggregation of unfolded and damaged proteins in cells. Severely damaged proteins are selected by a process termed protein quality control, in which the chaperone HSP70 in collaboration with other proteins such as E3 ubiquitin ligase target the damaged proteins for degradation via the ubiquitin-proteasome pathway (Connell *et al.*, 2001; McDonough and Patterson, 2003).

1.2 The heat shock protein family 110 (HSP110)

The Hsp110 gene family includes two genes in *Saccharomyces cerevisiae* known as *SSE1* and *SSE2* and four genes in the mammalian genome, namely, *Hspa4l/Apg1*, *Hspa4/Apg2*, *Hsph1/Hsp105* and *Hyou1/Grp175/orp150*. Except *HYOU1* that is present in endoplasmic reticulum, all other members of mammalian and yeast HSP110 are found in the cytosolic compartment. Constitutive expression of *Hspa4l* is high in testis and moderate in other tissues,

while *Hspa4* and *Hsph1* are expressed in various tissues (Morozov *et al.*, 1995; Kojima *et al.*, 1996; Kaneko *et al.*, 1997, Kojima *et al.*, 2004).

Table 1.1. Number of Hsp genes in different species (Vos *et al.*, 2008).

	HSPA/H	HSP40	sHSP	genome size (bp)
<i>H. sapiens</i>	13	41	11	3.3×10^9
<i>D. melanogaster</i>	12	36	11	1.2×10^8
<i>A. thaliana</i>	14	89	19	1.1×10^8
<i>Saccharomyces cerevisiae</i>	14	22	2	1.2×10^7
<i>E. coli</i>	3	6	2	4.6×10^6

Primary structure of HSP110 proteins is highly related to HSP70 and consists of a nucleotide-binding domain (NBD) and a peptide-binding domain (PBD) that are connected by a flexible linker region (Mayer and Bukau, 2005; Liu and Hendrickson, 2007). However, biochemical analyses revealed that HSP110 members serve as cochaperones of mammalian and yeast HSP70 chaperones and act as molecular exchange factors (NEF) during the ATP-hydrolysis cycle (Steel *et al.*, 2004; Dragovic, 2006; Shaner and Morano, 2007). Binding of newly synthesized polypeptides to HSP70 chaperones and the subsequent release of folded proteins is regulated by a continuous cycle of ATP-hydrolysis and exchange of ATP to ADP (Fig. 1.1). In the ATP-bound state, PBD of HSP70 chaperone binds to polypeptides with low affinity. However, ATP-hydrolysis to ADP by HSP40 cochaperone leads to conformational changes that result in high affinity substrate binding by HSP70. To complete the protein folding cycle, binding of HSP110 NEF to HSP70 in the ADP-state stimulates the release of ADP. Subsequent binding of ATP induces the disassociation of HSP70-HSP110 complexes (Polier *et al.*, 2008).

The cellular functions of the HSP110/SEE gene family members were determined in several species. In *S. cerevisiae*, deletion of SSE1 results in a reduction of cell proliferation and temperature sensitivity, whereas the depletion of SSE2 has no effect on proliferation. However

deletion of both SSE1 and SSE2 genes is reported to be lethal in some strain backgrounds, indicating a unique important cellular function of these proteins in yeast (Mukai, *et al.*, 1993; Shaner *et al.*, 2004; Raviol *et al.*, 2006).

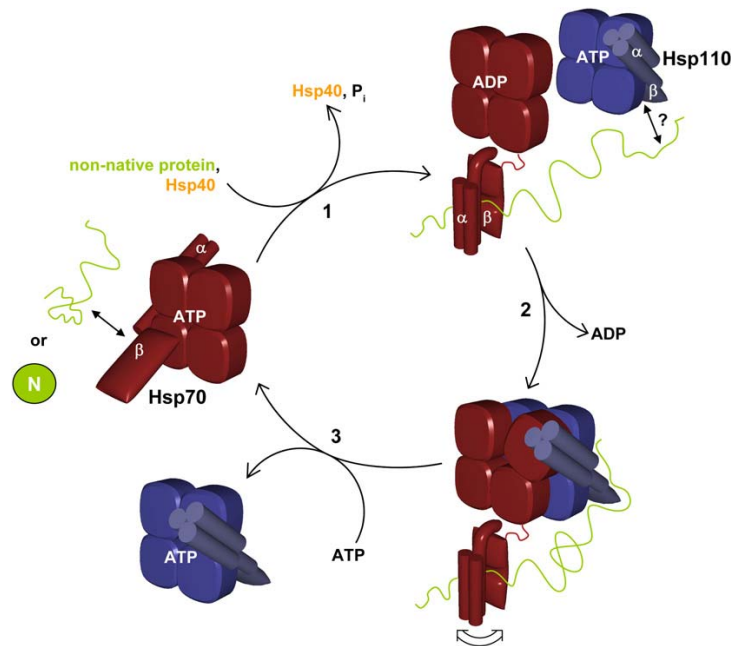


Fig.1.1 Model for the cooperation of HSP110 and HSP70 in protein folding. Recruitment of HSP70 (red) to unfolded substrate protein (green) is assisted by J-domain proteins (HSP40, orange; step 1). Complex formation between HSP70 and HSP110 (blue) displaces ADP from the HSP70 partner (step 2). Direct substrate binding to HSP110 may provide an anchor aiding the unfolding of kinetically trapped intermediates through thermal motions of the PBD of HSP70. Finally, upon binding of ATP to HSP70, the HSP70-HSP110 complex dissociates and the substrate protein is released for folding (step 3). The green circle indicates natively folded substrate protein (Polier *et al.*, 2008).

The physiological function of the mammalian HSP110 gene family has been studied by analysis of knockout mice. Analysis of *Hspa4*^{-/-} deficient mice revealed that *Hspa4l* is not essential for embryonic development and *Hspa4l*-deficient mice were indistinguishable from their wild-type littermates in appearance and gross behavior. However, approximately 42% of mutant males are infertile. The cause of the male infertility is due to reduction of sperm count and sperm motility. Further analysis revealed that the reduction of sperm number is due to the elimination of a significant number of developing germ cells via apoptosis. No defect in fertility was observed in *Hspa4l*-deficient females (Held *et al.*, 2006). In addition, Held *et al.* (2006) found that *Hspa4l*^{-/-} mice were preferentially susceptible to osmotic stress. Nakamura *et al.* (2008) have studied the physiological function of *Hsph1/Hsp110*, which is ubiquitously expressed. They found that the deletion of *Hsph1* did not affect the embryonic development, viability and fertility of mutant mice. However, *Hsph1/Hsp110* knockout mice are resistant to ischemic injury and that the protective effects of *Hsph1* deficiency in cerebral ischemia may be mediated by an increase in the chaperone activity of HSP70.

1.3 Expression and function of *Hspa4*

In mouse, *Hspa4* gene was mapped to chromosome 11, region B1.3 and consists of 19 exons. The *Hspa4* cDNA has a length of 2832 bp, encoding for a polypeptide of 841 amino acids with a molecular weight of 94,1 kDa. The HSPA4 protein shows about 65% sequence identity with HSPA4L protein (Kaneko *et al.*, 1997). Although HSPA4 protein is highly homologous in amino acid sequence to human HSP70RY (94%), HSPA4 is longer than HSP70RY by 140 amino acid sequence at its C-terminus. Expression analysis revealed that the transcript level of *Hspa4* is not induced by heat shock (Kaneko *et al.*, 1997; Nonoguchi *et al.*, 1999; Okui *et al.*, 2000). In the adult mouse, *Hspa4* mRNA is detected in most tissues, with the highest expression in testis, ovary and spleen (Nonoguchi *et al.*, 1999). *Hspa4* transcripts were detected in cells of various origins, including embryonic fibroblasts, embryonal carcinomas, myelomonocytic leukemia, mastocytoma, Sertoli cells and bone marrow stromal cells (Kaneko *et al.*, 1997).

In addition, the *Hspa4* gene has been found as one of 250 genes, which are highly expressed in the pluripotent stem cells (Ramalho-Santos *et al.*, 2002). Two *Hspa4* transcripts of 3.2 and 4.8-kb

were found by in Northern blot analysis. However, protein analysis revealed that an anti-HSPA4 antibody only detect a 94-kDa protein in all studied tissues. These results suggest that both *Hspa4* RNA isoforms result from alternative splicing of the 3'- untranslated region (Held, 2008). Analysis of HSPA4 expression during germ cell development revealed that the expression is highly enriched in male and female germ cells of prenatal gonad. Expression of HSPA4 in male gonocytes is gradually decreased after migration to basement layers of seminiferous tubules and differentiation to spermatogonia (Held, 2008). In brain, HSPA4 protein was found to be expressed constitutively in rat neuronal tissues throughout development (Ogita *et al.*, 2001) and primary human articular chondrocytes (Dehne *et al.*, 2010).

HSPA4 was identified as a new interaction partner of the protein zonula occludens (ZO-1), which is associated with tight junction proteins at cell membrane. This interaction between HSPA4 and ZO-1 regulates the function of ZO-1 in control of the cellular localization of the transcription factor ZO-1 associated nucleic acid binding protein (ZONAB/DbpA/Csda). Binding of ATPase domain of HSPA4 to the SH3 domain of ZO-1 competes with the binding of ZONAB to SH3 domain of ZO-1, resulting in the release the ZONAB from the complex with ZO-1, transport to the nucleus and stimulates the transcription of genes encoding cell cycle regulators such as cyclin D1 and PCNA. Cyclin D1 and PCNA regulate the G1/S phase transition (Balda *et al.*, 2003; Tsapara *et al.*, 2006). Both HSPA4 and ZONAB are required for normal proliferation and regulate entry to S-phase. Thus, only little HSPA4 is associated with ZO-1 under control conditions. On heat shock, however, HSPA4 is redistributed, not upregulated, resulting in accumulation in nucleoli and at intracellular junction. It is conceivable that HSPA4 stabilizes tight junctions during stress conditions (Tsapara *et al.*, 2006). In hepatocellular carcinoma and pancreatic cancer cells, HSPA4 as well as human ZONAB homologue DbpA are overexpressed (Nakatsura *et al.*, 2001; Hayashi *et al.*, 2002; Gotoh *et al.*, 2004) suggesting that ZONAB signaling becomes activated, because most of its interacting protein ZO-1 becomes associated with the HSPA4 (Tsapara *et al.*, 2006).

Recently, it has been showed that overexpression of *Hspa4* in chronic myelogenous leukemia cells (BaF3-BCR/ABL cells) increases cell proliferation and protects cells from oxidative damage, which may play an important role in chronic myelogenous leukemia carcinogenesis and progression (Li *et al.*, 2010).

To analyze the function of HSPA4 in mammalian species, *Hspa4* was disrupted by homologous recombination in the mice (Held, 2008). Two lines of *Hspa4*-deficient mice were generated in hybrid C57BL/6J x 129/SV and inbred 129/Sv genetic background. Analysis of *Hspa4*-deficient mice in hybrid C57BL/6J x 129/SV genetic background revealed that approximately 62% of *Hspa4*-deficient males in F2 generation are infertile due to a significant reduction in sperm number and motility. No defects in fertility were observed in female mutants. Analysis of *Hspa4*-deficient mice in the inbred background showed that 94,1% of *Hspa4*-deficient mice display growth retardation and died between the third and fourth week after birth. Male and female deficient animals, which overcome the early lethality display impaired fertility. Kyphosis was developed in *Hspa4*-deficient mice of advanced age. Anatomical analysis of adult *Hspa4*^{-/-} heart showed enlargement of heart size. In addition, deficiency of *Hspa4* gene causes skeletal muscle myopathy in adult *Hspa4*^{-/-} mice (Held, 2008).

1.4 Aims of the study

In context of this work, several questions must be addressed. What are the underlying causes of male infertility, growth retardation and skeletal muscle myopathy in *Hspa4*-deficient mice? What are the signaling pathways that are disturbed in the cardiac hypertrophy in mutant mice? Therefore, the aim of my study was to determine the underlying causes of male infertility, growth retardation and cardiac hypertrophy in *Hspa4*^{-/-} mice. To reach these goals, studies were performed and categorized as follows:

1. To determine the cause of disruption of spermatogenesis in *Hspa4*^{-/-} mice, the progress of male germ cell development in mutant mice was studied at different stages of postnatal development.
2. To determine whether growth retardation is due to skeletal muscle myopathy, histological analysis of different types of skeletal muscle were performed at different postnatal development.
3. Development of cardiac fibrosis and hypertrophy in the *Hspa4*^{-/-} heart was determined during postnatal life using different histological and molecular analyses.
4. To determine the molecular pathways, which are mediating the cardiac fibrosis and hypertrophy, a microarray assay was performed and the expression of differentially expressed genes in *Hspa4*^{-/-} heart was confirmed by quantitative RNA and protein analysis.

2. Materials and Methods

2.1 MATERIALS

2.1.1 Chemicals

Acetic acid	Merck, Darmstadt
Agar	Difco, Detroit, USA
Agarose	Invitrogen, Karlsruhe
Ammonium acetate	Fluka, Neu Ulm
Ammonium persulfate	Sigma, Deisenhofen
Ampicillin	Sigma, Deisenhofen
Ampuwa	Fresenius, Bad Homburg
Aqua Poly/Mount	Polysciences, Inc, USA
Bacto-tryptone	Difco, Detroit, USA
Bacto-Yeast-Extract	Difco, Detroit, USA
Blocking powder	Boehringer, Mannheim
BSA	Biomol, Hamburg
Chloroform	Baker, Deventer, NL
Cardiotoxin	Sigma, Deisenhofen
Coomassie Blue G-250	Sigma, Deisenhofen
Diethyl pyrocarbonate (DEPC)	Sigma, Deisenhofen
Dimethyl sulfoxid (DMSO)	Merck, Darmstadt
Dithiothreitol	Sigma, Deisenhofen
dNTPs	Invitrogen, Karlsruhe
EDTA	ICN Biomedicals, Eschwege
Ethanol	Baker, Deventer, NL
Ethidium bromide	Sigma, Deisenhofen
Eukitt-quick hardening mounting medium	Fluka, Neu Ulm
FBS	Invitrogen, Karlsruhe
Ficoll 400	Amersham Pharmacia, Freiburg
Formaldehyde	Invitrogen, Karlsruhe
Formamide	Fluka, Neu Ulm
Glutaraldehyde	Sigma, Deisenhofen

Materials and Methods

Glycerol	Invitrogen, Karlsruhe
Glycine	Biomol, Hamburg
Goat serum	PAN-Systems, Nürnberg
HCl	Merck, Darmstadt
H ₂ O ₂	Merck, Darmstadt
Isopropanol	Merck, Darmstadt
1 kb DNA Ladder	Invitrogen, Karlsruhe
100 bp DNA Ladder	Invitrogen, Karlsruhe
KCl	Merck, Darmstadt
KH ₂ PO ₄	Merck, Darmstadt
Methanol	Merck, Darmstadt
2-Mercaptoethanol	Serva, Heidelberg
MgCl ₂	Merck, Darmstadt
Milk powder	Roth, Karlsruhe
NaCl	Merck, Darmstadt
Na ₂ HPO ₄	Merck, Darmstadt
NaH ₂ PO ₄	Merck, Darmstadt
NaHCO ₃	Merck, Darmstadt
NaOH	Merck, Darmstadt
NuPAGE Novex Bis-Tris 4-12% Gel	Invitrogen, Karlsruhe
NuPAGE MOPS SDS running buffer	Invitrogen, Karlsruhe
NuPAGE SDS sample buffer	Invitrogen, Karlsruhe
Orange G	Sigma, Deisenhofen
Paraformaldehyde	Merck, Darmstadt
Paraquat	Sigma, Deisenhofen
PBS	PAN-Systems, Nürnberg
Penicillin/Streptomycin	PAN-Systems, Nürnberg
Peptone	Roth, Karlsruhe
Phenol	Biomol, Hamburg
Phosphoric acid	Merck, Darmstadt
Picric acid	Fulka, Neu Ulm
Protein marker	Biorad, Sigma
[³² P]-dCTP	Amersham Pharmacia, Braunschweig
Rediprime TM II	Amersham Pharmacia, Freiburg

RNase A	Qiagen, Hilden
RNase away	Biomol, Hamburg
RNase Inhibitor	Roche, Penzberg
RNA length standard	Invitrogen, Karlsruhe
Saccharose	Roth, Karlsruhe
Salmon sperm DNA	Sigma, Deisenhofen
SDS	Serva, Heidelberg
SeeBlue Plus2 Pre-Stained	Invitrogen, Karlsruhe
StandardSelect Peptone	Invitrogen, Karlsruhe
Gibco/BRL, Eggenstein	Merck, Darmstadt
S.O.C Medium	Merck, Darmstadt
Sodium acetate	Sigma, Deisenhofen
Sun flower oil	Sodium citrate
SuperScript II	Invitrogen, Karlsruhe
T4 DNA ligase	Promega, Mannheim
Trifast reagent	Sigma, Deisenhofen
Tris base	Sigma, Deisenhofen
Triton X-100	Serva, Heidelberg
Trypsin	PAN-Systems, Nürnberg
Tween-20	Sigma, Deisenhofen
Vectashield (DAPI)	Vector, Burlingame
X-Gal	Biomol, Hamburg
Xylene	Merck, Darmstadt
Yeast extract	Roth, Karlsruhe

2.1.2 Solutions, buffers and media

All standard buffers and solutions were prepared according to Sambrook *et al.* (1989).

Bouin's solution	15 volume of Picric acid (in H ₂ O) 5 volumes of 37% Formaldehyde 1 volume of Acetic acid
------------------	--

Ligation buffer (10x)	600 mM Tris/HCl (pH 7.5) 80 mM MgCl ₂ 100 mM DTT
Loading buffer	15% Ficoll 400 10 mM EDTA (pH 8) 0.25% Orange G 1% Glycerol
Lysis buffer I	100 mM Tris/HCl (pH 8.0) 100 mM NaCl 100 mM EDTA 0.5% SDS
SSC (20x)	3 M NaCl 0.3 M sodium citrate (pH 7.0)
TBE buffer (5x)	450 mM Tris base 450 mM Boric acid 20 mM EDTA (pH 8)
TE buffer	10 mM Tris/HCl (pH 8.0) 1 mM EDTA

2.1.3 Laboratory materials

The laboratory materials, which are not listed here, were bought from Schütt and Krannich (Göttingen).

Culture slides	BD Falcon, Heidelberg
Disposable filter Minisart NMI	Sartorius, Göttingen
Filter paper 0858	Schleicher and Schüll, Dassel
Hybond C	Amersham, Braunschweig
Hybond N	Amersham, Braunschweig
HPTLC Aluminum folio	Merck, Darmstadt

Microcentrifuge tubes	Eppendorf, Hamburg
Petri dishes	Greiner, Nürtingen
Pipette tips	Eppendorf, Hamburg
RotiPlast paraffin	Roth, Karlsruhe
Transfection flasks	Lab-Tek/Nalge, Nunc, IL, USA
Superfrost slides	Menzel, Gläser
Whatman blotting paper (GB 002, GB 003 and GB 004)	Schleicher and Schüll, Dassel
X-ray films	Amersham, Braunschweig

2.1.4 Sterilisation of solutions and equipments

All solutions that are not heat sensitive were sterilised at 121°C, 105 Pa for 60 min in an autoclave (Webeco, Bad Schwartau). Heat sensitive solutions were filtered through a disposable sterile filter (0.2 to 0.45 µm pore size). Plastic wares were autoclaved as above. Glasswares were sterilised overnight in an oven at 220°C.

2.1.5 Media, antibiotics and agar-plates

2.1.5.1 Media for bacteria

LB Medium (pH 7.5)	1% Bacto-trypton 0.5% Yeast extracts 1% NaCl
LB-Agar	1% Bacto-trypton 0.5% Yeast extracts 1% NaCl 1.5% Agar

The LB medium was prepared with distilled water, autoclaved and stored at 4°C.

2.1.5.2 Antibiotics

Stock solutions were prepared for the antibiotics. They were filtered through sterile disposable filters and stored at -20°C . When antibiotics were needed, in each case, they were added after the autoclaved medium has cooled down to a temperature lower than 55°C .

Antibiotics	Stock solution	Working solution
Ampicillin	50 mg/ml	50 $\mu\text{g/ml}$
Kanamycin	25 mg/ml	50 $\mu\text{g/ml}$

2.1.5.3 IPTG/X-Gal plate

LB-agar with 50 $\mu\text{g/ml}$ ampicillin, 100 μM IPTG and 0.4% X-Gal was poured into Petri dishes. The dishes were stored at 4°C .

2.1.6 Bacterial strains

E. coli DH5 α

K-12 strain, F- Φ 80d *lacZ* Δ M15 endA1
recA1 *hsdR17* (rk-, mk+) sup E44 *thi-1*
d- *gyrA96* (*lacZYA-arg*)
(Invitrogen, Karlsruhe)

2.1.7 Plasmids

pGEMTeasy

(Promega, Wisconsin, USA)

2.1.8 Synthetic oligonucleotides

The synthetic oligonucleotide primers used in this study were obtained from OPERON and dissolved in dH₂O (Ampuwa) to a final concentration of 100 pmol/ μl .

2.1.8 .1 Primers used for generation of cDNA probes

Name	Sequence
Acr_F	5`-CTTCTCGACCGCTTTACCTG-3'
Acr_R	5`-AGCTGAGCAGGGAGGATGTA-3'
Hsc70t_F	5`-GCTACAAAGCGGAGGATGAG-3'
Hsc70t_R	5`-AGGATGGTGACGTAGGCTTG-3'
Tnp2_F	5`-CATGGACACCAAGATGCAGA-3'
Tnp2_R	5`-CCTGTGACATCATCCCAACA-3'
Anf_F	5`-CCGGTAGAAGATGAGGTCATG-3'
Anf_R	5`-CAAGACCCCACTAGACCACTC-3'
Bnf_F	5`-CACTGAAGTTGTTGTAGGAAGACC -3'
Bnf_R	5`- CAAAAGCAGGAAATACGCTATG-3'
Apcs_F	5`-TCTTCCATAACCACGGACTGT -3'
Apcs_R	5`-CTCCACCCTTCATTGTCATC -3'
Slco1b2_F	5`-TGCGATGGATTCAGGATATT-3'
Slco1b2_R	5`-ACCCCTTTTCACAACCTTTC -3'
Sycp3_F	5`- GTTGCAGCAGTGGGAACTGG -3'
Sycp3_R	5`- CTAAAGGCATGCCTCTTAGC -3'
Pkg2_F	5`- TCTCATGAGTCACCTCGGTCG -3'
Pkg2_R	5`- AACTGTGAGCCCGATGTGCAG -3'
Pepck_F	5`- GTGGAGGAGATCGACAGGTATC -3'
Pepck_R	5`- CTCACACAGAGACACGTTAC-3'
ApoB_F	5`- CCAACAGAAATGTCCACAGAGA -3'
ApoB-R	5`- AGCCACTGGAGGATGTGAGTAT -3'

2.1.8.2 Genotyping primers

Apg2-genotyping_F	5`- GATCACGGGAAGTGAGTGGT -3'
Apg2-genotyping_R	5`- GAGCGGGAGTGAGACAGTTC -3'
Apg1- genotyping_F	5`- GGTCAGAAAGGCTCACCAAGG -3'
Apg1- genotyping_R	5`- ACTGAGGCCCTTGATTTGGCC -3'
PGK3	5`- TCTGAGCCAGAAAGCGAAGG -3'

2.1.8.3 Real time PCR primers

Myh7_F	5'-AAGGGCCTGAATGAGGGA-3'
Myh7_R	5'-TGCAAAGGCTCCAGGTCTGA-3'
Acta1_F	5'-TATGTGGCTATCCAGGCGGTG -3'
Acta1_R	5'-CCCAGAATCCAACACGATGC -3'
MCIP1.4_F	5'- AGCTCCCTGATTGCCTGTGT- 3'
MCIP1.4_R	5'-TTTGGCCCTGGTCTCACTTT- 3'
Apg2_F	5'- AGCTTCCTGAGATGGACATTG -3'
Apg2_R	5'- CGAGGTCCCCTAAAACTGA -3'
Hcn1_F	5'- CAATGAAGACAGCTCGGAAA -3'
Hcn1_R	5'- ATGAAGTCCACCACAAACCA-3'
Kcnd2_F	5'-TTGCCTGAGGTGAAGAAGTG -3'
Kcnd2_R	5'- GGGGTCACCCAAAATAACAC-3'
Mme_F	5'- GAGTTTGCAGATGCCTTTCA-3'
Mme_R	5'-AACCCGACATTTCTTTCTG- 3'
Scn4a_F	5'- CAGCATCGAGATGGACCACCTTAACT-3'
Scn4a_R	5'-GAGGCTGTAGTGGCTTCTTGATGTCC -3'
Irx4_F	5'-GAACAAGATGACCTGGCCACCTAGAA -3'
Irx4_R	5'-GGGTCTGAAGTCTTCCAAGTCACTGAG -3'
Ptp4a1_F	5'-AGCACGACCTCTATGCAGACAAGTGA -3'
Pt4a1_R	5'- GGCAATACAAAGGAAGTGCCTGAGG-3'
Maob_F	5'-AAACCAGATGGCACCTATGC- 3'
Maob_R	5'-GCTTCTTGGGAGTTCAGCAC- 3'
Kcne1_F	5'-AATTGTCCTCCGTTCTCCAC- 3
Kcne1_R	5'-CTGTGGGGGTTGCTTTTAAT- 3'
Gnao1_F	5'-AGTCAAAACAACCTGGCATCG- 3'
Gnao1_R	5'- TCAAACAGCCTGAAGTGGAG- 3'
Fktn1_F	5'-TTTTTGCCTGATGTGAGAGC- 3'
Fktn1_R	5'-TAGATGGCCCATGAATCAGA- 3'
Anf_F	5'-CCATATTGGAGCAAATCCTGTG- 3'
Anf_R	5'-CGGCATCTTCTCCTCCAGGT- 3'
Bnf_F	5'-TGGAAGTCCTAGCCAGTCTC-3'
Bnf_R	5'-CTGTCTCTGGGCCATTTCT-3'

Sdha_F	5'-GCTTGCGAGCTGCATTTGG-3'
Sdha_R	5'-CATCTCCAGTTGTCCTCTTCCA-3'
Hprt_F	5'-AGCCCCAAAATGGTTAAGGTTGC-3'
Hprt_R	5'-TTGCAGATTCAACTTGCGCTCAT-3'
Igfbp3_F	5'-CCAGGAAACATCAGTGAGTCC-3'
Igfbp3_R	5'-GGATGGAAGTTGGAATCGGTCA-3'
ET-AR_F	5'-GGTGGCTCTTTGGGTTCT-3'
ET-AR_R	5'-GACGCTGTTTGAGGTGCT-3'
ET-BR_F	5'-TGCGAAATGCTCAGGAAG-3'
ET-BR_R	5'-ACGAGGACCAGGCAGAAG-3'
Collagen 1_F	5'-AGGCTTCAGTGGTTTGGATG-3'
Collagen 1_R	5'-CACCAACAGCACCATCGTTA-3'
Calmodulin 1_F	5'-AGGGGTTTGGAGGTGACTTT-3'
Calmodulin 1_R	5'-TTCCTCGGAGGTTAGGGTTT-3'
TGF- β 1_F	5'-TGAGTGGCTGTCTTTTGACG-3'
TGF- β 1_R	5'-GGTTCATGTCATGGATGGTG-3'
Mef2C_F	5'-ATTTGGGAACTGAGCTGTGC-3'
Mef2C_R	5'-CGCTCATCCATTATCCTCGT-3'
Hdac 7a_F	5'-ATCTCTTCCTGGCAGGCTTA-3'
Hdac 7a_R	5'-TTCTGCTTGACCACACTGCT-3'

2.1.9 Mouse strains

Strains C57BL/6J, 129/Sv, CD-1 and NMRI were initially ordered from Charles River Laboratories, Wilmington, USA, and kept at Animal Facility of Institute of Human Genetics, Göttingen, in air-conditioned and light-controlled rooms.

2.1.10 Antibodies

Rabbit anti -HSP110 polyclonal antibody	Sigma, Steinheim
Rabbit anti -Apg1 polyclonal antibody	Santa Cruz Biotechnology, Heidelberg
Rabbit anti -Apg2 polyclonal antibody	Santa Cruz Biotechnology, Heidelberg
Mouse monoclonal anti - α -tubulin	Sigma, Deisenhofen
mouse anti -GCNA1 monoclonal antibody	G. Enders, University of Kansas, USA

Rabbit anti -SCP3(Syp3) polyclonal antibody	Abcam, Cambridge, UK
Goat anti-mouse IgG alkaline phosphatase conjugate	Sigma, Deisenhofen
Goat anti-rabbit IgG alkaline phosphatase conjugate	Sigma, Deisenhofen
Rabbit anti-mouse IgG Cy3 conjugate	Sigma, Deisenhofen
Rabbit anti-mouse IgG FITC conjugate	Sigma, Deisenhofen
Goat anti-rabbit IgG horse radish preoxidase conjugate	Sigma, Deisenhofen
Rabbit anti-mouse IgG horse radish preoxidase conjugate	Sigma, Deisenhofen
Rabbit anti-STAT3 polyclonal antibody	New England Biolabs, Frankfurt
Rabbit anti-phospho-STAT3 polyclonal antibody	New England Biolabs, Frankfurt
Rabbit Anti-MAP Kinase (ERK-1, ERK-2) polyclonal antibody	New England Biolabs, Frankfurt
Rabbit Anti-phospho- ERK-1 and Anti-phospho- ERK-2 polyclonal antibody	New England Biolabs, Frankfurt

2.1.11 Enzymes

Immolase DNA Polymerase	(Bioline, Luckenwalde)
Proteinase K	(Sigma, Deisenhofen)
Platinum Taq polymerase	(Invitrogen, Karlsruhe)
Restriction enzymes (with supplied buffers)	(Invitrogen, Karlsruhe)
RNase A	(Qiagen, Hilden)
RNase inhibitor	(Invitrogen, Karlsruhe)
Superscript-II	(Invitrogen, Karlsruhe)
T4 DNA ligase	(Promega, Mannheim)
Trypsin	(Invitrogen, Karlsruhe)
DNase I Amplification Grade	(Invitrogen, Karlsruhe)

2.1.12 Kits

Labelling System	Qiagen, Hilden
Megaprime DNA Labeling Kit	Amersham Pharmacia, Freiburg
Mini Plasmid Kit	Qiagen, Hilden
PCR Purification Kit	Qiagen, Hilden
QIAquick Gel Extraction Kit	Qiagen, Hilden
Rediprime™ II Random Prime	Amersham Pharmacia, Freiburg
Masson's trichrome stain Kit	Sigma, Deisenhofen
Periodic Acid Schiff Kit (PAS)	Sigma, Deisenhofen
ApopTag® plus peroxidase	Qbiogene, Heidelberg, Germany

2.1.13 Equipment

Autoclave	(Webeco, Bad Schwartau)
Centrifuge 5415D	(Eppendorf, Hamburg)
Centrifuge 5417R	(Eppendorf, Hamburg)
Biophotometer	(Eppendorf, Hamburg)
DNA Sequencer Modell Megabace 1000	(Amersham, Freiburg)
Microscope BX60	(Olympus, München)
GeneAmp PCR System 9600	(Perkin Elmer, Berlin)
Histocentre 2 embedding machine	(Shandon, Frankfurt aM.)
Microtiterplate-Photometer	(BioRad laboratories, München)
Molecular Imager FX	(BioRad laboratories, München)
Phosphoimager Screen	(BioRad laboratories, München)
Semi-Dry-Blot Fast Blot	(Biometra, Göttingen)
Spectrophotometer Ultraspec 3000	(Amersham, Freiburg)
SpeedVac concentrator SVC 100H	(Schütt, Göttingen)
Thermomixer 5436	(Eppendorf, Hamburg)
Turboblotter™	(Schleicher & Schüll, Dassel)
UV Stratalinker™1800	(Leica, Nußloch)

2.2 Methods

2.2.1 Isolation of nucleic acids

2.2.1.1 Small-scale isolation of plasmid DNA

(adapted from Birnboim and Doly, 1979).

A single *E.coli* colony was inoculated in 5 ml of LB medium with the appropriate antibiotic and incubated in a shaker for 16 hrs at 37°C with a vigorous shaking. 0.5 ml of this culture was used for making glycerol stock (0.5 ml of culture and 0.5 ml of glycerol) and rest of the culture was centrifuged at 5000 x g for 10 min. The pellet was resuspended in 100 µl of solution P1. The bacterial cells were lysed with 200 µl of P2 solution and then neutralized with 150 µl of P3 solution. The precipitated solution was centrifuged for 10 min at 10,000 xg at 4 °C. The supernatant was transferred into a new tube and centrifugation was done again. The supernatant was transferred again into a new tube and 1 ml of 100% ethanol was added to precipitate the DNA. It was then stored in ice for 15 min, centrifuged at full speed for 20 min, and finally the pellet was washed with 70% ethanol and after air-drying was dissolved in 50 µl of Ampuwa water.

P1: 50 mM Tris/HCl, pH 8.0; 10 mM EDTA; 100 µg/ ml RNase A

P2: 200 mM NaOH; 1% SDS

P3: 3 M Potassium acetate, pH 5.5

2.2.1.2 Isolation of genomic DNA from tissue samples

(Laird et al., 1991)

Routinely 0.5 cm of the mouse tail was incubated in 700 µl of lysis buffer I containing 35 µl proteinase K (10 µg/µl) at 55°C overnight in thermomixer . The tissue lysate was centrifuged at 10,000 xg for 15 min. Then, DNA was precipitated from supernatant by adding an equal volume of isopropanol, mixed and centrifuged at 10,000 xg at RT for 15 min. DNA was washed with 1 ml of 70% ethanol, dissolved in 50-100 µl of dH₂O and incubated at 60°C for 10 min.

2.2.1.3 Isolation of total RNA from tissue samples

(Chomczynski and Sacchi, 1987).

The composition of Trifast Reagent, which was used for RNA extraction contained phenol and guanidine thiocyanate in a monophasic solution. In order to avoid any RNase activity, homogenizers which were used for RNA isolation were treated before with RNase away and DEPC water. 100 mg tissue sample was homogenised in 1 ml of RNA reagent by

using a glass-teflon homogenizer. The sample volume should not exceed 10% of the volume of reagent used for the homogenisation. The homogenate was vortexed and incubated on ice for 5 min to permit the complete dissociation of nucleoprotein complexes. Then, 0.2 ml of chloroform was added, mixed and stored at 4°C for 10 min. After centrifugation at 12000 xg for 15 min at 4°C, the upper aqueous phase was transferred into a new tube. The RNA was precipitated by adding 0.5 ml of isopropanol. Finally, the pellet was washed twice with 75% ethanol and dissolved in 50-100 µl of RNase free water (DEPC-dH₂O). The RNA was stored at -80°C.

2.2.2 Determination of nucleic acid concentration

The concentration of nucleic acids was determined spectrophotometrically by measuring absorption of the samples at 260 nm. The quality of nucleic acids i.e. contamination with salt and protein was checked by the measurements at 230, 280, and 320 nm. The concentration was calculated according to the formula:

$$C = (E_{260} - E_{320}) / f \cdot c$$

C = concentration of sample (µg/µl)

E 260 = ratio of extinction at 260 nm

E 320 = ratio of extinction at 320 nm

f = dilution factor

c = concentration (standard) / absorption (standard)

for double stranded DNA : c = 0.05 µg/µl

for RNA : c = 0.04 µg/µl

for single stranded DNA : c = 0.03 µg/µl

2.2.3 Gel electrophoresis

2.2.3.1 Agarose gel electrophoresis of DNA

Agarose gels are used to electrophorese nucleic acid molecules from as small as 100 bp to more than 50 kb. For preparation of 1% agarose gel, 1 g of agarose was added in 100 ml 0.5 x TBE buffer, boiled in the microwave to dissolve the agarose, then cooled down to about 60°C before adding 3 µl ethidium bromide (10 mg/ml). This 1% agarose gel was poured into a horizontal gel chamber. 0.5x TBE buffer was used also as electrophoresis buffer. Before loading the samples, about 0.1 volume of loading buffer was added and mixed. The samples were then loaded into the wells of the gel and electrophoresis was carried out at a steady voltage (50 – 100 V). Size of the DNA fragments on agarose gels was determined using 1 kb

DNA ladder, which was loaded with samples in parallel slots. DNA fragments were observed and photographed under UV light.

2.2.3.2 Agarose gel electrophoresis of RNA

(Hodge, 1994)

Single-stranded RNA molecules often have complementary regions that can form secondary structures. Therefore, RNA was run on a denaturing agarose gel that contained formaldehyde. RNA was pre-treated with formaldehyde and formamide to denature. To prepare a denaturing agarose gel, 2 g of agarose was added to 20 ml of 10x MOPS buffer and 148 ml of DEPC water and dissolved by heating in microwave oven. After cooling it to about 50°C, 33.2 ml of formaldehyde (37%) was added, stirred and poured into a horizontal gel chamber. RNA samples were treated as follows:

- 10 – 20 µg RNA
- 2 µl 10 x MOPS Buffer
- 3 µl Formaldehyde
- 7 µl Formamide (40%)
- 1 µl Ethidium bromide
- 5 µl Loading buffer

Samples were denatured at 65°C for 10 min and chilled on ice before loading into the gel.

The gel was run at 40 V at 4°C overnight. To determine the size of the nucleic acid fragments on agarose gels, molecular weight ladder (0.24 – 9.5 RNA ladder) was loaded with samples in parallel slots.

2.2.4 Purification of DNA fragments from agarose gel

To purify DNA fragments from agarose gel, QIAquick gel extraction kit was used. The principle of this method depends on selective binding of DNA to uniquely designed silica-gel membranes. After running DNA in the agarose gel, agarose gel piece containing the DNA fragment was cut and incubated in 3 volumes of QG buffer at 50 °C for 10 min. Then, dissolved gel slice was applied to a QIAquick column and centrifuged for 1 min at 10,000 xg. The flow through was discarded and the column was washed with 0.75 ml of PE buffer. After drying, the column was placed into a fresh microcentrifuge tube. To elute DNA, 50 µl of dH₂O was added to the QIAquick membrane and the column was centrifuged for 1 min at 10,000 xg.

2.2.5 Enzymatic modifications of DNA

2.2.5.1 Digestion of DNA using restriction enzymes

Restriction enzymes are class of bacterial enzymes that recognizes and cut DNA at specific nucleotide sequence of 4 - 8 bp. Restriction enzyme digestions were carried out by incubating double-stranded DNA with an appropriate amount of restriction enzyme in its respective buffer as recommended by the supplier, and at the optimal temperature for that specific enzyme. Standard digestions include 2-10 U enzyme per microgram of DNA. Reactions were usually incubated for 1-3 hrs to ensure complete digestion at the optimal temperature for enzyme activity.

2.2.5.2 Ligation of DNA fragments

The ligation of an insert DNA into a vector, which was digested with appropriate restriction enzyme, was performed in the following reaction mix:

30 ng linearized vector DNA
50-100 ng insert DNA
1 μ l ligation buffer (10x)
1 μ l T4 DNA ligase (5U / μ l)
in a total volume of 10 μ l

Blunt-end ligations were carried out at 16°C for overnight, whereas overhang-end ligations were carried out at RT for 2-4 hrs. For cloning of PCR products, a pGEMTeasy vector system that has 5' T overhangs was used. The following substances were mixed:

50 ng of pGEMTeasy vector
150 ng PCR product
1 μ l of T4 DNA Ligase buffer (x10)
1 μ l of T4 DNA Ligase

The reactions were done in a total volume of 10 μ l and incubated overnight at 4°C.

2.2.6 Transformation of competent bacteria

(Ausubel *et al.*, 1994)

Transformation of the competent *E. coli* bacteria (invitrogen) was done by gently mixing one aliquot of competent bacteria (50 μ l) with 10 μ l of ligation reaction. After incubation for 30 min on ice, bacteria were heat shocked for 45 sec at 40°C and then cooled

down for 2 min on ice. After adding 600 µl of S.O.C medium, bacteria were incubated at 37°C for 1 hr. Bacteria were plated out either on LB-agar plates containing appropriate antibiotic (50 µg/ml) or X-Gal plates.

2.2.7 Polymerase chain reaction (PCR)

2.2.7.1 PCR amplification of DNA fragments

The standard PCR assay contained the following components:

10 ng DNA

1 µl Forward primer (10pmol)

1 µl Reverse primer (10pmol)

1 µl 10mM dNTPs

5 µl 10x PCR buffer

1.5 µl 50mM MgCl₂

1 µl *Taq* DNA polymerase (5U/µl)

Up to 50 µl H₂O

The reaction mixture was added in a 200 µl reaction tube, vortexed slightly and placed in the thermocycler.

Standard PCR program:

<i>Initial denaturation</i>	95°C 5 min
<i>Elongation</i>	95°C 30 sec (denaturation)
30-35 cycles	58°C 45 sec (annealing)
	72°C 1-2 min (extension)
<i>Final extension</i>	72°C 10 min

2.2.7.2 Genotyping of knockout mice by using PCR

All offspring of *Hsp4a* and *Hspa41* mutant lines were genotyped by polymerase chain reaction (PCR). For amplification of the wild type and the mutant allele, the DNA was extracted from mouse tails as described in 2.2.1.2 and pipetted to the following reaction mixture:

0.5 µl DNA (300-500 ng)

0.5µl Forward primer (10 pmol/µl)

0.5 µl Reverse primer (10 pmol/µl)

Materials and Methods

0.5 μ l P_{gk}_3 (10 pmol/ μ l)
 0.5 μ l dNTPs (10 mM)
 0.5 μ l Taq Platinum buffer (10x)
 0.75 μ l MgCl₂ (25 mM)
 0.25 μ l Taq Platinum
 Up to 25 μ l H₂O

The mixture was subjected to the following program in the thermocycler,

<i>Denaturation</i>	95°C for 7 min
Elongation (for 35 cycle)	95°C for 30 sec (Denaturation) 58°C for 30 sec (Annealing) 72°C for 1 min (Elongation)
<i>Final extension</i>	72°C for 10 min

2.2.7.3 Reverse transcription PCR (RT-PCR)

2.2.7.3.1 DNase I digestion

RNA samples, which were used in RT-PCR assay, were treated firstly with DNase to eliminate the contaminated DNA. The reaction mixture contained the following components:

1-5 μ g of RNA	≤ 8 μ l
10X DNase I Reaction Buffer	1 μ l
1 μ l of DNase I, diluted 1:5	1 μ l
DEPC-treated water	to 10 μ l

The reaction mixture was incubated for 30 min at 37°C. To inactivate the DNase I, 1 μ l of 25 mM EDTA solution was added to the reaction mixture and incubated for 10 min at 65°C.

2.2.7.3.2 Reverse transcription technique

To determine the expression of genes in specific tissues or in different development stages RT-PCR assay was performed. 1 -5 µg of total RNA was mixed with 1 µl of oligo (dT) primer (10 pmol/µl) in a total volume of 12 µl. To disrupt the secondary structure of the RNA, which might interfere with the cDNA synthesis, the mixture was heated to 65°C for 5 min and then quickly chilled on ice. After a brief centrifugation the followings were added to the mixture:

- 4µl 5x First strand buffer
- 2µl 0.1MDT
- 1µl 10 mMdNTPs
- 1µl Rnase inhibitor (10U/µl)

The content of the tube was mixed and incubated at 42°C for 2 min. Then, 1µl of reverse transcriptase enzyme (Superscript II) was added and further incubated at 42°C for 50 min for the first strand cDNA synthesis. The reaction was then inactivated by heating at 70°C for 15 min. One µl of the first strand reaction was used for the PCR reaction.

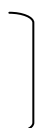
2.2.7.4 Quantitative Real-Time PCR

Extraction of total RNA from tissues was performed using Trifast Reagent as described above (2.2.1.3). RNA was treated with DNase I and was then reverse-transcribed according to section 2.7.3. Serial dilutions of sample and standard DNA's were made. To generate a standard curve, standard DNA was serially diluted to 20, 10, 5, 2.5, 1.25 and 0.625 ng/µl, while each RNA sample was diluted to a concentration of 10 ng/µl. To enhance the efficiency of PCR amplification, primers were designed to generate amplicons less than 200 bp. Real-Time quantitative PCR was performed using QuantiTect SYBR Green PCR Master mix (Quiagen) in an ABI Prism 7900HT sequence detection system. Each reaction was run in triplicate , repeated three times using three animals of each genotype. Levels of mRNA expression were normalized to those of the mouse housekeeping genes *Sdha* (succinate dehydrogenase) and *Hprt* (phosphoribosyl-transferase). 5 µl of 2x QuantiTect SYBR-Green PCR-Master-Mix, 1 µl Forward Primer (9µM), 1 µl Reverse Primer (9µM), 0.3µl MgCl₂ (50mM) and 1µl of cDNA (in a 1/20 dilution) were mixed with RNase free water to a total volume of 10 µl. The following PCR program was used:

2 min 50°C

15 min 95°C

15 sec 95°C



30 sec 54°C 40x
30 sec 72°C
15 sec 95°C }
15 sec 60°C } Dissociation stage
15 sec 95°C }

2.2.8 Protein and biochemical methods

2.2.8.1 Isolation of total protein from mouse tissues

100 mg of tissue was homogenized in 500 µl of RIPA buffer containing protease inhibitors. Tissues extract was incubated for 30 min at 4°C and then sonicated two times for 1 min with Branson ultra-Sonifier. The lysates were centrifuged at 8000xg for 10 min. The supernatant containing total proteins was taken and aliquoted in e-cups. The protein samples were stored at -80°C.

2.2.8.2 Isolation of total protein from cell culture

5 x 10⁶ cells/ml were washed with cold phosphate buffered saline (PBS) and resuspended in 50 - 200 µl of lysis buffer A. The cell lysate was incubated on ice for 30 min, treated with ultrasound on ice two times for 30 sec and centrifuged at 24000 x g for 15 min at 4°C. The supernatant with protein extract was stored at -80°C.

2.2.8.3 Determination of protein concentration

(Bradford, 1976)

Bio-Rad protein assay was used to determine the protein concentration. The assay is based on the observation that the absorbance maximum for an acidic solution of Coomassie Blue G-250 shifts from 494 to 595 nm when it is associated to protein. In order to obtain standard dilutions in range of 10 µg/ml to 100 µg/ml, BSA stock solution of 1 mg/ml was diluted. The dye reagent was diluted 1:5 with H₂O and a 2 µl sample was added. The absorption of the color reaction was measured at 595 nm in a spectrophotometer.

2.2.8.4 SDS-PAGE gel for separation of proteins

(Laemmli, 1970)

NuPage 4-12% Bis-Tris gel ((Invitrogen) was used for separation of proteins according to their molecular weight. To 15 µl of whole protein lysate, 5 µl of 4 x LDS sample buffer and 3 µl of 1 M DTT were added. Then, the samples were denatured in 95°C for 10 min and chilled in ice. The gel electrophoresis was run in 1 x MOPS buffer (Invitrogen). As a

weight marker, a pre-stained molecular weight standard (See Blue Plus2, Invitrogen) was loaded. The gel was run at 100 V for 2 – 3 hrs at RT.

2.2.9 Blotting techniques

2.2.9.1 Northern blotting of RNA

To transfer the RNA to the nitrocellulose membrane, we used a Turbo-Blot apparatus (Schleicher & Schuell, Dassel). About 25-28 Whatman filter papers (GB 003) were layered on a Stack Tray, followed by 4 Whatman filter papers (GB 002) and 1 Whatman filter paper (GB 002), which were soaked with 20 x SSC. The nitrocellulose filter, which was also soaked with 20 x SSC, was laid on the top. The agarose gel was placed on the nitrocellulose filter and was covered with 3 Whatman filter papers GB 002 soaked with 20 x SSC. The buffer tray was filled with 20 x SSC. Then, a wick that was soaked with 20 x SSC, was put on top of the blot. The transfer was performed for overnight. Finally, after disassembling of the blot, the RNA was fixed onto the filter by baking at 80°C for at least 2 hours.

2.2.9.2 Western blotting of protein

(Gershoni and Palade, 1982)

After electrophoresis of proteins on the SDS-PAGE, the nitrocellulose membrane Hybond-C (Amershan) was cut at the size of the gel and soaked with transfer buffer. Four pieces of Whatman filter paper were soaked in transfer buffer and placed on the semi dry transfer machine's lower plate (Biometra, Göttingen). Then, the wet membrane and the gel were put over them. Another four soaked Whatman papers were placed over to complete the sandwich model. The upper plate of semi dry transfer machine was placed over this sandwich and the transfer was carried out at 10 W (150-250 mA, 39 V) for 1 hr. Next, the nitrocellulose membrane was blocked and incubated with antibodies. To assess transfer efficiency of proteins onto nitrocellulose membranes, the gel was stained for 30 min in Coomassie blue solution at RT. Finally, gel was destained in Coomassie destaining solution for 3-8 hrs at RT.

Transfer buffer	pH 9.2	5.8 g Tris-HCl
		2.9 g Glycine
		3.7 ml 10% SDS
		dH ₂ O to 1000 ml

Membrane staining

Membrane was stained with Coomassie blue at RT.

Coomassie blue: 0.1% Coomassie
90% Methanol
10% CH₂COOH

Destaining of the membrane

Destaining solution: 40% Methanol
10% CH₂COOH
up to H₂O

2.2.9.3 Incubation of protein –bound membranes with antibodies

The blotted membrane was first incubated with 5% non-fat milk in PBT for 1-2 hrs at RT and then it was incubated overnight at 4 °C with a primary antibody at the recommended antibody dilution in 2% non fat milk in PBT. Then, the membrane was washed 3x 20 min with 2% non fat milk in PBT and incubated with horse radish peroxidase conjugated secondary antibody diluted 1:10000 in PBT containing 2% non fat milk in PBT for 1 hr at RT. After this step the membrane was washed 3x for 10 min at RT in PBT with 2% non fat milk in PBT and one time for 5 min at RT in PBS. Finally, the proteins from the membrane were visualized by using SuperSignal® West Pico Chemiluminescent Substrate (Pierce, USA) . Membrane was incubated for 3-5 min with 1 ml of developing mixture (0.3 ml stable peroxidase solution and 0.3 ml Luminal/enhancer solution) and then was wrapped in saran foil and exposed to Roentgen films (Hyperfilm MP, Amersham, Braunschweig) for 0.5 to 10 min. The films were developed in X-Ray Automatic processor Curix .

2.2.10 “Random Prime” method for generation of ³²P labeled DNA

(Denhardt, 1966; Feinberg and Vogelstein, 1989)

For generation of ³²P labeled DNA Rediprime™ II Random Prime Labeling System (Amersham Pharmacia) was used. The method depended on the random priming principle developed by Feinberg and Vogelstein (1989). Firstly, 25-50 ng DNA were denatured in a total volume of 46 µl at 95°C for 10 min and quickly chilled on ice for 5 min. After pipetting the denatured probe into Rediprime™ II Random Prime Labelling System cup, 4 µl of [α -³²P] dCTP (3000 Ci/mmol) were added to the reaction mixture. The labelling reaction

incubated at 37°C for 45 min. The labelled DNA was purified from free [α - 32 P] dCTP by using illustraTMProbe QuantTM G-50 Micro Columns (GE Healthcare).

2.2.11 Hybridisation of nucleic acids

(Denhardt, 1966)

The membrane to be hybridised was equilibrated in 2 x SSC and transferred to a hybridisation tube. After adding 12 ml of Rapid-hyb buffer (GE Healthcare) and sheared denaturated salmon DNA, the membrane was incubated for 2 hrs in the hybridisation oven at 65°C. The 32 P labeled DNA probe was denaturated at 95°C for 10 min, chilled on ice for 5 min, and added to the hybridisation solution. The hybridisation was carried out overnight in the hybridisation oven. The membrane was washed for 10 min with 2 x SSC, and then with 2 x SSC containing 0.2% SDS at 65°C for 10 – 20 min. Finally, the membrane was washed with 0.2 x SSC containing 0.1 % SDS at the hybridisation temperature. After drying the filter, it was sealed in plastic foil and exposed to autoradiography overnight at -80°C. The film was developed in X-Ray Automatic Processor Curix 60. If the membrane has to be used again, it was stripped in 0.2 x SSC at 80°C until radioactive signal was no longer detected.

2.2.12 DNA sequencing

DNA sequencings was performed with the Dye Terminator Cycle Sequencing-Kit (ABI PRISM). The reaction products were analysed with automatic sequencing equipment, MegaBase DNA Sequencer. For the sequencing reaction, four different dye labelled dideoxy nucleotides were used (Sanger *et al.*, 1977), which, when exposed to an argon laser, emit fluorescent light that can be detected and interpreted.

The reaction was carried out in a total volume of 10 μ l containing 1 μ g plasmid DNA or 100-200 ng purified PCR products, 10 pmol primer and 4 μ l reaction mix (contained dNTPs, dideoxy dye terminators and *Taq* DNA polymerase). Elongation and chain termination took place during the following program in a thermocycler: 4 min denaturation followed by 25 cycles at 95°C, 30 sec; 55°C, 15 sec, annealing; 60°C, 4 min, elongation. After the sequencing reaction, the DNA was precipitated with 1/10 volume 3 M sodium acetate and 2.5 volume 100% ethanol and washed in 70% ethanol. The pellet was dissolved in 4 μ l of loading buffer, denaturated at 95°C for 3 min, and finally loaded on the sequence gel.

2.2.13 Histological techniques

2.2.13.1 Tissue preparation for paraffin-embedding

Tissues were isolated from mice and fixed in Bouin's solution or 4% (w/v) paraformaldehyde for 6 - 24 hrs to prevent alterations in the cellular structure. The dehydration process was accomplished by passing the tissues through a series of increasing alcohol concentrations, i.e. 70%, 80%, 90%, 96%, 100% ethanol for 1 hr at RT and isopropanol overnight. The alcohol was removed from the tissues by incubation in 25%, 50%, 75% and 100% xylene. Tissues were then incubated in paraffin at 60°C for 12-24 hrs. The paraffin was changed at least three times. Finally, tissue was placed in embedding mold and melted paraffin was poured into the mold to form a block. The paraffin block was cooled at 4°C.

2.2.13.2 Sections of the paraffin block

Paraffin blocks were clamped into the microtome (Hn 40 Ing., Nut hole, Germany). The thickness of the sections was 5-7 µm. The sections were floated on 40°C water to allow actual spread. Then, they were put onto slides. After complete drying at 37°C, slides were stored at 4°C for further analysis.

2.2.13.3 Immunofluorescence staining

Tissue cross sections were incubated twice for 10 min in xylene to remove the paraffin. Then, they were rehydrated by descending ethanol concentrations. For immunofluorescence staining, sections were placed into a plastic staining dish containing the antigen retrieval buffer. This plastic staining dish was placed into boiling water bath for 15 min and then placed in ice for 10 min. Then slides were incubated with a blocking solution containing 10% goat or sheep serum in 0.02% Tween-20 in PBS for 2 hrs at RT. Slides were then incubated with primary antibodies for overnight in a humidified chamber at 4°C. Subsequently, they were rinsed three times for 5 min in PBS and incubated with secondary antibody for 1 hr. Finally, the slides were washed three times for 5 min in PBS and the nuclei were counterstained with DAPI. Immunostaining of the sections was examined using a fluorescence equipped microscope (BX60; Olympus). When alkaline phosphatase secondary antibody was used, immunostaining was detected by adding alkaline phosphatase substrate (Fast Red TR/Naphthol AS-MX[®], Sigma) to the sections for 15 min. To stop the reaction, the slides were immersed in Copling jars filled with distilled water, slides were then covered with Aqua-Poly-Mount.

Antigen retrieval buffer:

Sodium Citrate Buffer (10mM Sodium Citrate, 0.05% Tween 20, pH 6.0)

2.2.13.4 Immunocytochemical staining of germ cell suspension

Germ cell suspension was prepared from mouse testes by using the collagenase/trypsin method according to published procedure (Romrell *et al.*, 1976). Testes from 60 days old mice were collected in serum-free culture medium, rinsed in 0.1 M PBS, pH 7.2. After removal of the tunica albuginea, seminiferous tubules were enzymatically dissociated by the addition of 1ml collagenase (1mg/ml). The slurry maintained at 37°C for 30 min was triturated every 5 min. 5 ml of Hank's solution was added and then spun at 500 xg to sediment the dissociated cells. The pellet was resuspended in 3 ml trypsin, incubated for 5 min and then trypsin (0.5 mg/ml) was inactivated by adding 2 ml FKS. The slurry was passed through 80µm nylon mesh. The filtrate was spun at 500 xg to sediment the cells. Cells were resuspended in PBS and spread onto superfrost slides, air-dried and fixed in 4% PFA for 10 min at RT. Next, they were washed twice in PBS and immunostained as described above (2.2.13.3).

2.2.13.5 Hematoxylin-eosin (H&E) staining of histological sections

Histological sections were incubated three times in xylene for 3 min each, followed by incubation in 100% for 3 min, 95% and 80% ethanol for 2 min each. Slides were then washed in dH₂O for 5 min and stained for 3 min in hematoxylin. The staining was followed by rinsing with deionised water and washing in tap water for 10 min. Slides were dipped in acid ethanol (1ml concentrated HCl in 400 ml 70% ethanol) for 8-12 times to destain, then in ammonium water (0,25%), rinsed in tap water for 2 min and in deionised water for 2 min. Thereafter slides were stained with eosin (0.1% + 2% acetic acid) for 1 min, then in dH₂O for 1 min and incubated in 50%, 70%, 80%, 90%, 96% and 100% ethanol for 2 min in each. Finally they were incubated two times in histoclear (Xylol) for 5 min and mounted with Eukitt-quick hardening mounting medium.

2.2.13.6 Apoptosis detection

The slides containing the thin (5 µm) sections of testis were processed for a TUNEL assay to assess the possible number of cells undergoing apoptosis by an ApopTag detection kit. The sections were firstly deparafinized, hydrated and washed 2 x 5 min in PBS. Slides

were then incubated for 15 min at RT in 20 µg/ml Proteinase K and washed 2 x 2 min in dH₂O. To block endogenous peroxidase, tissues were incubated in 3 % H₂O₂ for 5 min at RT. After 2 x 5 min washing in PBS, the tissues were covered for 10 sec with equilibration buffer. Slides were incubated with Working Strength TdT Enzyme (30% enzyme in reaction buffer) for 1 hr at 37°C in darkness. Slides were incubated for 10 min shaking at RT in Stop/Wash buffer (1:34 in dH₂O) , washed 3 x 1 min with PBS. Thereafter, slides were incubated with anti-digoxigenin for 30 min at RT in darkness and then washed 4 x 2 min with PBS. Slides were stained with Working Strength Peroxidase Substrate (2% DAB Substrate in DAB Dilution buffer) for 6 min at RT, washed 3 x 1 min and 1 x 5 min with dH₂O. Finally, slides were covered by AquaPolyMount liquid. . The percentage of cell death was determined by counting the cells exhibiting brown nuclei (TUNEL-positive) and compared with cells from wildtype littermate.

2.2.14 Masson's Trichrome staining

Masson's Trichrome stain identifies nuclei in black, cytoplasm , keratin and muscle fibers in red, and collagen, mucin in blue. Trichome stains are used primarily for distinguishing collagen from muscle tissue. Accustain trichome stains (Masson) from Sigma-Aldrich was used. Heart and skeletal muscle sections were stained with Masson's Trichrome stain to identify any fibrotic areas. Briefly , slides were deparaffinized and rehydrated before placing in Bouin's fixative overnight at RT. Slides were placed in Working Weigert's Iron Hematoxylin solution for 5 min , rinsed in running tap water for 10 min , placed in Beibrich scarlet-acid fuchsin solution for 5 min and then rinsed until clear. Next, slides were immersed in phosphomolybdic-phosphotungstic acid solution for 5 min , followed by aniline blue solution for 5 min, rinsed and then placed in 1% acetic water for 2 min. Finally, rinsed slides were dehydrated and protected with Eukitt-quick hardening mounting medium.

2.2.15 Tissue preparation for electron microscopy

The left ventricle of freshly isolated heart was cut in small pieces and treated with fixation solution for 8-12 hrs in 4°C. Tissues were then washed in washing buffer for a few hours and sent to Dr. C. Mühlfed (Department of Anatomy and Cell Biology, University of Giessen), who did the electron microscopy analysis.

Fixation solution: 1% Paraformaldehyde

3% Glutaraldehyde

In 0.1 M Cacodylat buffer, pH 7.4

Washing solution 3.4 % Saccharose

in 0.1 M Cacodylat buffer, pH 7.4

2.2.16 Echocardiogram

Echocardiographic assessments were done in collaboration with Prof. Dr. Maier, Departement of Cardiology and Pneumology, Göttingen University. Echocardiography was performed on a Toshiba Power Vision 6000 system with a 15-MHz ultrasound probe under general anesthesia with tribromoethanol/amylyene hydrate (Avertin; 2.5% wt/vol, 6 μ L/g body weight i.p.) under spontaneous respiration (Natalie. *et al.*, 2007).

2.2.17 Microarray analysis

Microarray analysis was performed at the Göttingen Transcriptome Analysis Laboratory, Medical Faculty, University of Göttingen . RNA was isolated from heart as described in 2.2.1.3. 0.3 μ g of total RNA were used as a starting material to prepare cDNA. The synthesis of double-stranded cDNA was done with the WT Target Labeling and Control Reagents (Affymetrix; Cat. N° 900652). The cleanup of double-stranded cDNA was done using the GeneChip® Sample Cleanup module (Affymetrix). The in-vitro transcription was conducted with the WT Target Labeling Kit (Affymetrix). The total amount of the reaction product was purified with the GeneChip® cRNA Samle Cleanup Module (Affymetrix) and quantified using the NanoDrop ND-1000. A cDNA synthesis (ss) were performed using the WT Target Labeling Kit (Affymetrix). 5.5 μ g of ssDNA were cleaved into fragments of 35-200 bases by enzymatic processes. The degree of fragmentation and the length distribution of the ssDNA were checked by capillary electrophoresis using the Agilent 2100 Bioanalyzer. A terminal labeling reaction (Biotin) was performed after fragmentation using the WT Labeling Kit (Affymetrix; Cat. N° 900652). Biotinylated fragmented ssDNA was hybridized onto the GeneChip® Mouse Gene 1.0 ST Array (Affymetrix; Cat. N°901171) according to the manufacturer's recommendation. The hybridization were performed for 16 hrs at 60 rpm and 45°C in the GeneChip® Hybridization Oven 640 (Affymetrix). Washing and staining of the arrays were done on the Gene Chip® Fluidics Station 450 (Affymetrix) according to the manufacturers recommendation. The antibody signal amplification, washing and staining protocol were used to stain the arrays with streptavidin R-phycoerythrin (SAPE; Invitrogen, USA). To amplify staining, SAPE solution were added twice with a biotinylated anti-

streptavidin antibody (Vector Laboratories, CA) staining step in between. Arrays were scanned using the GeneChip® Scanner 30007G.

2.2.18 Computer analysis

For the analysis of the nucleotide sequences, programs like BLAST, BLAST2, MEGABLAST and other programs from National Center for Biotechnology Information (NCBI) were used (www.ncbi.nlm.nih.gov). For protein studies ExPASy tools (www.expasy.ch) were used. Mouse genome sequence and other analysis on mouse genes, transcripts and putative proteins were done in Ensembl database (www.ensembl.org).

3. Results

3.1 Analysis of *Hspa4*- deficient mice on the hybrid C57BL/6J x 129/SV genetic background

Analysis of *Hspa4*-deficient mice in hybrid C57BL/6J x 129/SV genetic background showed that male infertility is the most apparent phenotype. However, the fertility was heterogeneous in male. Thus, 8 of 13 male mutants did not produce a single litter, whereas the remaining 5 males produced litter size similar to that of wild type males. Histological analysis of testes from adult *Hspa4*- deficient mice revealed that the disruption of spermatogenesis is the main cause of male infertility (Held, 2008).

3.1.1 Impaired progression of the first wave of spermatogenesis in juvenile *Hspa4*-deficient mice

To identify the spermatogenic stage at which spermatogenesis is affected by *Hspa4*-deficiency, testicular sections from different postnatal days (P5, P10, P15, P20 and P25) were stained with hematoxylin and eosin. Histological analysis of 5-day-old *Hspa4*^{-/-} testis showed normally developed Sertoli cells and gonocytes at the basement membrane of seminiferous tubules (Fig. 3.1A, B). In wild-type testis, at postnatal day 10 spermatogonia proliferate and develop to primary spermatocytes. No apparent differences were found in histological structure of seminiferous tubules between wild type and mutant mice at postnatal days 5 and 10 (Fig.3.1A-D). These results suggest that the proliferation and differentiation of spermatogonia to primary spermatocytes did not require *Hspa4*, despite the high expression of *Hspa4* in gonocytes (Held, 2008). At postnatal day 15, when spermatogenesis progresses to mid-and late pachytene spermatocytes in wild-type testis (Fig. 3.2A), the number of pachytene spermatocytes was found to be drastically reduced in *Hspa4*-deficient testes (Fig. 3.2B). By postnatal day 20, spermatogenesis has reached the stage of round spermatids in wild-type tubules (Fig.3.2C). In contrast, mutant tubules are almost completely devoid of round spermatids and contain a reduced number of pachytene spermatocytes (Fig. 3.2D). At day 25, when tubules of wild-type littermates showed elongated spermatids as most advanced germ cells (Fig. 3.2E), *Hspa4*^{-/-} testis showed severe depletion of germ cells. Very few seminiferous tubules contained round spermatids as most advanced germ cells in *Hspa4*-deficient testes (Fig. 3.2 F).

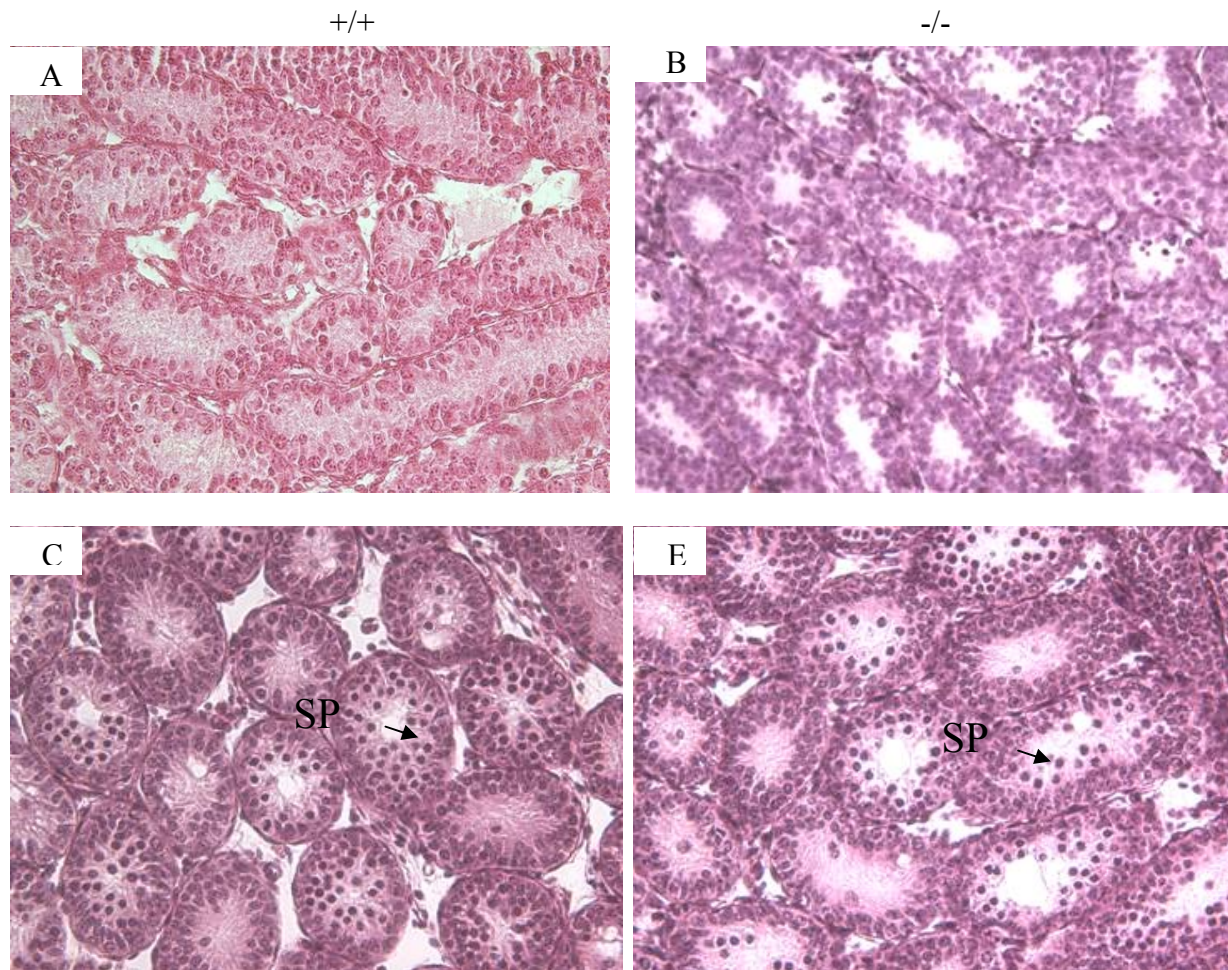


Fig.3.1. Histological analysis of testes from 5- and 10- day-old wild type (+/+) and *Hspa4*-deficient mice (-/-) reveals normal histological structure of seminiferous tubules. (A, B) 5-day-old testis (C, D) 10-day- old testis. Sp –primary spermatocytes... Photos were taken in 20 x magnification.

These results suggest that spermatogenesis in *Hspa4*^{-/-} testis is arrested at first meiotic prophase.

3.1.2 Immunohistochemical analysis of *Hspa4*^{-/-} testes

To confirm the results of histological analysis, we performed immunohistochemical analysis using different germ cell markers. Using the anti-heat shock protein 110 (HSPH1) antibody to label gonocytes (Held, 2008), the *Hspa4*^{+/+} and *Hspa4*^{-/-} tubules contained an equivalent number of gonocytes (Fig. 3.3A-C), suggesting that the *Hspa4* deficiency does not

impair the gonocytes. Using anti-germ cell nuclear antigen 1 (GCNA) antibody, which recognizes the spermatogonia and primary spermatocytes (Enders and May, 1994), the number of spermatogonia per tubule was not significantly different between 5-day-old wild-type and mutant testis (Fig. 3.3D-F). This result suggests that the differentiation of gonocytes to spermatogonia is not affected in 5-day-old *Hspa4*^{-/-} testis. In wild type testis, at postnatal day 10 spermatogonia underwent mitotic division and differentiate to spermatocytes. The mean number of GCNA1-positive germ cells in mutant and wild-type tubules was not significantly different at postnatal day 10, suggesting that mitotic division in mutant testes is not affected (Fig. 3.3G-I). However, few seminiferous tubules of *Hspa4*^{-/-} testes lacked meiotic germ cells (pachytene spermatocytes) at postnatal day 15. By immunohistological staining for heat shock protein 4-like (HSPA4L) protein, which is highly expressed in pachytene spermatocytes (Held *et al.*, 2006), a reduction was observed in the mean number of HSPA4L-immunopositive cells per tubule in testis of *Hspa4*^{-/-} mice compared to wild-type mice (Fig.3.4A-C). Such reduction of HSPA4L-immunopositive cells was also observed in 20-day-old *Hspa4*^{-/-} testis (Fig. 3.4D-H). To prove whether the arrest of meiotic division is due to defects in pairing of homologous chromosomes during prophase I, we examined chromosomal synapses in *Hspa4*^{-/-} spermatocytes. Germ cell suspension was prepared from adult wild-type and mutant testes, spread on slides, fixed with paraformaldehyde and immunostained with an antibody against synaptonemal complex protein 3 (SYCP3). The SYCP3 is a part of the synaptonemal complex between synapsed chromosomes during pachytene and remains on the disynapsed axis during diplotene. Analysis of germ cell spreads revealed that the formation of synaptonemal complexes in the meiotic cells of mutant testis was indistinguishable from that in wild-type. This indicates the proper accumulation of the synaptonemal complex protein SYCP3 (Fig. 3.5A-F).

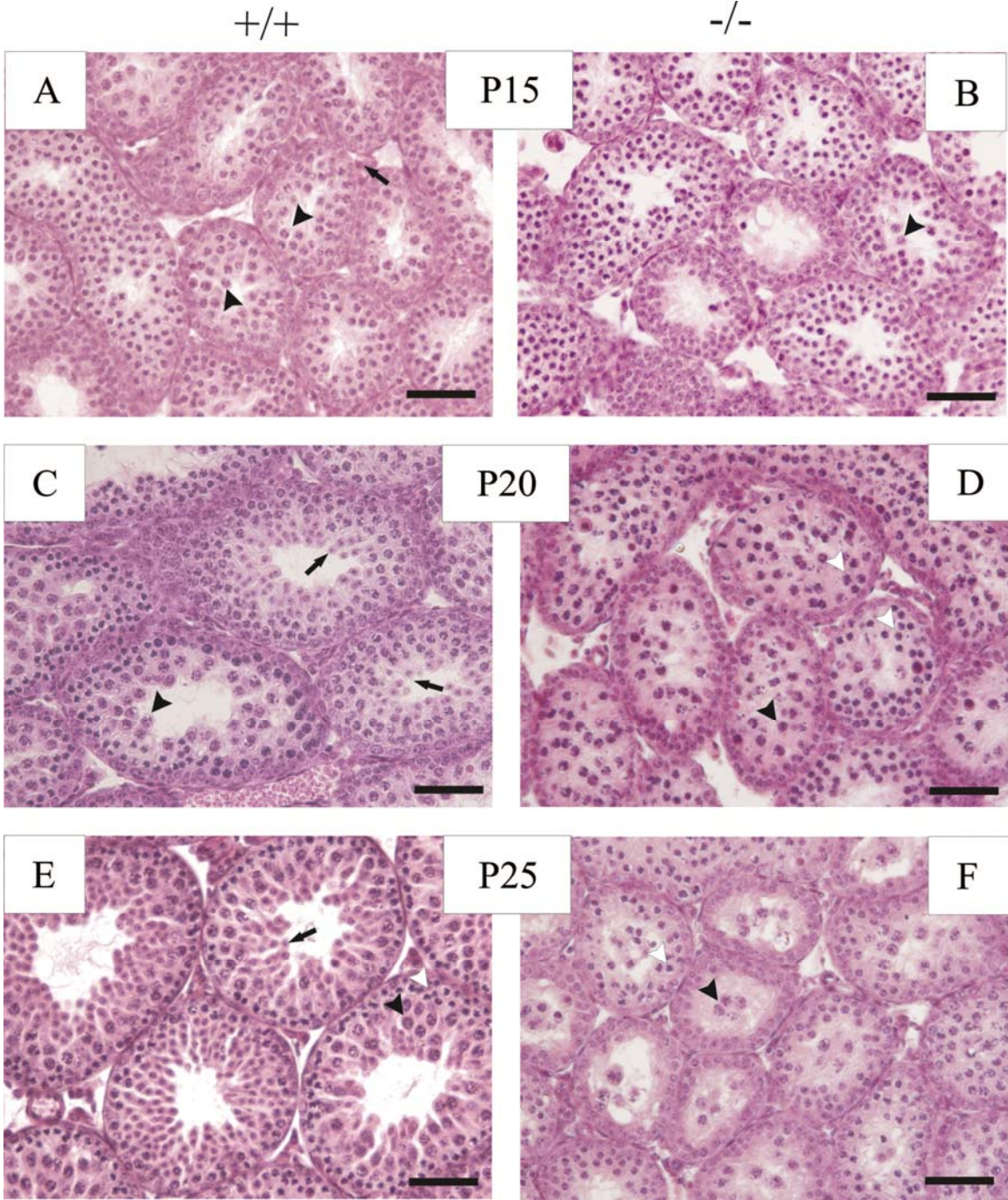


Fig. 3.2. Delayed and disrupted first wave of spermatogenesis in *Hspa4* mutant mice. Testicular sections from wild-type and *Hspa4*-null mice of various postnatal days (P) were stained with H&E. At P15, spermatogenesis has progressed up to pachytene spermatocyte stage (black

arrowhead) in wild-type mice (A), whereas very few pachytene spermatocytes are present in testes of mutant mice (B). At P20, spermatogenesis reached the stage of round spermatids (arrow) in wild-type mice (C), whereas germ cell development in *Hspa4*-null mice is mostly impaired, seminiferous tubules are filled with premeiotic germ cells (white arrowhead) and contain very few pachytene spermatocytes. At P25, spermatogenesis is progressed to stages of round and elongated spermatids in wild-type tubules (E). In contrast, meiotic germ cells are sloughing off and vacuolization is visible in seminiferous tubules of *Hspa4*^{-/-} mice (F). Scale bar, 50 μ m.

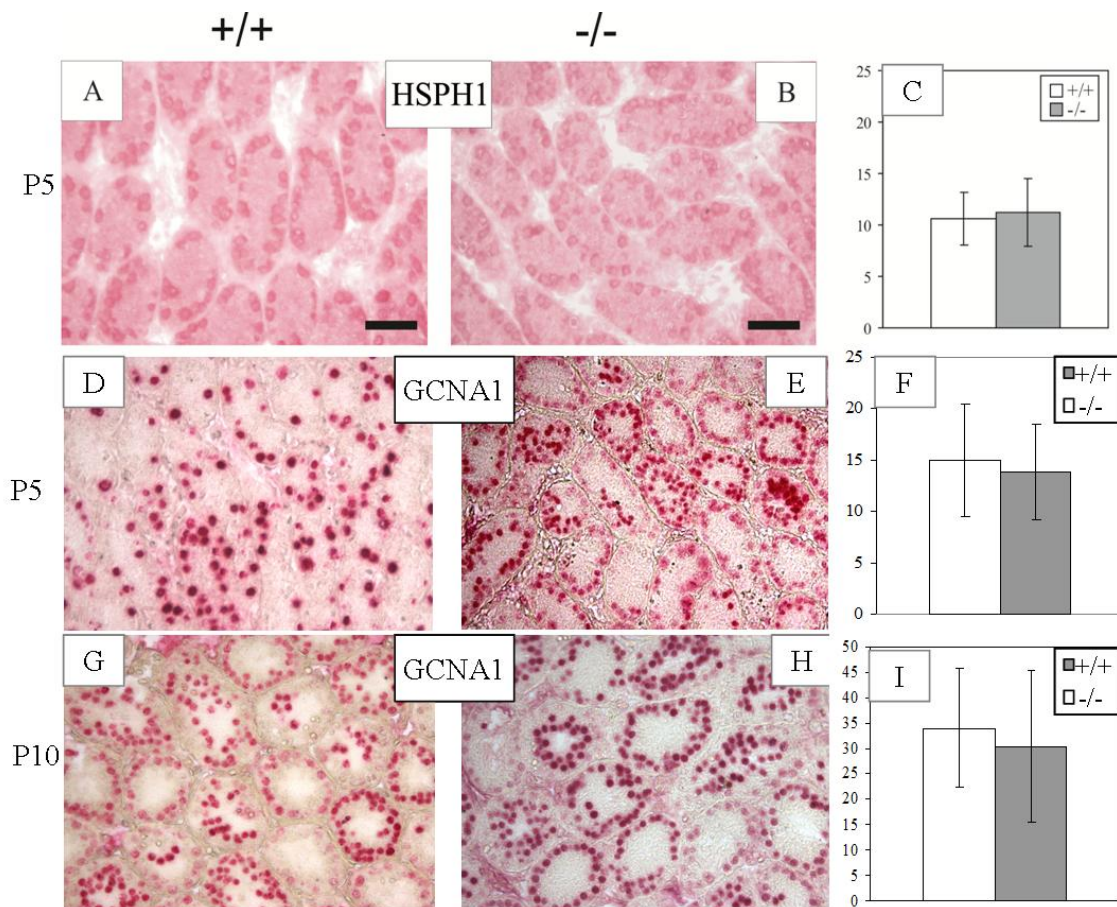


Fig. 3. Expression profile of premeiotic and meiotic markers in *Hspa4*^{+/+} and *Hspa4*^{-/-} testes. Histological sections of wild-type (A, D and G) and null-mice (B, E, I) at different postnatal days (P5 and P10) were immunostained with HSPH1 (A, B) and GCNA1 (D, E, G, H) antibodies. No significant difference is observed in the mean number of HSPH1- (C) and GCNA1-positive cell at P5 (F) and P10 (I) per tubule between wild-type and mutant testes. Scale bar, 50 μ m.

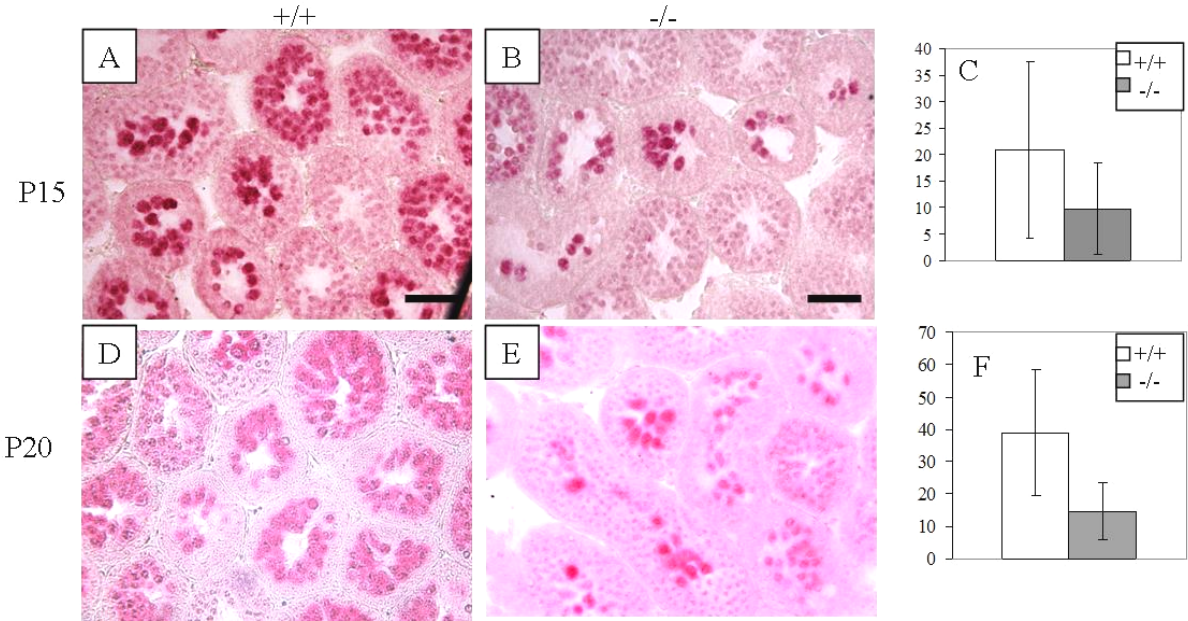


Fig. 3.4. Expression of HSPA4L in *Hspa4*^{+/+} and *Hspa4*^{-/-} testes. Histological sections of wild-type (A, B) and null-mice (D, E) at different postnatal days (P15 and P20) were immunostained with HSPA4L antibody. A significant reduction in the mean number of HSPA4L-positive cells per tubule was found in *Hspa4*^{-/-} testes at days 15 (C) and 20 (F). Scale bar, 50 μ m.

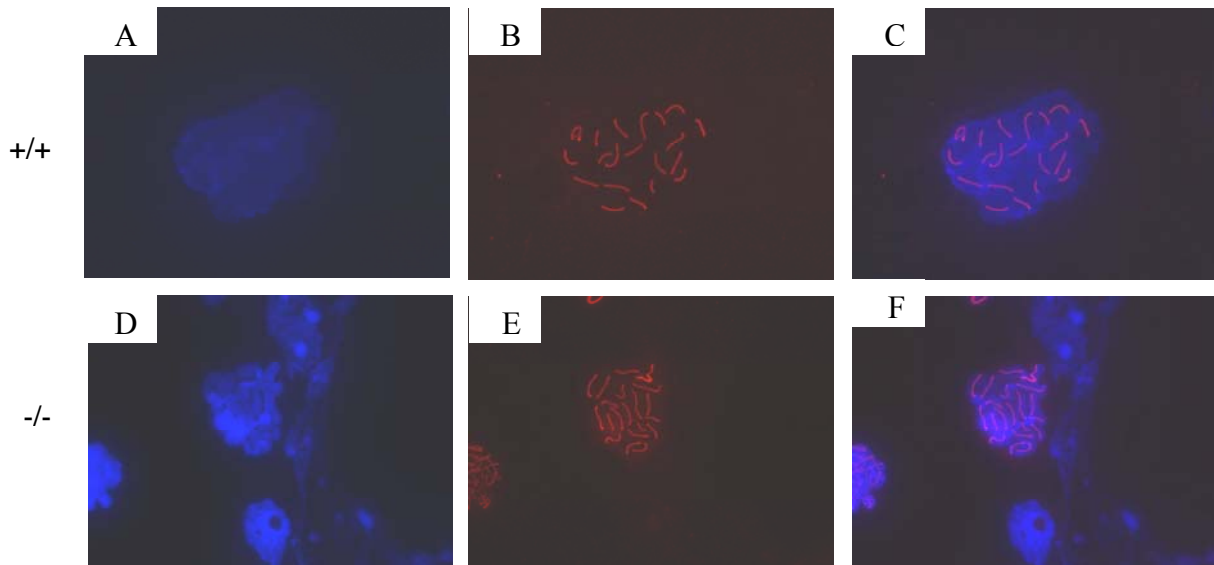


Fig. 3.5 . Immunofluorescent localization of SYCP3 on synaptonemal complexes of wild-type (A-C) and *Hspa4*-deficient (D-L) pachytene spermatocytes . Representative sections were obtained from 5-month old *Hspa4*^{-/-} and WT. Cells stained with anti-SYCP3 (Red) and DAPI (blue). 60 fold magnification.

3.1.3 Increase of apoptotic germ cells in *Hspa4*^{-/-} testes

To determine whether the observed absence of differentiated germ cells is the result of enhanced apoptosis in *Hspa4*-null mice, TUNEL assay was performed to identify apoptotic cells during first wave of spermatogenesis in testes of postnatal day 10, 15, 20 and 25 (Fig. 3.6A-H). There are no significant differences in the number of apoptotic cells between *Hspa4*^{-/-} and *Hspa4*^{+/+} testes at P10 (Fig. 3.6A, B and Fig. 3.7). A significant increase of TUNEL-positive spermatocytes was found in *Hspa4*-null mice at P15, 20 and 25 (Fig.3.6 D- H and Fig. 3.7). The frequency of TUNEL-positive cells was variable among tubules, but overall there were significantly more apoptotic cells in the seminiferous tubules of infertile *Hspa4*^{-/-} mice than in those of their wild-type littermates.

Most of TUNEL -positive cells were seen to be in meiotic prophase (Fig.3.6 D- H). These results indicate that germ cells at meiotic stages appear to be the most affected cells in *Hspa4*-deficient testes.

3.1.4 Expression analysis of germ cell marker genes in *Hspa4*-deficient testes

To further identify the spermatogenic stage at which spermatogenesis is impaired in adult *Hspa4*-null mice, we analysed the expression of different meiotic and postmeiotic marker genes. Testicular RNA was isolated from 5-month old wild type, fertile and infertile *Hspa4*^{-/-} mice, and probed subsequently with a cDNA probe for Sycp3, Pkg2, Acr, Hsc70t and Tnp2 genes. The amount of loaded RNA used in this experiment were proved by rehybridization of blots with a cDNA probe for β -actin (Fig. 3.8A). Expression of Sycp3 gene encoding synaptonemal complex protein-3, which is exclusively expressed in leptotene and zygotene spermatocytes, revealed that the expression levels of Sycp3 in testes of fertile and infertile *Hspa4*^{-/-} mice are similar with that in wild-type testes. In contrast, expression of testis-specific phosphoglycerate kinase gene (Pkg2) and acrosin (Acr), which were reported to peak in pachytene spermatocytes, was significantly reduced in testes of infertile *Hspa4*-null mice. Similar results were also shown for the transcript level of postmeiotic-specific genes *Hsc70t* (*Hsp70* homolog gene) and *Tnp2* (transition nuclear protein 2). These results confirm that the spermatogenic arrest in *Hspa4*-deficient mice occurred late in meiotic prophase I.

3.1.5 Expression analysis of other members of HSP110 family in *Hspa4*^{-/-} testis

The leaky phenotype in spermatogenesis of *Hspa4*-null mice may be due compensation by overexpression of other members of HSP110 family. Therefore, we analysed the expression of HSPA4L and HSPH1 in testes of fertile *Hspa4*^{-/-} mice (Fig. 3.8B). Western blot analysis did not reveal a marked increase in the expression of HSPA4L and HSPH1 in testes of *Hspa4*-null mice. These results suggest that the deficient of HSPA4 expression in the testes is not compensate for by increased expression of other cytolc proteins of HSP110 family.

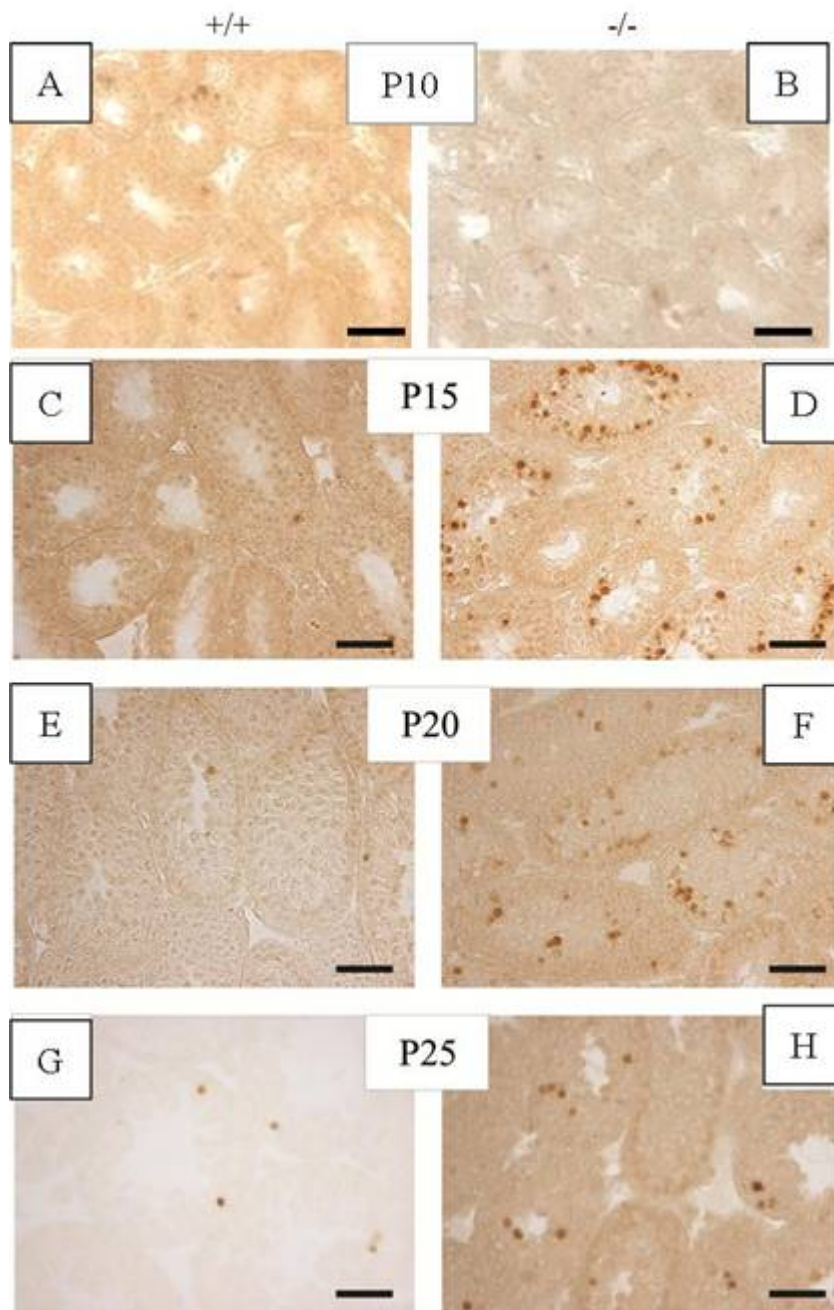


Fig. 3.6. Enhanced apoptosis during germ cell differentiation of *Hspa4*-null mice. Histological sections of *Hspa4*^{+/+} (A, B, E and G) and *Hspa4*^{-/-} mice (B, D, F and H) at different postnatal days (P) were subjected to TUNEL staining. The proportion of TUNEL-stained apoptotic cells (brown nuclei) at P15, P20 and P25 is higher in testes of *Hspa4*-deficient than in testes of wild-type

mice. Apoptotic germ cells are mainly pachytene spermatocytes as indicated by their nuclear size and their position in the seminiferous tubules. Scale bar, 50 μ m.

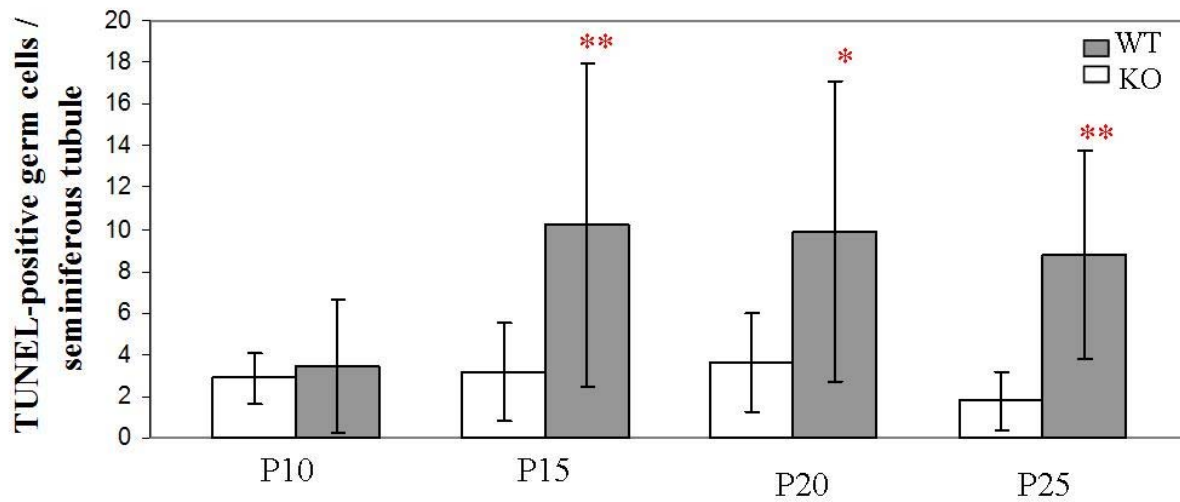


Fig.3. 7. Quantification of TUNEL –positive germ cells in *Hspa4*- deficient mice and wild type mice at different postnatal days(P10, P15, P20 and P25) . Mean (\pm SEM) number of apoptotic germ cells per seminiferous tubule. WT, Wild –type; KO, *Hspa4a*-deficient mice; *, $p < 0.05$; **, $p < 0.001$.

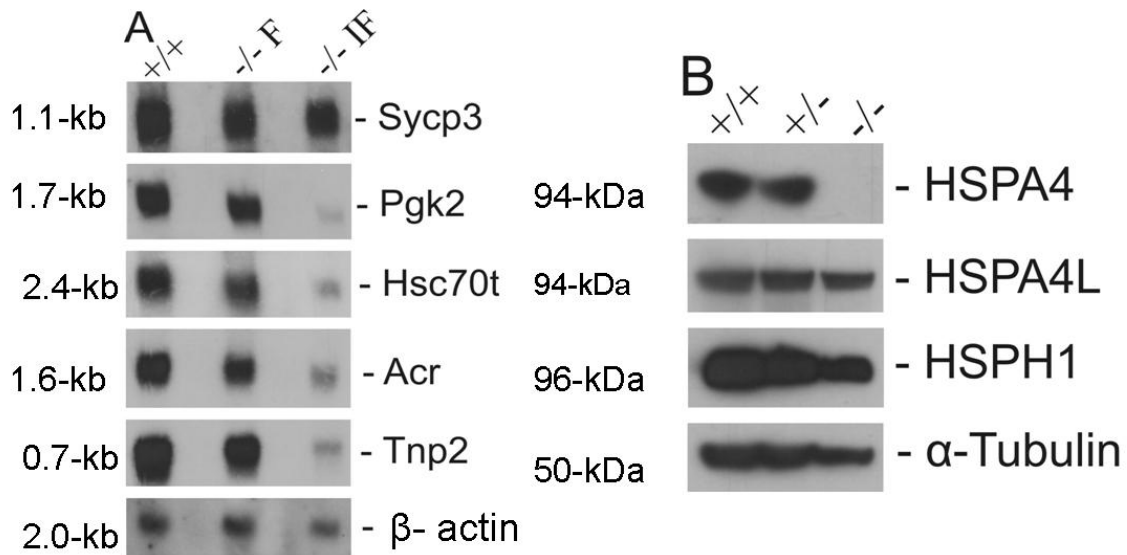


Fig. 3.8. Expression profile of different germ cell markers and members of HSP110 family in $Hspa4^{-/-}$ testes. (A) Northern blot with total RNA from testes of $Hspa4^{+/+}$ (+/+), fertile (-/-F) and infertile $Hspa4^{-/-}$ (-/-IF) mice was sequentially hybridized with cDNA probes for the indicated genes. (B) Expression pattern of other members of the HSP110 family in testes of wild-type and $Hspa4$ -null mice. Immunoblots were probed with the antibodies against proteins shown at the right margin.

3.2 *Hspa4*-deficient mice with the inbred 129/Sv genetic background display postnatal growth retardation

In contrast to the *Hspa4* deficiency in the hybrid C57BL/6J x 129/Sv genetic background, analysis of *Hspa4*-deficient mice with the inbred 129/Sv genetic background revealed that 85% of *Hspa4*-deficient mice display growth retardation and 94,1% of newborn animals died between the third and fourth week after birth (Held, 2008). The cause of postnatal growth retardation shown in *Hspa4*-deficient mice could be due either to:

- 1- Metabolic failure or malabsorption of nutrients in the intestine
- 2- Defect in growth hormone (GH)-signaling
- 3- Increased degeneration of skeletal muscle and/or failure in muscle regeneration

Several experiments are performed to differentiate between these possible causes.

3.2.1 Metabolic state in *Hspa4*-deficient mice

3.2.1.1 Measurement of glucose levels in sera of *Hspa4*-deficient mice

To determine whether growth retardation in *Hspa4*-deficient mice is due to impaired glucose homeostasis, we have determined the glucose levels in serum of 10-, 15-, (22-28) and 60-day-old wild-type and mutant mice. The presence of milk food in the stomach of mutant neonatal animals was also monitored. Blood glucose concentrations in 10-, 15- and 20-day-old *Hspa4*^{-/-} mice were significantly lower than in control littermates (Fig. 3.9). Dissection of mutants at these postnatal stages revealed that these mice had milk in their stomach. Although these mutant mice have lower glucose levels, they did not suffer with hypoglycemia, which is characterized by decrease of glucose levels in blood to less than 60 mg/dl. In contrast to their siblings, all the mutant mice (between 22- to 28-day-old) had less or no food in their stomachs and their glucose levels were decreased to 56±17.3 mg/dl (Fig. 3.9). Blood glucose concentrations in adult mutants, which had overcome the neonatal lethality, were not significantly different from those of wild-type. These results suggest that the growth retardation shown in *Hspa4*^{-/-} animals during postnatal life is not due to hypoglycemia. Hypoglycemia found in *Hspa4*^{-/-} animals at age between 22 to 28 days could a result either of fasting or of impairment in glucose homeostasis.

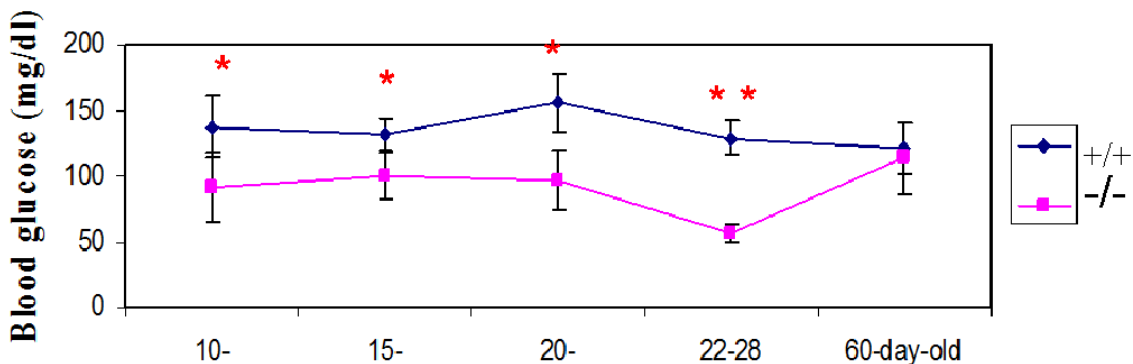


Fig. 3.9. Glucose levels in the blood of *Hspa4*^{-/-} and *Hspa4*^{+/+} mice at different postnatal stages. Blood glucose was determined in the tail veins of 10-, 15-, 20-, (22-28)-, and 60 day-old mice. The glucose levels are significantly lower in *Hspa4*-deficient mice at different postnatal stages. In contrast, adult mutants have normal glucose level. Data are presented as mean \pm SD of at least 4 animals of each age; *, $p < 0.05$, **, $p < 0.001$.

3.2.1.2 Expression of Pepck in liver of fasted *Hspa4*^{-/-} mice

The gluconeogenesis is the main source of liver glucose output upon long term fasting. There are several enzymes which are involved in gluconeogenesis (Irimia, *et al.* 2010). To determine whether the hypoglycemia found in *Hspa4*^{-/-} mice is a result of impaired gluconeogenesis, four mutants and three wild-type mice were fasted for 24 hrs and glucose concentrations in their blood were measured before and after fasting. Total RNA was isolated from the liver of fasting animals and used to determine the expression profile of phosphoenolpyruvate carboxykinase (*Pepck*), which is a key enzyme of gluconeogenesis in liver (Rajas *et al.*, 2000). In contrast to the fed animals, the glucose levels in blood of fasted *Hspa4*^{-/-} mice were significantly lower than in of their control littermates (Fig. 3.10A and B). Northern blot analysis revealed that the expression of *Pepck* is not downregulated in liver of mutant mice (Fig. 3.10C). These results suggest that hypoglycemia showed in fasted *Hspa4*^{-/-} is not due to impaired gluconeogenesis.

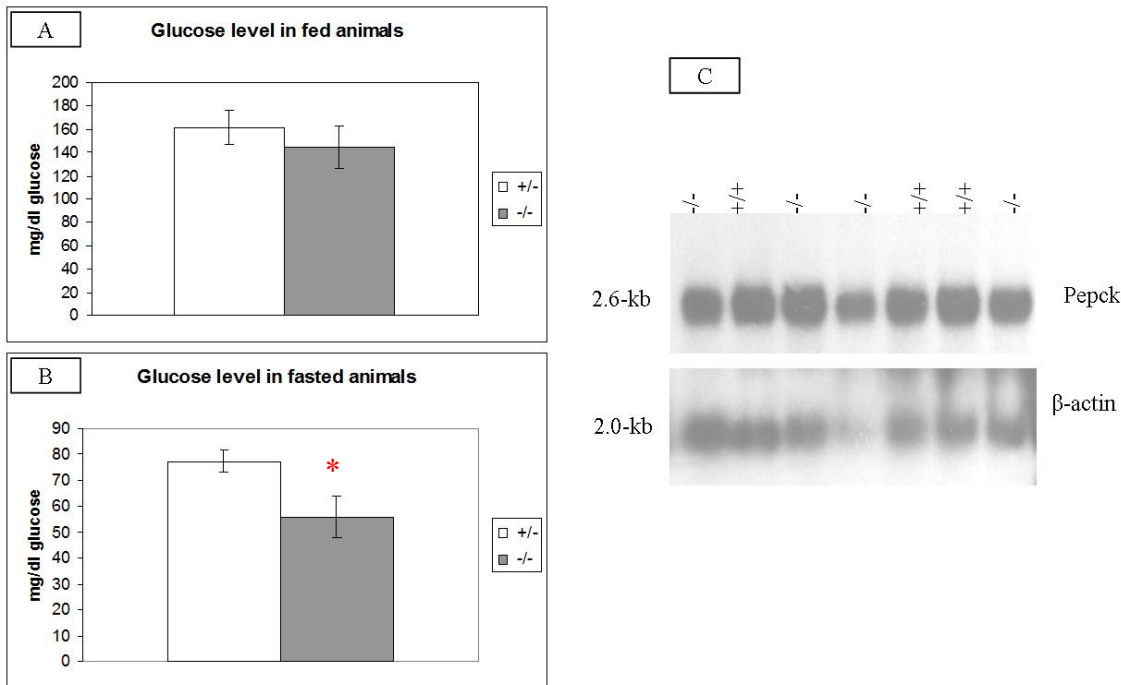


Fig. 3.10. (A, B) Glucose levels were measured in blood of 2-month-old wild-type (n=3) and *Hspa4*^{-/-} (n=4) animals before (A) and after fasting (B). Data are presented as mean \pm SD; *, $p < 0.05$. Northern blot with RNA isolated from liver of these fasted animals was hybridized with a *Pepck* cDNA probe (C). Blot was rehybridized with β -actin to determine the integrity and equal amount of RNA loading (C).

3.2.2 Is growth retardation due to malabsorption of lipids in intestine?

The decrease of glucose levels in blood despite the presence of normal amount of milk and food in stomach of *Hspa4*^{-/-} mice at age 10- to 25-day lead us to determine whether their growth retardation may be a result of malabsorption of lipids in the intestine. In newborn mice, dietary fat is absorbed in intestine, predominantly as triacylglycerol (TG). In the endoplasmic reticulum of enterocytes, the lipoproteins are assembled in chylomicrons, which transport the lipids to peripheral tissues. The assembly of these chylomicrons by intestinal epithelial cells is dependent on the presence of microsomal triglyceride transfer protein (MTP) and apolipoprotein B (ApoB) and apolipoprotein AIV (apoAIV). The B apolipoproteins, apo48 and apoB100, play important structural roles in the formation of lipoproteins in intestine and liver. In the intestine,

the microsomal triglyceride transfer protein (MTT) transfer triglyceride to ApoB and apoAIV proteins (Black, 2007).

3.2.3 Expression analysis of apolipoprotein B and AIV in intestine and liver during postnatal development of *Hspa4*^{-/-} mice

To determine whether the growth retardation in *Hspa4*^{-/-} mice is due to a defect in lipid absorption, expression of apoB and apoAIV was determined in liver and intestine of 10-, 15-, 20- and 25-day-old *Hspa4*^{+/+} and *Hspa4*^{-/-} mice. As shown in figure 11A and B, no difference between wild-type and *Hspa4*^{-/-} mice was found in expression of ApoB in liver and intestine (10- and 15-day-old mice). Similar results were obtained for ApoAIV in intestine of both genotypes at these postnatal stages (Fig. 3.11A, B). Apo AIV is not expressed in liver of 10- and 15-day-old *Hspa4*^{+/+} and *Hspa4*^{-/-} mice. In contrast, overexpression of ApoB was found in liver and intestine of 20- and 25-day-old *Hspa4*^{-/-} mice, compared to that of wild-type. Expression of apoAIV was also found upregulated in *Hspa4*^{-/-} intestine of both ages (Fig. 3.11C, D). At postnatal day 20, expression of Apo AIV was higher in intestine of *Hspa4*^{-/-} than in that of *Hspa4*^{+/+} mice, while no expression of Apo AIV could be detected in 20-day-old liver of both genotypes (Fig. 3.11C). Expression of ApoAIV in liver of 25-day-old *Hspa4*^{-/-} mice was higher than in *Hspa4*^{+/+} liver (Fig. 3.11D). These results revealed that the ApoB gene is upregulated in intestine and liver of *Hspa4*^{-/-} mice at postnatal day 20 and 25-day, while the levels of ApoAIV mRNA are higher in 20- and 25-day-old *Hspa4*^{-/-} mice in intestine.

3.2.4 Growth hormone (GH) signaling is not affected in *Hspa4*^{-/-} mice

It is known that postnatal growth, such as muscle and longitudinal growth, is mediated by growth hormone (GH) signaling. Furthermore, several lines of evidence reveal the crucial role of the hepatic glucocorticoid receptor (GR) to modulate the large set of GH-responsive genes (Tronche *et al.*, 2004; Engblom *et al.*, 2007). To determine whether the growth retardation of *Hspa4*^{-/-} mice is due to defect in GH-signaling, we analyzed the expression of two GH-responsive genes, Amyloid P component (APCS) and solute carrier organic anion transporter family, member 1b2 (SLCO1B2) (Lin *et al.*, 2008), in liver of wild-type and *Hspa4*^{-/-} animals (Fig. 3.12). Northern blots with RNA isolated from 10- and 14-day-old wild-type and *Hspa4*^{-/-} were hybridized with APCS and SLCO1B2 cDNA probe. The results of Northern blot show that

Results

there are no differences in expression of APCS and SLCO1B2 in liver of *Hspa4*^{-/-} and wild-type mice. This result suggested that GH-signaling is not impaired in *Hspa4*- deficient mice.

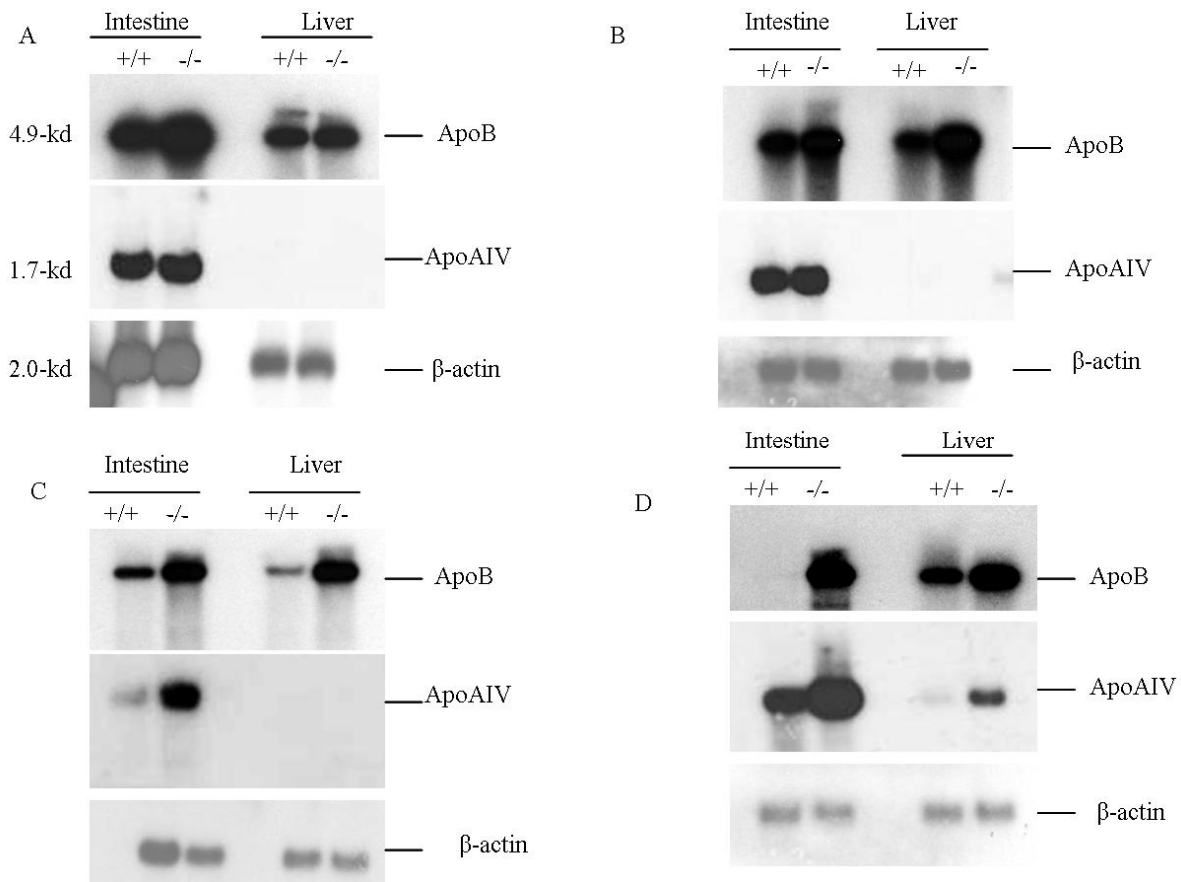


Fig.3.11. Expression analysis of apolipoprotein B (*apoB*) and apolipoprotein A4(*apoAIV*) during the postnatal development of *Hspa4*^{+/+} and *Hspa4*^{-/-} mice . Total RNA was extracted from liver and intestine at different postnatal developmental stages. Northern blots with total RNA from liver and intestine of 10- (A), 15- (B), 20 (C)- and 25- (D) day-old *Hspa4*^{+/+} and *Hspa4*^{-/-} mice were hybridized with *ApoB* and *ApoAIV* cDNA probes. The blots were rehybridized with a mouse β -actin probe to determine the integrity of RNA and amount of RNA loading.

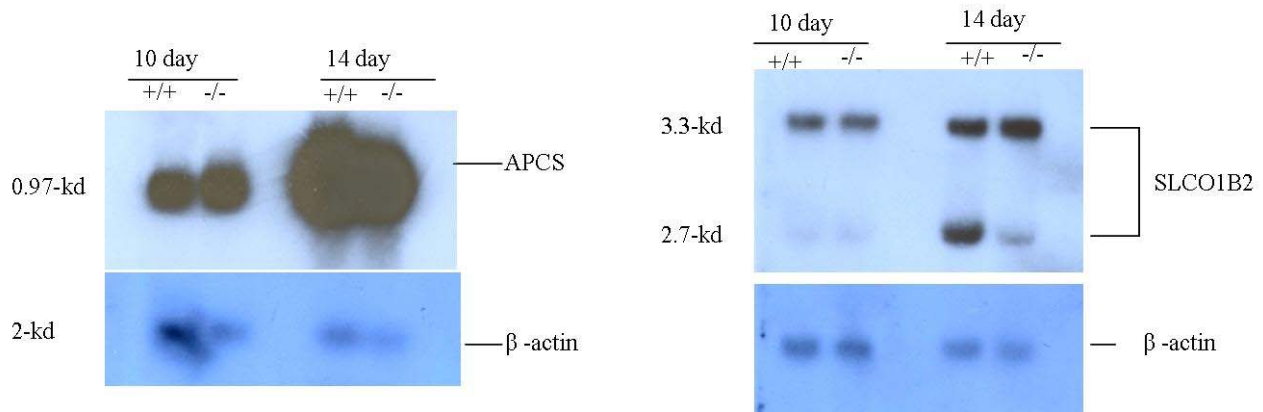


Fig. 3.12. Expression analysis of GH- responsive genes in *Hspa4*-deficient and wild-type liver. Total RNA was extracted from 10- and 14-day-old *Hspa4*^{+/+} and *Hspa4*^{-/-} liver and subjected to Northern blots hybridization using the Amyloid P component (APCS) and the solute carrier organic anion transporter (*SLCO1B2*) cDNA probe, respectively. For RNA quality control Northern blots were rehybridized with mouse β -actin.

3.2.5 Analysis of skeletal muscles of *Hspa4*- deficient mice.

3.2.5.1 Hspa4-deficient mice display skeletal muscle myopathy

The presence of kyphosis in *Hspa4*-deficient mice of advanced age and reduction of skeletal muscle mass in *Hspa4*-deficient mice compared with wild-type lead us to suggest that the skeletal muscle of *Hspa4*^{-/-} mice is affected. In order to determine the effect of *Hspa4* deficiency on skeletal muscle, histological analysis of different skeletal muscles was performed. Tibialis anterior, Vastus intermedius, Soleus and diaphragm muscles were isolated from 4-month-old *Hspa4*-deficient and wild-type mice, fixed in Bouin solution and embedded in paraffin. Analysis of hematoxylin & eosin stained sections of Soleus muscle revealed clear differences between wild-type and *Hspa4*-deficient mice (Fig. 3.13 A-D). Soleus muscle of mutant mice displayed severe myopathic changes. The myopathic changes are characterized by a marked variation in myofibrer size, percentage of muscle fibers with central nuclei, which represent regenerated muscle fibers, and accumulation of nuclei representing necrotic fibers (Fig. 13B and D). Vastius intermedius (Fig.3.13F and H) and Tibialis anterior (Fig 3.13 J and L) also displayed myopathic changes. No myofibers with centrally located nuclei and variation in size of myofibers was detected in the diaphragm muscle of *Hspa4*^{-/-} mice at 4-month of age (data not shown). To determine whether the skeletal muscle myopathy represents the major cause for observed kyphosis in *Hspa4*^{-/-} mice of advancing age, histological analysis of paraspinal muscle of 18-month-old wild type and *Hspa4*^{-/-} mice was performed and an abundant pathology was found (Fig. 3.14A-G). These results suggest that myopathy of the paraspinal muscle is a cause of kyphose development in aging *Hspa4*^{-/-} mice.

3.2.5.2 Skeletal muscle myopathy develops during early postnatal development

The growth retardation of *Hspa4*^{-/-} mice was observed after postnatal day 10. Therefore, histological sections of the Soleus muscle of 13- and 19-day-old wild-type and *Hspa4*^{-/-} mice were analyzed (Fig 3.15A-F). Careful analysis of cross-section areas showed a significant increase in the percentage of myofibers with central nuclei in 13-day-old Soleus muscle of *Hspa4*^{-/-} mice compared to wild-type (Fig.3.15C). The decrease of fiber size and the presence of myofibers with central nuclei are associated with skeletal muscle myopathy (Buj-Bello *et al.*, 2008; Guo *et al.*, 2006; Joya *et al.*, 2004). This result further support that the growth retardation in *Hspa4*^{-/-} mice is a result of myopathy of skeletal muscle. Similar muscle histopathology was

shown with histological sections in the Soleus muscle from 19-day-old *Hspa4*^{-/-} and wild-type mice (Fig. 3.15D-F).

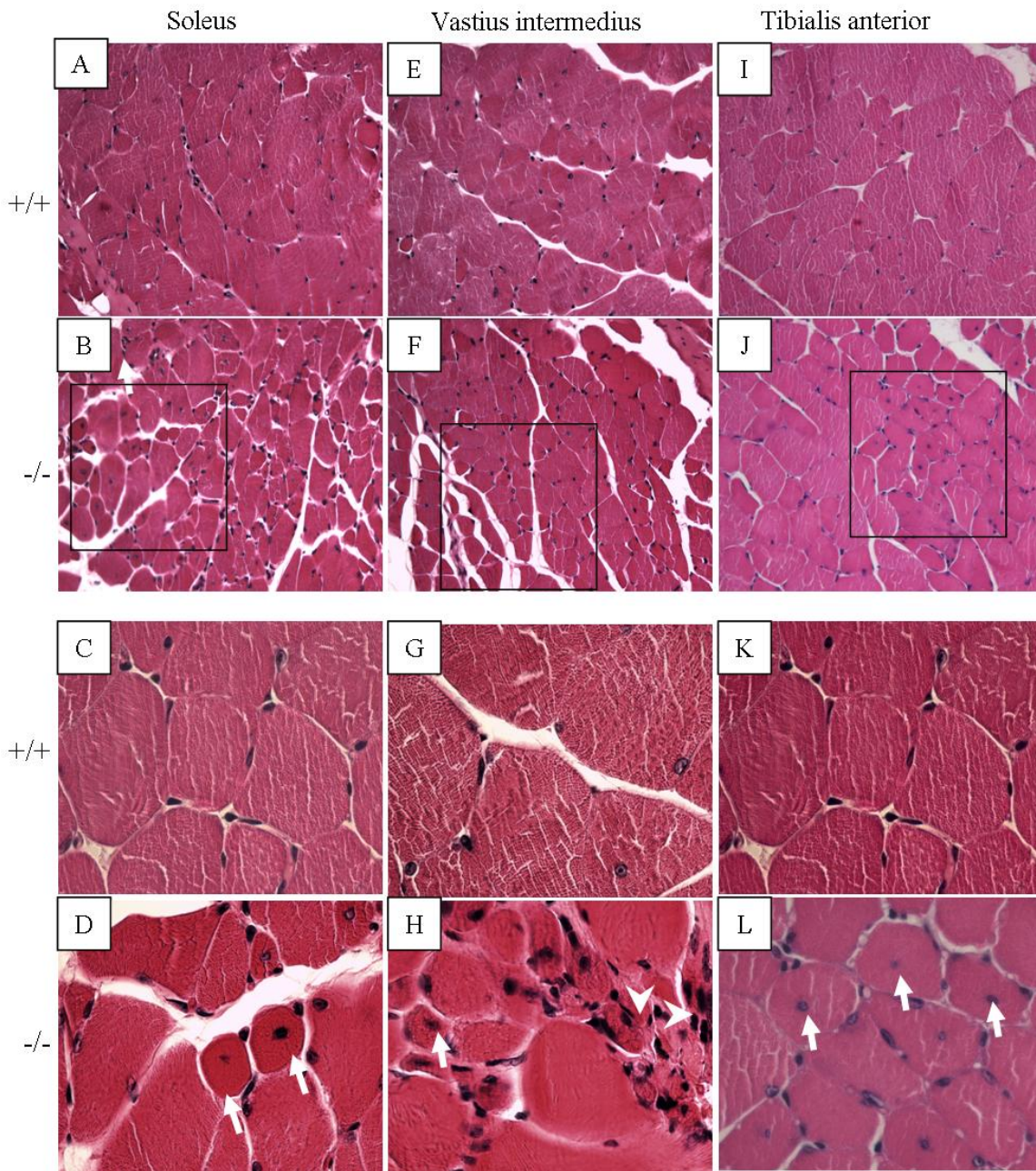


Fig. 3.13 . Histological evidence of myopathy in 4-month-old *Hspa4*^{-/-} mice. Histological sections of a region of Soleus (A-D), Vastus intermedius (E-H) and Tibialis anterior (I-L) muscles of 4-month-old wild-type (+/+) and mutant (-/-) mice. The boxed areas in B, F, J are shown in higher magnification in D, H and L. The white arrows and white head arrows indicate fibers with centrally located nuclei and accumulation of nuclei, respectively. In the boxed area show also the

variation in myofiber size. Sections were photographed at 20x (A, B, E, F, I, J) and at 60x (B box area, C, D, G, H, K, L) magnification.

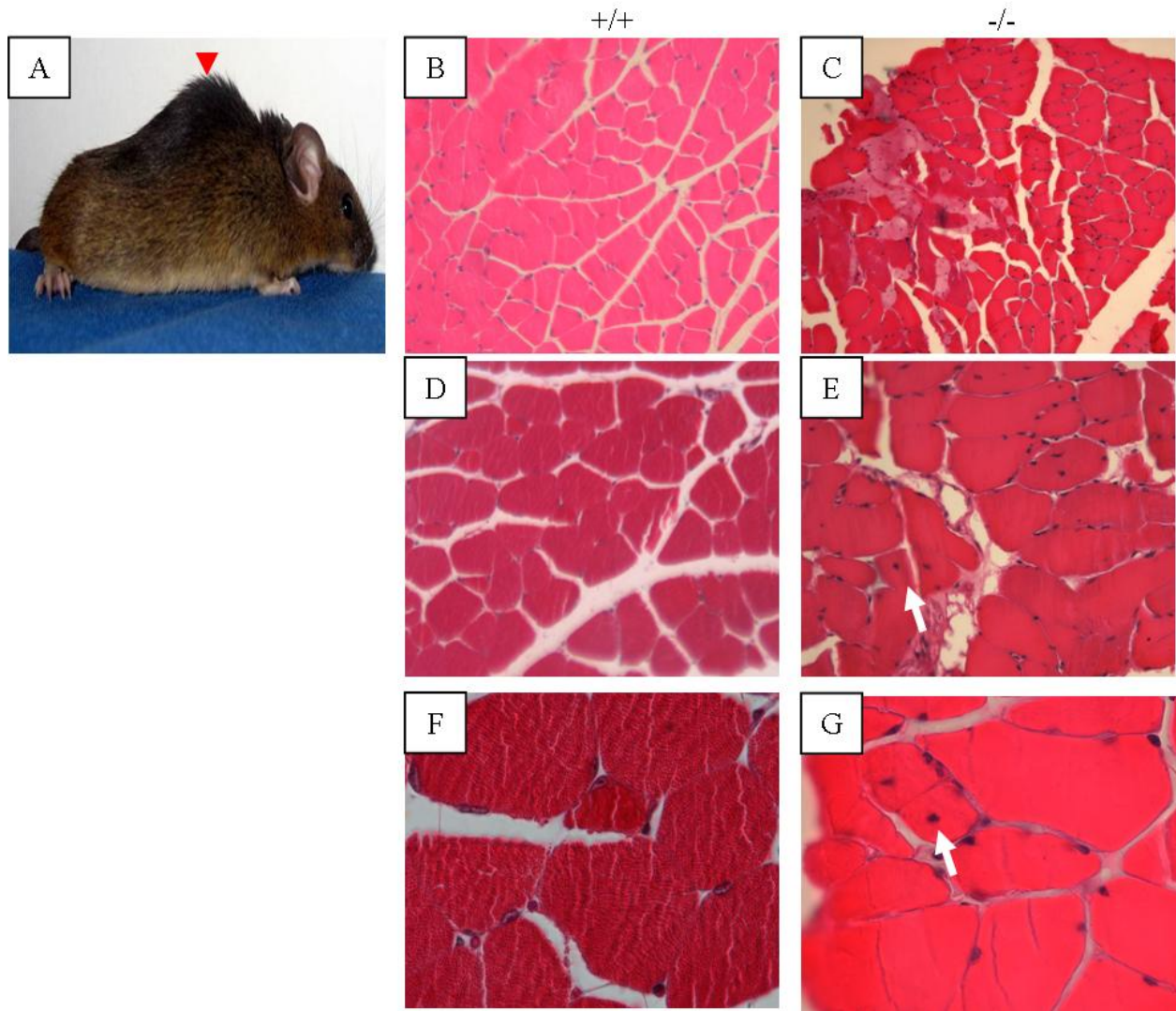


Fig.3.14. Myopathy in the paraspinal muscle is a cause of kyphosis in $Hspa4^{-/-}$ mice. (A) Development of kyphosis in 18-month-old $Hspa4^{-/-}$ mice. H&E-stained section from paraspinal muscle of wild-type (+/+) and mutant mice (-/-) at 18-months of age. Myofibers with central nuclei (white arrows). B, C: 10x magnification; D, E: 20x magnification; F, G: 60 x magnification.

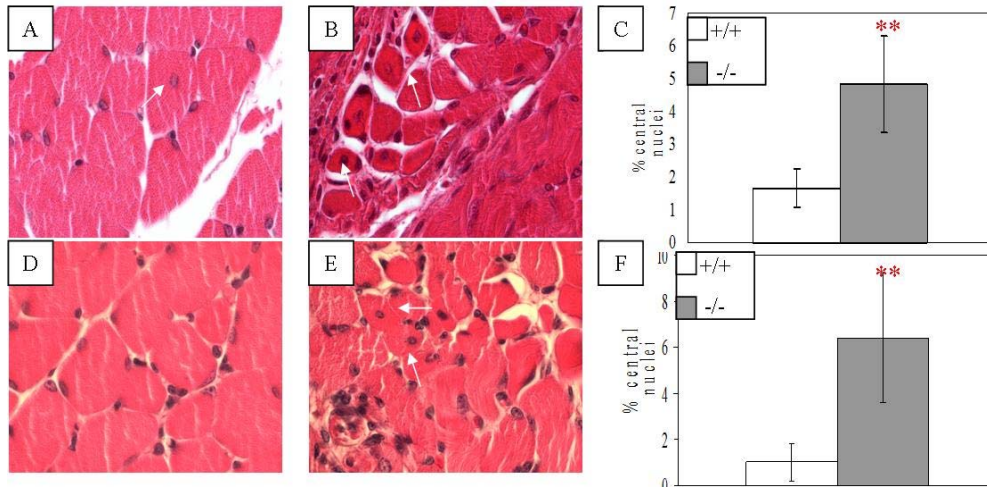


Fig. 3.15. Histological studies of 13- (A-C) and 19-day-old (D-E) muscle in *Hspa4*-mutant (-/-) and wild type (+/+). (B and E) Sections of skeletal muscle from *Hspa4*-mutant mice showed marked increase of myofibers with central nuclei (white arrows) compared to control. Histogram comparing the percentage of fibers with centrally located nuclei in *Soleus* from 13- (C) and 19-day (F) *Hspa4*^{-/-} and wild-type mice. **; $P < 0.05$.

3.2.6 Analysis of the heart in *Hspa4*-deficient mice

3.2.6.1 Development of cardiac hypertrophy in *Hspa4*-deficient mice

To determine whether myopathy of skeletal muscle is also realized in heart as hypertrophic cardiomyopathy, we analyzed hearts from 12-month-old wild-type and *Hspa4*-mutant mice. Heart showed marked enlargement in comparison to that of wild-type control (Fig. 3.16A). Histological examination revealed prominent myocyte degeneration and loss and intracellular vacuoles in cardiomyocytes surrounded by fibrotic tissue (Fig. 3.16B, C). This histopathology are features of sustained hypertrophy. To confirm that loss of myocytes is accompanied by extensive fibrosis, heart sections were stained with Massion's trichome staining. As shown in figure 3.16A and D, the increase of *Hspa4*^{-/-} heart size is consistent with the thickened interventricular septum and ventricular wall and decreased left ventricular cavity size. Significant levels of fibrosis are indicated by accumulation of collagen compared to heart of wild-type mice (Fig. 3.16. E, F). The fibrosis is more severe in septum and left ventricular wall than in right ventricular (Fig. 3.16D). These results reveal that *Hspa4* disruption in the inbred 129/Sv genetic background causes cardiac hypertrophy and fibrosis. To determine the development of cardiac hypertrophy in *Hspa4*^{-/-} mice, histological analysis of hearts and heart weight to body weight ratios (HW/BW) were performed in wild-type and *Hspa4*-mutant mice at different postnatal stages. In animals between 7- to 25-days of age, heart weight to body weight ratios (HW/BW) were not significant different from that of wild-type littermates (Fig. 3.17). In contrast, *Hspa4*^{-/-} mice at 2- and 6- months of age showed a significant increase in HW/BW ratio compared to wild-type littermates (Fig. 3.17). Analysis of cross-sectional cardiomyocyte areas revealed no overt differences in morphology and size of myocytes between wild-type and mutant hearts isolated from mice at age between postnatal days 7 to 25 (Fig. 3.18A-F, 3.19O). Histological sections of hearts from these animals were stained with Massion's trichome staining to detect the extent of fibrosis. As shown in figure 3.16 G-L, the fibrosis is not yet realized in mutant hearts at these postnatal stages. Histological analysis of hearts from 2-3 and 6-month-old mice revealed that the size of left ventricular myocytes was markedly increased in *Hspa4*^{-/-} mice compared with wild-type mice (Fig. 3.19M, N, O). Vacuoles in cardiomyocytes and development of fibrosis were also prominent in hearts of 2-, 3- and 6-month-old *Hspa4*^{-/-} mice (Fig. 3.19D-F, J-N). Increase of fibrosis areas was found in hearts of 2-, 3- and 6-month-old *Hspa4*^{-/-} mice. These areas were mostly marked in left ventricle and septum.

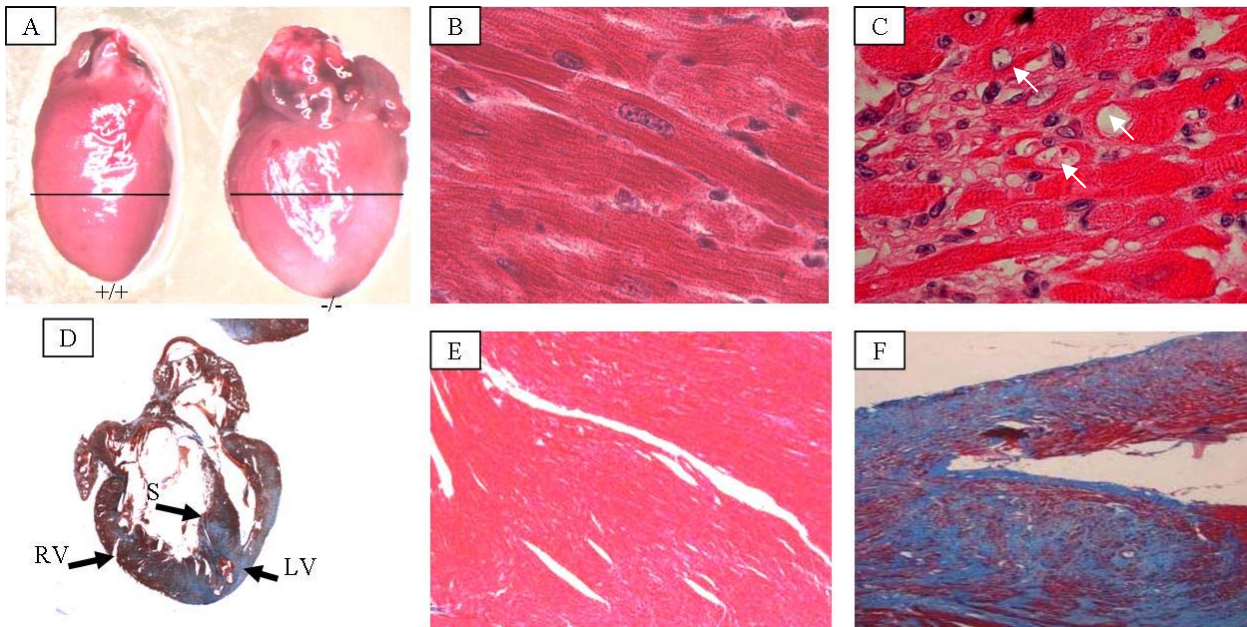


Fig. 3.16. *Hspa4* deficiency causes cardiac hypertrophy and fibrosis. (A) External view of representative hearts from 12-month-old *Hspa4*^{+/+} (left) and *Hspa4*^{-/-} (right) mice. (B and C) Histological sections of wild-type (B) and *Hspa4*^{-/-} hearts (C) stained with H&E show degeneration and vacuoles in cardiomyocytes (white arrows). (D-F) Representative Massion's trichrome-stained heart sections showing collagen-distribution (blue) in heart of *Hspa4*^{-/-} mice, indicative for fibrosis (D). In sections of wild-type heart (E), no fibrosis was found. Right ventricle (RV); left ventricle (LV); Septum (S). Optical magnifications: 4x in E, F; 60x in B, C.

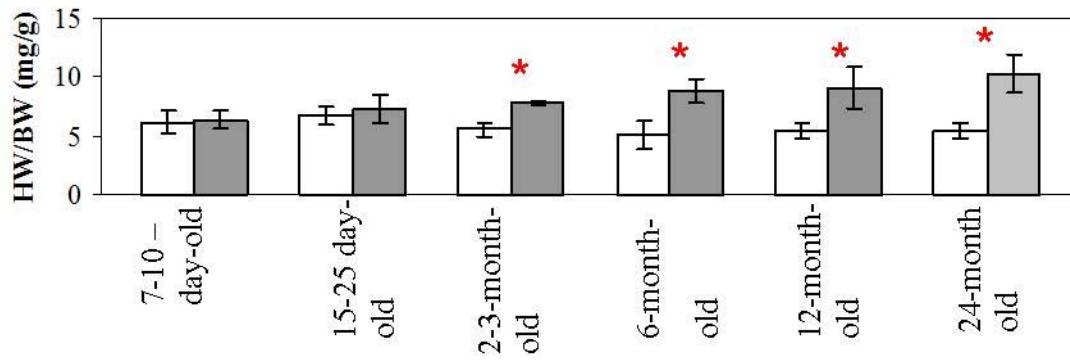


Fig. 3.17. Heart weight to body weight (HW/BW) ratios in wild type and *Hspa4*-null mice. There was no significant difference in HW/BW ratio before 2 months of age between the *Hspa4*-null mice when compared with littermate controls. HW/BW ratios of *Hspa4*^{-/-} mice were significantly greater in 2-3-, 6-, 12-, 24 month-old compared with those of wild-type mice. Data are mean \pm SD from 4-15 mice for each group; *, $p < 0.001$, HW: heart weight; BW: body weight.

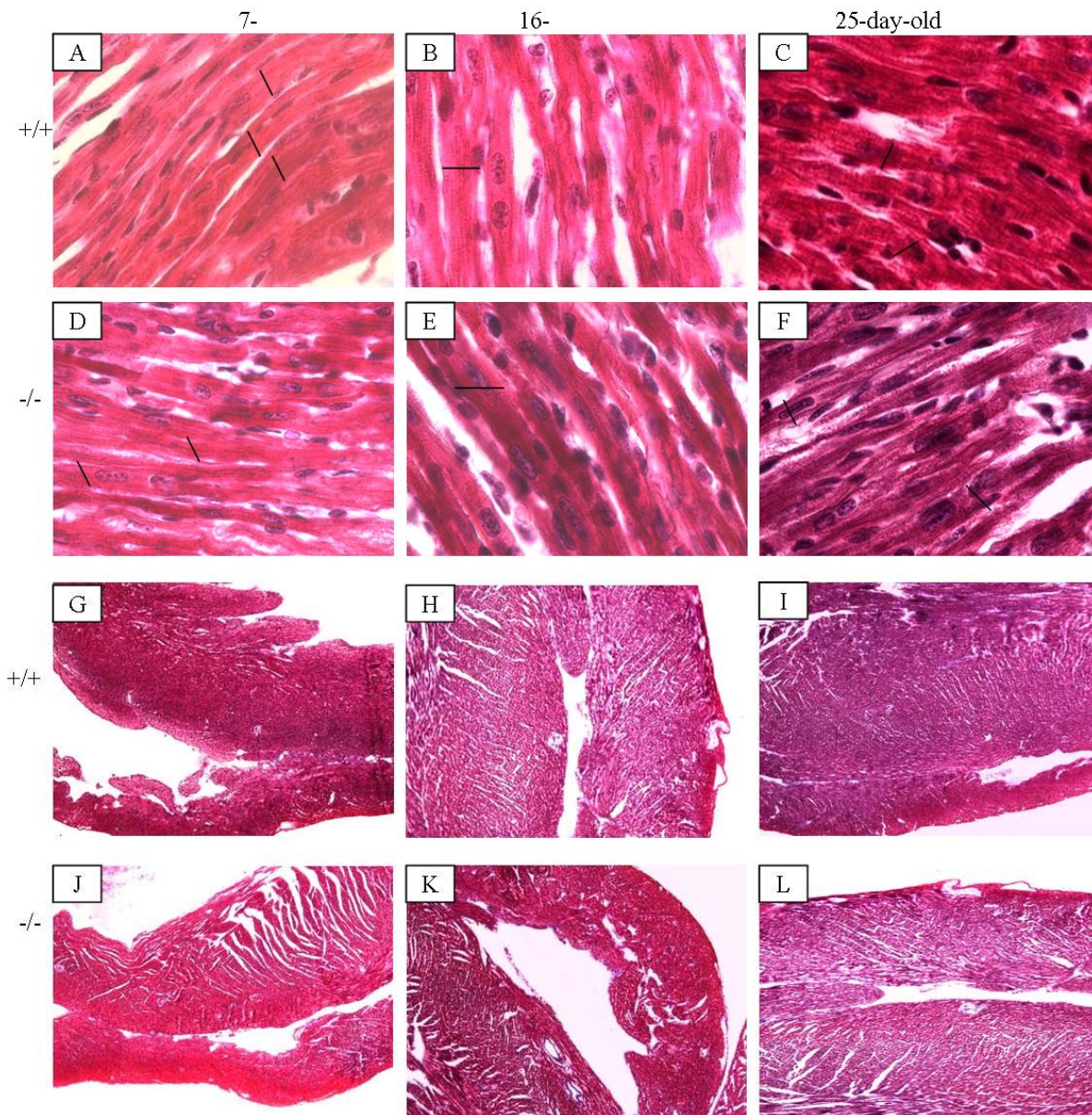


Fig. 3.18. Cardiac hypertrophy and fibrosis were not observed in 7 to 25 day- old *Hspa4*-mutant mice. Hematoxylin and eosin-stained cross sections of hearts obtained from wild-type (A, B, C) and *Hspa4*-mutant (D, E, F) mice at postnatal day 7 (A, D), 16 (B, E), 25 (C, F) are shown. At P7 (D), P16 (E) and P25 (F) heart sections did not show differences in morphology and size of cardiomyocytes between wild-type and mutant mice. (G-L) Representative Massion's trichome – stained heart sections at postnatal day 7 (G, J), 16 (H, K), 25 (I, L) without fibrosis in *Hspa4*^{-/-} mice (J, K, L). Black lines indicate cardiomyocyte diameters in the region of the cell nucleus. Optical magnifications: 4 x in G-L; 60 x in A-F.

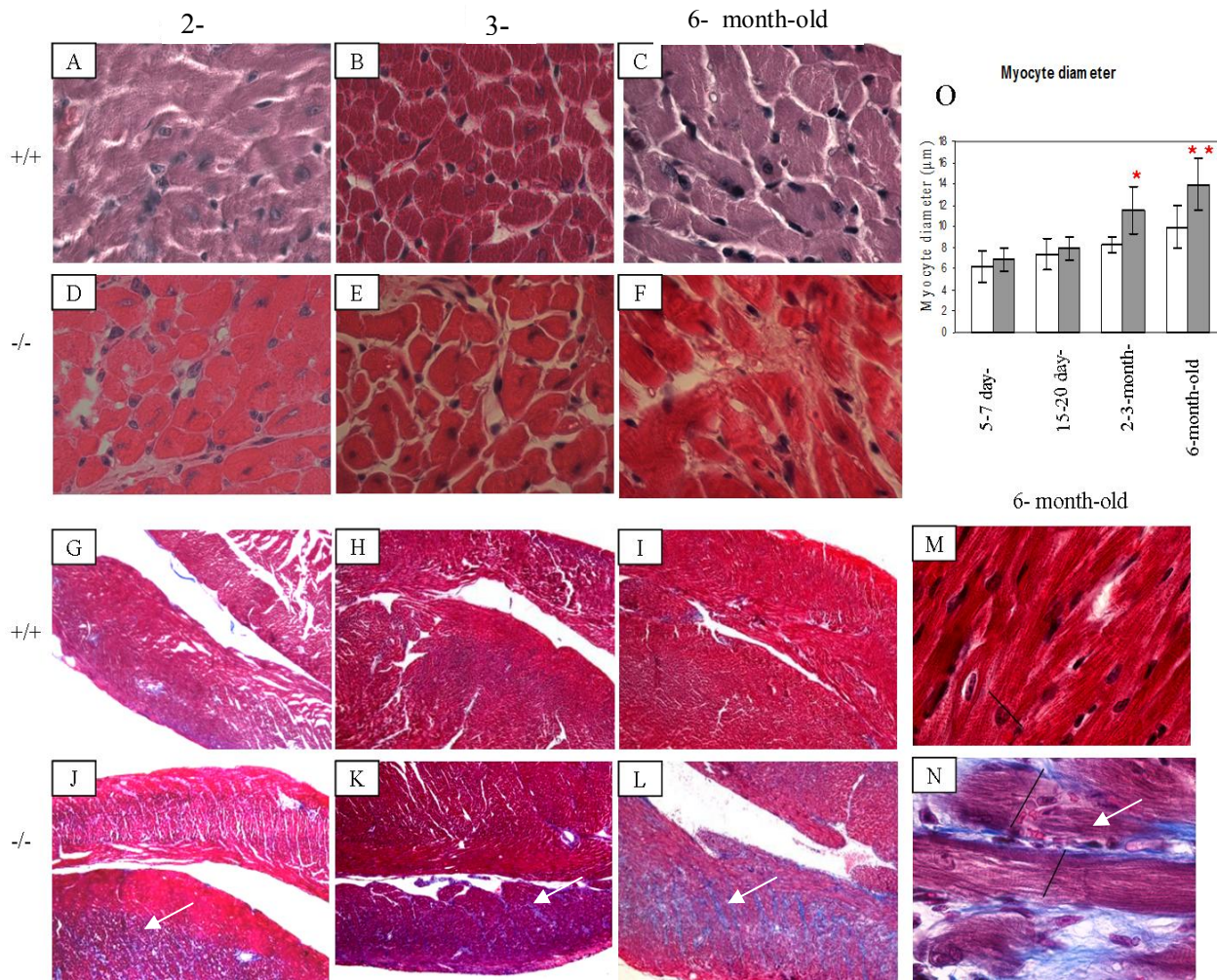


Fig.3.19. Cardiac hypertrophy and fibrosis were first observed in hearts of 2-month-old *Hspa4*^{-/-} mice. Hematoxylin and eosin- stained cross sections of hearts obtained from wild type (+/+) (A, B, C) and *Hspa4*-mutant (-/-) (D, E, F) mice at month 2 (A, D), 3 (B, E), 6 (C, F) are shown. The 2-, 3- and 6-month-old *Hspa4*^{-/-} (D, E, F) hearts display severe signs of hypertrophy including increase of myocyte size, degeneration and loss of myocytes compared to control littermates. (G-N) Representative Massion's trichome heart sections from 2- (G, J), 3- (H, K) and 6- (I, L, M, N) month-old *Hspa4*^{+/+} and *Hspa4*^{-/-} mice showing increased fibrotic areas (blue) in *Hspa4*^{-/-} heart (J, K, L, N). Myocyte diameter of mutant and wild-type hearts (O). Black lines indicate cardiomyocyte diameters in the region of the cell nucleus, which were significantly increased in hearts of 6-month mutant mice. Collagen-containing fibrotic region is stained with blue color (white arrow). Optical magnifications: 4x in G-L; 60x in A-F, M, N, *, p <0.05; **, p <0.001.

3.2.6.2 Echocardiographic measurements in wild type and mutant mice

To further confirm the cardiac hypertrophy phenotype in *Hspa4*-mutant mice, echocardiogram was performed in 4-month-old wild-type (n=7) and *Hspa4*-null mice (n=10) (Fig. 3.20A, B). Two-dimensional directed M-mode echocardiograms were recorded to measure left ventricle end-diastolic and end-systolic dimensions, right ventricle and septal thickness. As shown in figure 3.20A-C, *Hspa4*^{-/-} mice exhibit significant hypertrophy with increase of intraventricular septal thickness, left ventricle posterior wall thickness during diastole compared with age-matched wild-type control mice. The lumen of *Hspa4*^{-/-} left ventricle was thinner than wild-type control (Fig. 3.20A, B). Left ventricular mass (LVM) as well as the left ventricular mass to body weight ratio (LVM/BW) were higher than in wild-type mice. However, the increase of LVM/BW ratio was not significant (Fig. 3. 20E, F). Furthermore, the calculated ratio of wall thickness to heart radius at diastole (H/R) was significantly increased compared to that in wild type mice, suggesting a concentric pattern of enlargement (Fig. 3.20G). At 17 days of age, the *Hspa4*- null mice showed a small degree of hypertrophy, but with a significant increase in septal wall thickness compared with wild- type controls (Fig.3. 20D).

3.2.6.3 Ultrastructural analysis of sections *Hspa4*^{-/-} heart

To further evaluate the morphological changes in cardiomyocytes of *Hspa4*^{-/-} mice more precisely, we performed ultrastructural analysis on sections from left ventricular wall of 2-month-old *Hspa4*^{+/+} and *Hspa4*^{-/-} mice (Fig. 3.21A-F). Ultrastructural analysis revealed myofibrillar disarray and disassembly in *Hspa4*^{-/-} heart . The structure of the myocyte nuclei was also markedly abnormal, with redundancy of vacuoles in the nuclei. Nuclei have bizarre shapes (Fig 3.21E). Furthermore, increased collagen accumulation (fibrosis) was frequently observed in *Hspa4*^{-/-} hearts (Fig 3.21C, F). In contrast, ultrastructure of wild-type heart did no show these pathological changes (Fig. 3.21A, D).

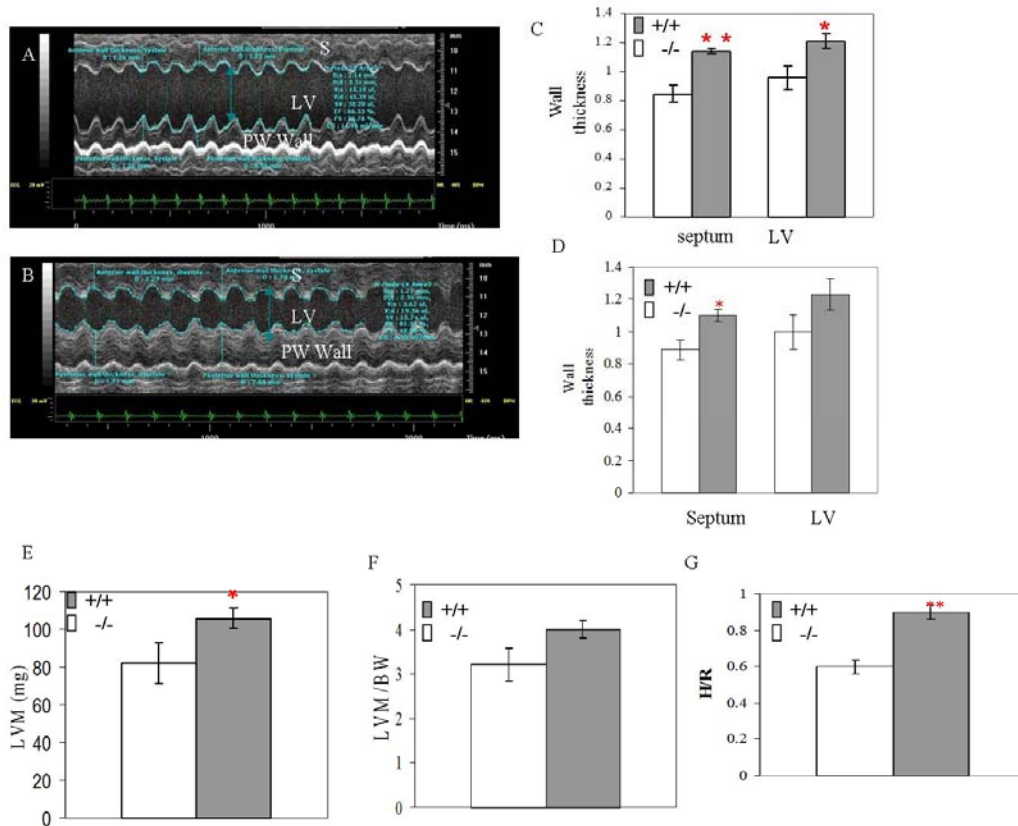


Fig. 3.20. Transthoracic echocardiography revealed affected dimensions and functions of *Hspa4*^{-/-} hearts. (A and B) Shown two representative M mode images from heart of wild type (A) and null-mice (B). (C-G) Quantitative analysis of the diameter of diastolic left ventricular wall and septal of heart from 4-month- (C) and 17-day-old mice (D), left ventricular mass (LVM) (E) and LVM/BW ratio (F) of 4-month-old animals. (G) The H/R (left ventricular thickness/radius) ratio of 4-month-old heart shown marked increase of the H/R ratio in *Hspa4*-null mice. Data are mean \pm SEM of 7 wild type and 10 *Hspa4*^{-/-} mice; *, $p < 0.05$; **, $p < 0.001$, ventricular end-diastolic (right arrows) and end-systolic (left arrows). Ventricular cavity (double head arrows).

3.2.6.4 Analyses of molecular markers of cardiac hypertrophy

Ventricular hypertrophy induced by pressure or volume overload is known to lead to reactivation of several specific embryonic genes, such as atrial natriuretic factor (*Anf*), Brain natriuretic peptide (*Bnf*), β -myosin heavy chain 7 (*Myh7*) and skeletal α actins 1 (*Acta1*) (Komura and Yaakov, 1993; Chine *et al.*, 1991). In order to show at which postnatal stage the development of heart hypertrophy starts, we studied the expression of hypertrophic marker genes in the heart from different postnatal stages. Northern blots with RNA isolated from hearts at P10, P14, P15, P17, P19, P37 and 3.5-month-old *Hspa4*^{+/+} and *Hspa4*^{-/-} mice were hybridized with ³²P-labeled *Anf* cDNA probe (Fig. 3. 22). To check the integrity and equal amounts of RNA, the blots were rehybridized with β -actins cDNA probe. Northern blot analysis showed no difference in expression levels of *Anf* in hearts of wild-type and null-mice at postnatal days 10 and 14. Expression level of *Anf* was increased in RNA of *Hspa4*-null hearts at postnatal day 15 (P15) compared with the control littermates. Thereafter, a significant increase in the level of *Anf* expression was observed through the postnatal developmental stages of *Hspa4*-null hearts. To further confirm these results, expression levels of *Anf*, *Bnf*, *Acta1* and β -*Myh7* were determined at different postnatal stages by quantitative real-time RT-PCR (Fig. 3. 23A-D). The results revealed that the expression levels of hypertrophic marker genes are significantly higher in *Hspa4*^{-/-} hearts at postnatal days 15- 25 than in wild-type hearts. The expression levels of *Anf*, *Bnf*, *Acta1* and β -*Myh7* were increased 7.0-, 4.7-, 3.8- and 2.8- fold in *Hspa4*^{-/-} mice, respectively, compared with wild type. These results suggest that reactivation of the fetal gene program in the *Hspa4*-null hearts. Furthermore, the expression pattern of hypertrophy marker genes indicates that the development of hypertrophy in *Hspa4*-null mice starts in early postnatal life.

3.2.6.5 Upregulation of fibrosis marker genes in heart of *Hspa4*^{-/-} mice

The development of cardiac fibrosis in *Hspa4*^{-/-} lead us to determine at molecular level the progression of fibrosis in heart of *Hspa4*^{-/-} mice at different postnatal ages. We determined the expression levels of fibrosis marker genes collagen I, collagen III and transforming growth factor- β 1 (TGF- β 1). Quantitative real-time PCR was used to characterize expression level of fibrosis marker genes.

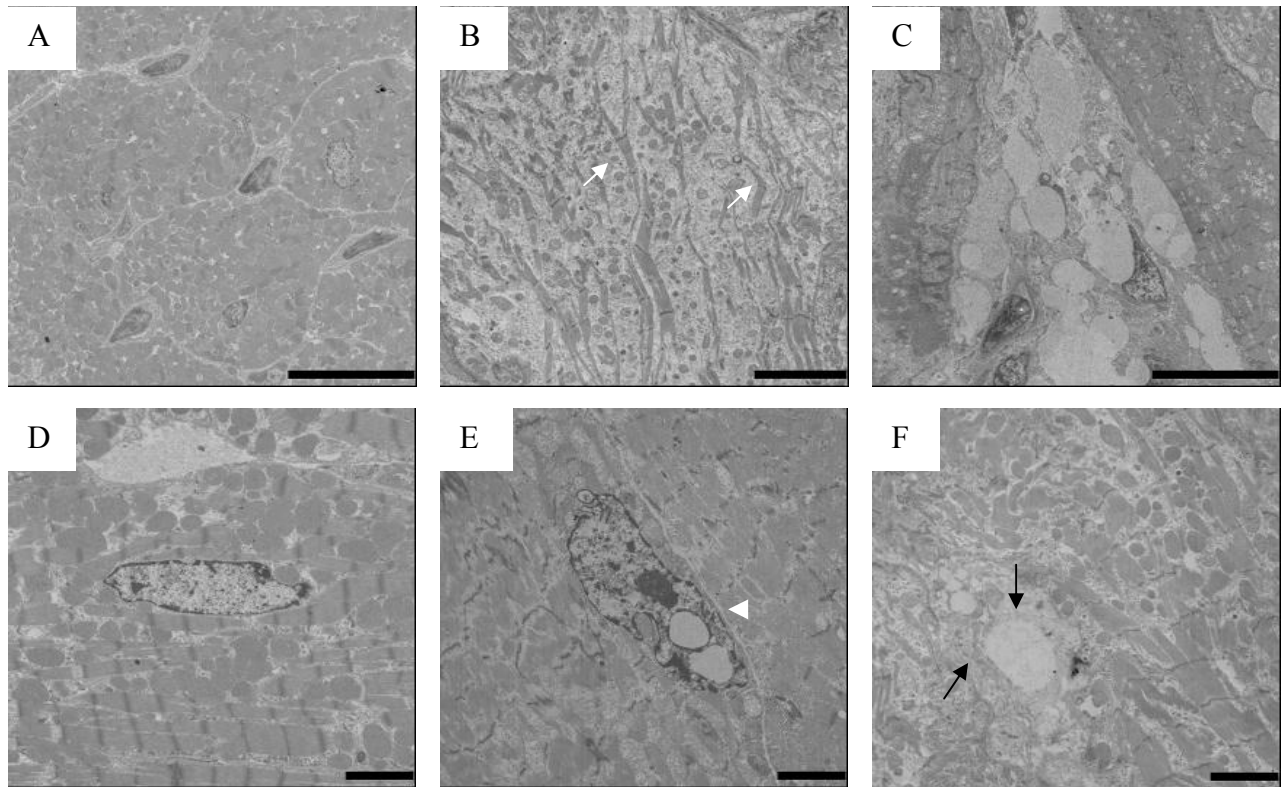


Fig. 3.21. *Ultrastructural analysis by transmission EM of $Hspa4^{+/+}$ (A, D) and $Hspa4^{-/-}$ mice (B, C, E, F) reveals disarray and disassembly of myofibrils (white arrows) in $Hspa4^{-/-}$ (B) heart versus the normal architecture of wild-type heart (A, D). Nuclei of myofibrils from $Hspa4$ -null mice exhibit irregular morphology with multiple inclusions (white arrow head) compared to the normal nuclear shape of control myocyte (D). Collagen accumulations are frequently observed in mutant myocytes (black arrows).*

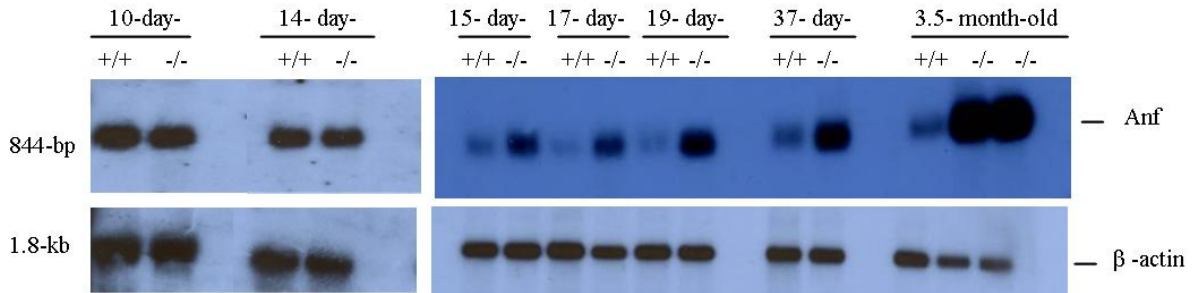


Fig. 3.22. Expression of the *Anf* gene in heart of wild-type and null mice at different postnatal stages. Total RNA was extracted separated in 1% formaldehyde-agarose gel (15 μ g/lane), transferred onto nylon membrane and hybridized with 32 P-labelled *Anf* and β -actin cDNA probes, respectively. Northern blot showing an increase in *Anf* mRNA expression in heart of *Hspa4*^{-/-} mice at postnatal day 15 and advancing ages.

Results

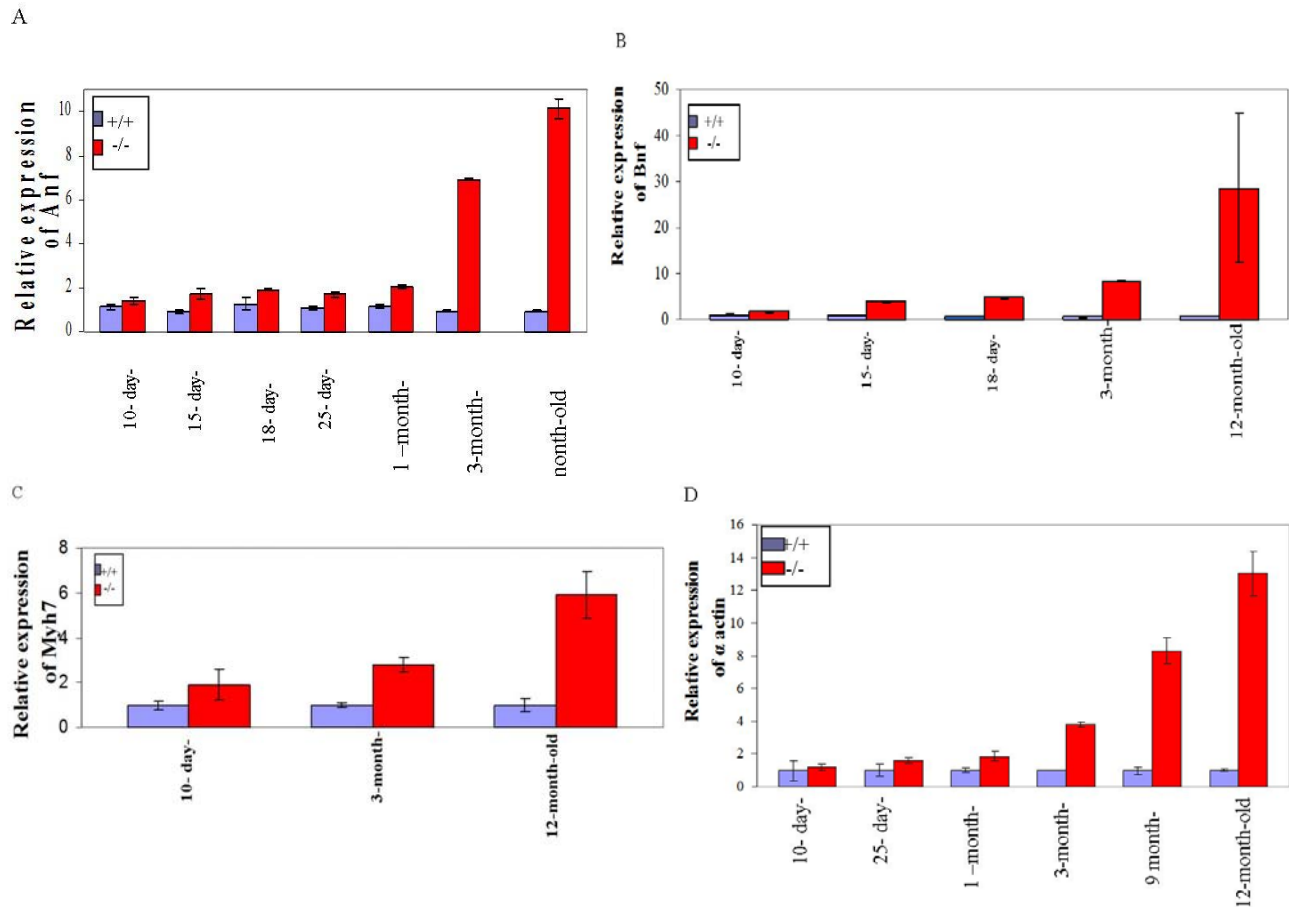


Fig.3.23. Expression of hypertrophy genes in hearts of wild-type and null-mice at different postnatal ages. The mRNA levels of *Anf* (A), *Bnf* (B), *Myh7*(C) and *Acta1* (D) were quantified by real time RT-PCR ($n=3$ per group). The relative mRNA level of each gene was normalized to that of house keeping succinate dehydrogenase (*Sdha*). Values indicate relative expression to wild-type littermate.

As expected from the results of histological analysis for development of fibrosis in *Hspa4*^{-/-} heart, no significance different in expression levels of collagen I, collagen III and TGF- β 1 in heart of 20-day-old wild-type and *Hspa4*^{-/-} mice (Fig. 3.24 A-C), while significant increase in expression of collagen III and TGF- β 1 were observed in heart of 50-day-old *Hspa4*^{-/-} mice at compared to that of littermate control (Fig 3.24. B, C). Expression levels of all three genes were markedly increased in 3-month old *Hspa4*^{-/-} heart compared to that of wild-type. These results reveal that the cardiac fibrosis is developed in *Hspa4*^{-/-} heart at early postnatal age.

3.2.6.6 Molecular pathways in the regulation of cardiac hypertrophy

Several molecular pathways have been implicated in the molecular response of cardiomyocytes to external stimuli or stress and in the development of cardiac hypertrophy. Gp130/STAT3, MAPK, Calcineurin-NFAT and P13K/Akt/GSK-3-depenent- signalings are among the best established mediators of cardiac hypertrophy. Alteration in the activity of one of these molecular signalings leads to development of cardiac hypertrophy (Frey and Oslon, 2003). To determine the signal pathway that is affected in *Hspa4*^{-/-} mice and responsible for the development of cardiac hypertrophy, we determined the expression of some genes and proteins involved in Gp130/STAT3, MAPK and Calcineurin-NFAT signalings in heart of wild-type and *Hspa4*^{-/-} mice.

3.2.6.6.1 Analysis of STAT3 and MAPK signaling in heart of *Hspa4*^{-/-} mice

Several studies have reported that IL-6-related cytokines such as LIF induced hypertrophy in cardiac myocytes through gp130 receptor. Activation of gp130 receptor leads to downstream activation of two signaling pathways, one is the JAK/STAT-, the other the MAPK pathway (Kishimoto *et al.*, 1994; Kunisada *et al.*, 1996). The transcription factor STAT3 is essential for gp130-mediated hypertrophy in heart. To study whether the STAT pathway is affected in *Hspa4*-null heart, expression of STAT3 and phosphorylated STAT3 in heart of wild-type and mutant mice at different ages was determined by Western blot analysis. Total protein extracts were isolated from 3-week-, 3-, 6-, and 12-month-old wild-type and *Hspa4*^{-/-} mice, separated on PAGE-SDS gel and blotted on nitrocellulose filters. Blots were probed with anti-STAT3, anti-phospho STAT3 and anti- α -tubulin antibodies. As shown in figure 3.25A, expression of STAT3 and activated STAT3 (phospho-STAT3) in heart of *Hspa4*^{-/-} mice at different ages was not different from that of wild-type mice.

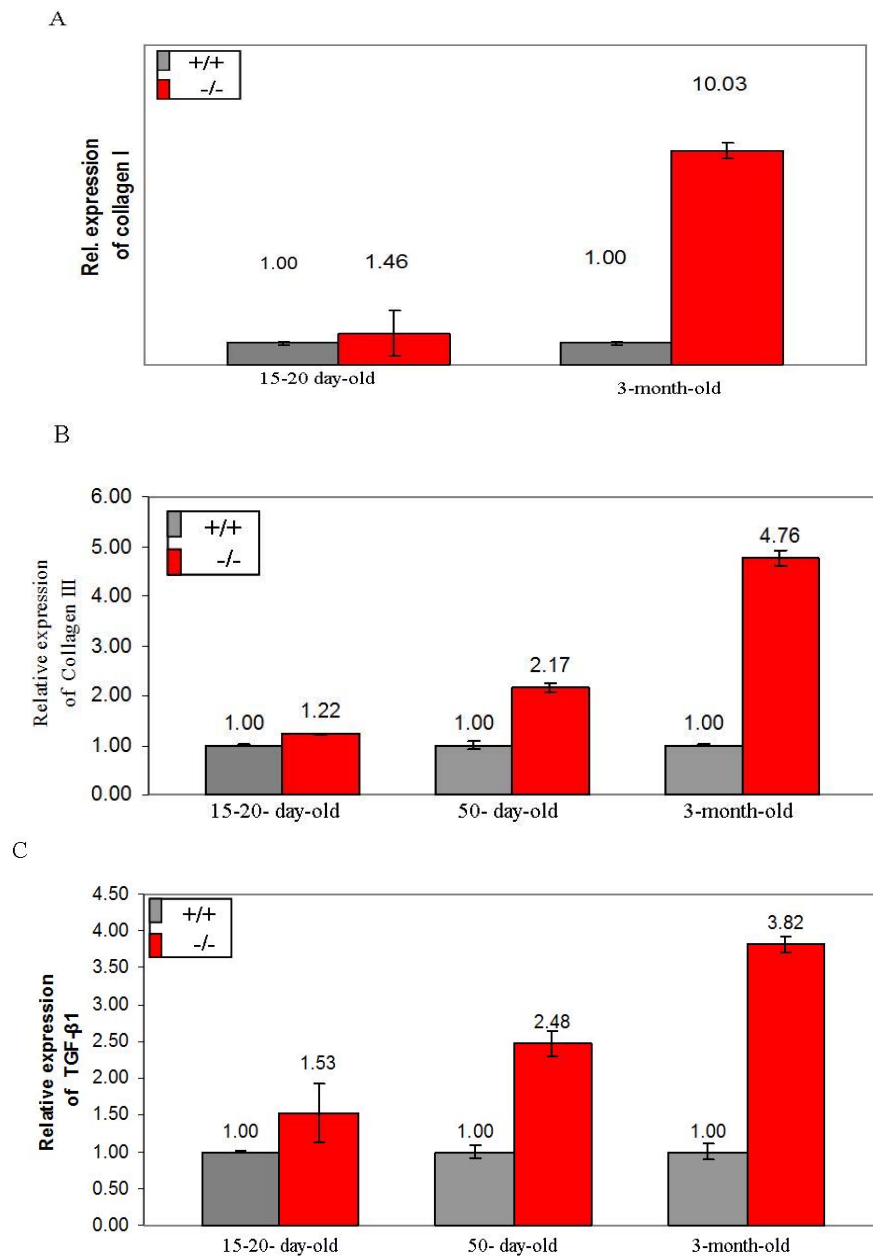


Fig. 3.24. Increase of fibrosis marker gene expression in *Hspa4*-mutant adult mice. *Relative levels of collagen I (A), collagen III (B), and TGF β 1 (C) mRNA expression in heart of Hspa4-null and wild type mice during cardiac postnatal development (15-20-, 50- and 90-day-old) are illustrated. Expression levels were normalized to the expression of endogenous control (Sdha). RNA from hearts of three mice was used for each stage and genotype.*

MAPK signaling pathway consists of a sequence of successively acting kinases that result in dual phosphorylation and activation of terminal effector kinases such as ERK1/2 (Widmann *et al.*, 1999). To determine whether the MAPK signaling is altered in heart of *Hspa4*^{-/-} mice, expression of ERK1/2 and activated form (phospho-ERK1/2) was studied by Western analysis. Blots with heart protein extracts from wild-type and *Hspa4*-null mice at different ages were probed with ERK1/2, phospho-specific ERK1/2 and anti- α -tubulin antibodies. Western blot analysis revealed that the ERK1/2 and phospho-related ERK1/2 protein levels are similar in heart of wild-type and mutant mice at different ages (Fig. 3.25B). These results suggest that the both signaling pathways are not responsible for the development of cardiac hypertrophy in *Hspa4*-null mice.

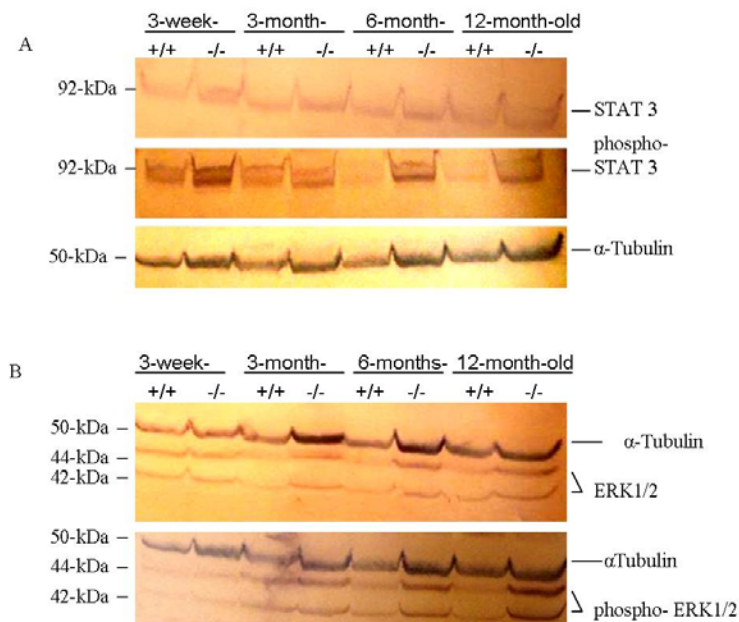


Fig. 3.25. Expression of inactive and active STAT3 and *Erk1/2* proteins in heart. Western blots with protein extracts from heart of 3-week, 3-, 6- and 9-month-old *Hspa4*^{+/+} and *Hspa4*^{-/-} mice were probed with STAT3, phospho-specific STAT3 and α -tubulin antibodies (A). Blots with the same proteins as in A were probed with anti-ERK1/2, anti phospho-ERK1/2 and anti- α -tubulin (B).

3.2.6.6.2 Genes involved in calcineurin/NFAT pathway are upregulated in heart of *Hspa4*^{-/-} mice

Several studies have shown that the angiotensin-endothelin system induce the activity of calcineurin-NFAT signaling pathway (Abbasi, *et al.*, 2006). Therefore, we determined the expression of genes coding for receptors that regulate the activity of downstream proteins in the calcineurin/NFAT pathway in heart of wild-type and *Hspa4*-null mice. These receptors include endothelin A (ET_A) and B (ET_B), angiotensin II type 1 (AT₁) and type 2 (AT₂) receptors. We measured the expression of these genes by real time PCR in heart at two postnatal ages. At P18, expression of most genes in heart of *Hspa4*^{-/-} was slightly higher than that in wild-type littermates (Fig.3.26 A, B, D, E). Only expression of the gene coding for ET_B endothelin receptor did not show any significant difference between heart of *Hspa4*^{-/-} and control mice at this postnatal age. In contrast, expression of the genes coding for these receptors was significantly up-regulated (at least 2-fold) in heart of 3-month-old *Hspa4*^{-/-} compared to heart of control mice (Fig.3.26 A, B, D, E). The expression of angiotensin II gene that codes for the ligand of AT₁ **and** AT₂ receptors was also determined in the heart of both genotypes and ages. Similar to expression pattern of its receptor, expression of angiotensin II gene was slightly higher in heart of 18-day-old *Hspa4*^{-/-} and 4-fold higher in heart of 3-month-old *Hspa4*^{-/-} mice than in heart of control littermates (Fig.3.26 C). The expression of endothelin (ET-1) coding for ligand of ET_A and ET_B also showed the same pattern (Fig.3.26 F). These results suggest that the *Hspa4* deficiency alters the activity of angiotensin-endothelin pathway. To study whether the upregulation of these genes coding for ligands and receptors of angiotensin-endothelin pathway of 3-month-old *Hspa4*^{-/-} mice is accompanied by increase of the activity of Calcineurin-NFAT signaling pathway, quantitative real-time PCR assays were performed to determine the mRNA levels of several genes that are involved in this signaling. The studied genes include natriuretic peptide receptor A (Npr1), calmodulin 1 (Calm), protein kinase C (PKC), myocyte-specific enhancer factor 2C (Mef2C), GATA4 binding protein 4 and histone deacetylase 7A (Hdac7a). As shown in figure 3.27, except for Calm, mRNA levels of all other genes were slightly higher in heart of 18-day-old *Hspa4*^{-/-} mice than in control mice. In heart of 3-month-old mice, expression levels of all these genes were more than 2-fold higher in *Hspa4*^{-/-} mice compared to control mice. These results suggest that the expression of genes involved in calcineurin/NFAT signaling is altered in heart of *Hspa4*^{-/-} mice.

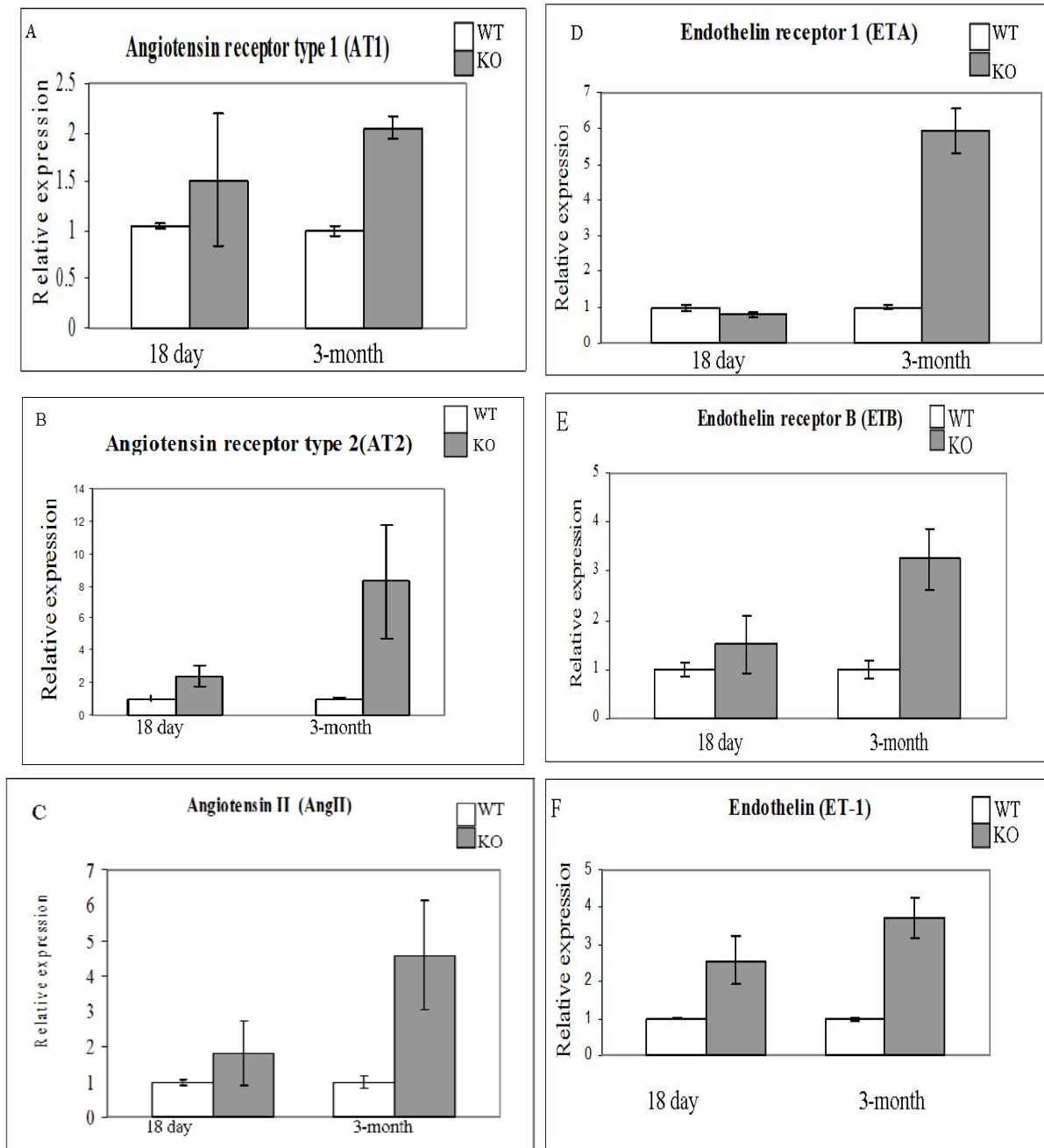


Fig. 3.26. Upregulation of genes that are involved in angiotensin- endothelin system in heart of *Hspa4*-mutants and controls. Quantitative real-time PCR analysis of mRNA levels for angiotensin II type 1 (AT_1) (A) and type 2 (AT_2) (B) receptors, angiotensin II (AngII) (C), endothelin A (ET_A) (D) and B (ET_B) (E) receptors and endothelin (ET-1)(F) wild type (WT) and mutant (KO) mice was determined at 18-day- and 3-month-old. Expression levels were normalised to the expression of endogenous control (*Sdha*). 2-3 biological replicates were performed for each stage and genotype.

In calcineurin/NFAT signaling, calcineurin dephosphorylates and activates *the* NFAT transcription factors. *The activated* NFAT protein promotes together with other transcription factors such as Mef2C and GATA4 the expression of several hypertrophic induced genes. To determine whether calcineurin/NFAT pathway is highly activated in heart of *Hspa4*^{-/-} mice, we determined the expression of the NFAT-target gene, cardiac-specific transcript modulatory calcineurin interacting protein 1.4 (MCIP1.4). The promoter of MCIP1.4 gene contains specific-acting element for NFAT proteins. Expression analysis revealed that the MCIP1.4 transcript level was 15-fold higher in heart of 3-month-old *Hspa4*^{-/-} mice than in control mice. These results demonstrate that Calcineurin/NFAT signaling pathway is highly activated in heart of *Hspa4*^{-/-} mice (Fig. 3.28). These results further suggest that elevated calcineurin/NFAT activity can modulate the cardiac hypertrophy of *Hspa4*^{-/-} mice.

3.2.6.7 Microarray analysis of cardiac gene expression

To investigate the pathways regulating the development of cardiac hypertrophy in *Hspa4*-deficient mice, microarray analysis was used as a screening tool to indicate genes with altered expression in the *Hspa4*-null hearts at 25 days compared with that of wild type mice. We selected 25-day-old *Hspa4*^{-/-} and control mice because at that age expression of marker genes for cardiac hypertrophy and fibrosis is slightly increased in heart of *Hspa4*^{-/-} mice (sections 3.2.6.4 and 3.2.6.5). RNA from these wild-type and *Hspa4*^{-/-} mice, respectively, was prepared and labeled cDNA was hybridized to GeneChip® Mouse Gene 1.0 ST Arrays. The specificity of results obtained by microarray analysis was firstly confirmed by studying downregulation of *Hspa4* gene (4-fold decrease) and upregulation of hypertrophic markers such as *Anf*, *Bnf*, *Myh7* and *Acta1*, which were found to be upregulated in *Hspa4*^{-/-} heart by real time PCR described in section 3.2.6.4. There were 98 genes with statistically significant altered expression of at least +/-1.5 fold with P values of < 0.05, of which 42 were upregulated and 56 downregulated in *Hspa4*^{-/-} heart compared to corresponding wild-type (Table 3.1). Several genes were selected and classified according to their function in the development of cardiac hypertrophy (Table 3.2).

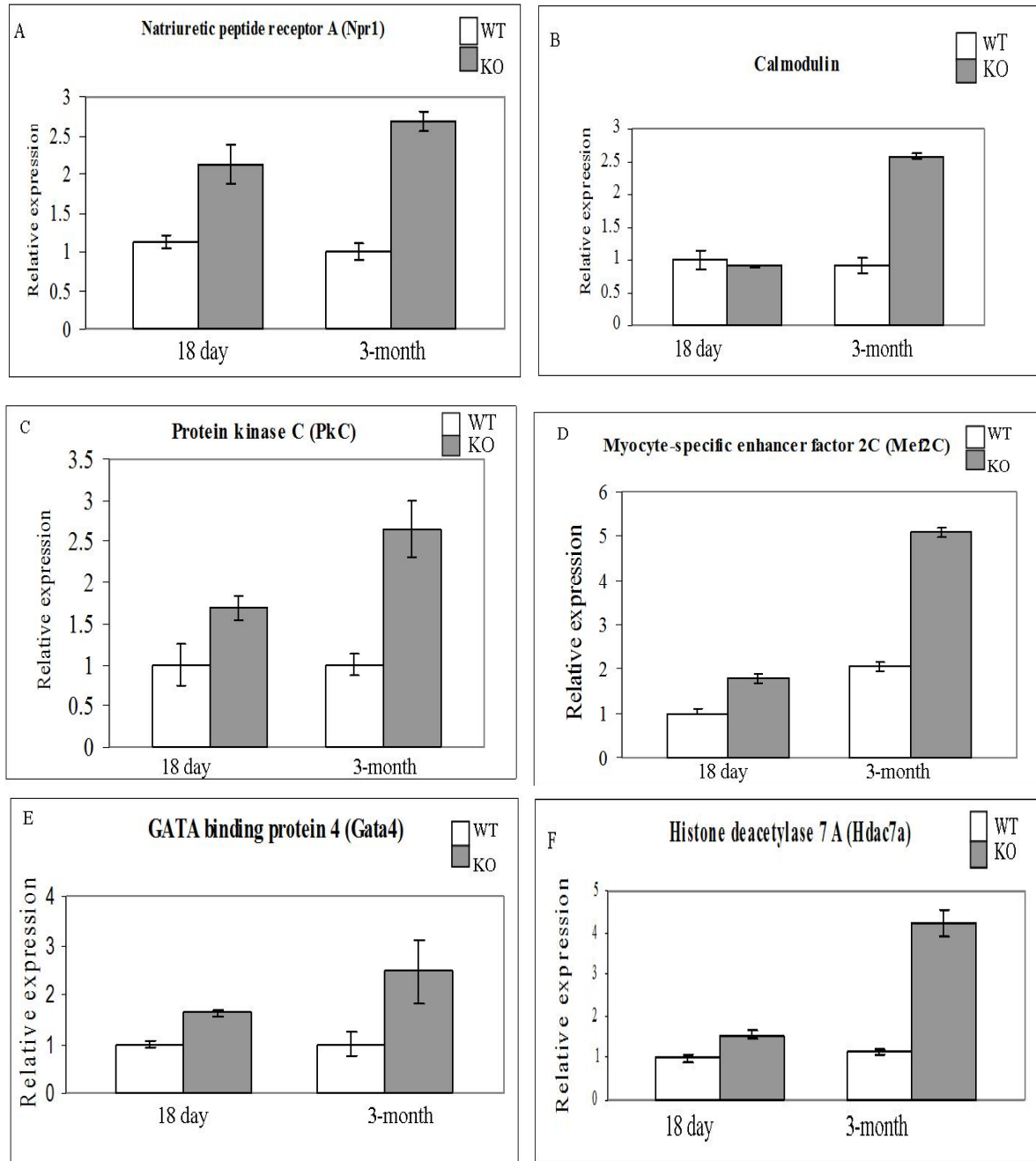


Fig. 3.27. Expression levels of *Npr1* (A) calmodulin 1 (B), *PKC* (C), *Mef2C* (D), *GATA4* (E) and *Hdac 7a* (F) in heart of *Hspa4*^{-/-} and control mice at 18 days and 3 months of age. Expression levels were normalized to the expression of endogenous control (*Sdha*). 2-3 biological replicates were used for each stage and genotype.

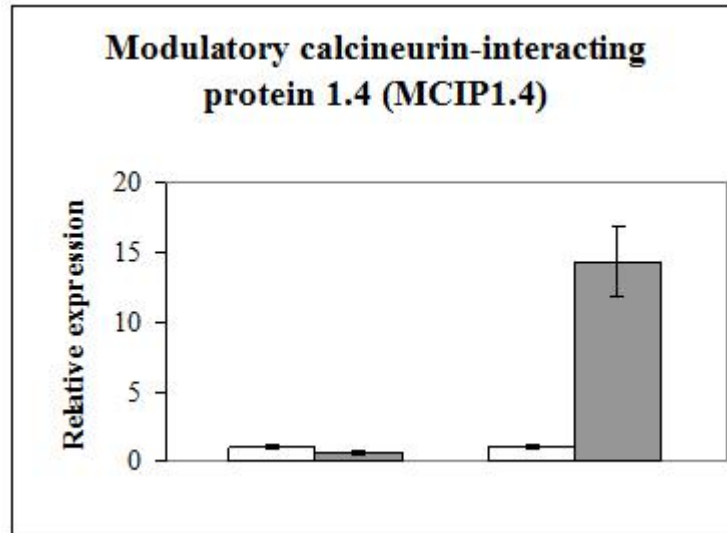


Fig.3.28. Overexpression of MCIP1.4 in heart of *Hspa4*-deficient mice. Values represent relative levels of MCIP1.4 in heart of 25-day- and 3 month- old animals. mRNA expression levels in each sample were normalized to the expression of *Sdha*. 2-3 biological replicates were used for each stage and genotype.

Table 3.1 Microarray analysis showing genes altered in *Hspa4*^{-/-} as compare to wild-type.

Symbol	Description	Function	log2FC KOvsWT
Nppa (Anf)	natriuretic peptide precursor type A	Hormone activity,regulation of blood vessel size	1.79
Kcne1	potassium voltage-gated channel, Isk-related subfamily, member 1	Potassium ion transport, epithelial cell Maturation	1.02
Acta1	actin, alpha 1, skeletal muscle	striated muscle thin filament, skeletal muscle fiber development	1.01
BC023105	cDNA sequence BC023105	unkown	0.90
MyI9	myosin, light polypeptide 9, regulatory	Calcium ion binding, motor activity	0.80
Dpys3	dihydropyrimidinase-like 3	Hydrolase activity, SH3 domain binding	0.76
Gnao1	guanine nucleotide binding protein, alpha O	GTP binding, GTPase activity, signal transduction	0.75
Leng8	leukocyte receptor cluster (LRC) member 8	Protein binding	0.72
Fhl1	four and a half LIM domains 1	metal ion binding	0.72
Rasd2	RASD family, member 2	nucleotide binding, GTP binding	0.69
Adh1	alcohol dehydrogenase 1 (class I)	NAD or NADH binding, oxidoreductase activity, zinc ion binding	0.66
Igfbp3	insulin-like growth factor binding protein 3	regulation of cell growth, , insulin-like growth factor binding, Negative regulation of protein amino acid phosphorylation	0.64
Rps26	ribosomal protein S26	structural constituent of ribosome	0.63
Timp4	tissue inhibitor of metalloproteinase 4	Metal ion binding, metalloendopeptidase inhibitor activity	0.62
Casq1	calsequestrin 1	Calcium ion binding, regulation of muscle contraction	0.61
Pfn1	profilin 1	actin binding, regulation of actin polymerization or depolymerization	0.61

Results

Symbol	Description	Function	log ₂ FC KOvsWT
Myh7	myosin, heavy polypeptide 7, cardiac muscle, beta	calmodulin binding , striated muscle thick filament , striated muscle contraction , myosin complex	0.58
Irx4	Iroquois related homeobox 4 (Drosophila)	Regulation of transcription, heart development, regulation of transcription	0.57
Pitpnm2	phosphatidylinositol transfer protein, membrane-associated 2	calcium ion binding, phospholipid binding	0.56
Nrbp2	nuclear receptor binding protein 2	protein kinase activity, ATP binding, protein amino acid phosphorylation	0.55
Rnf207	ring finger protein 207	protein binding, intracellular , zinc ion binding, metal ion binding	0.55
9030624G23Rik	RIKEN cDNA 9030624G23 gene	Unknown	0.54
Zyx	zyxin	protein binding, cell-cell adherens junction, cell adhesion	0.54
Eif4ebp1	eukaryotic translation initiation factor 4E binding protein 1	translation initiation factor activity regulation of translation, regulation of translational initiation	0.53
Hspg2	perlecan (heparan sulfate proteoglycan 2)	protein binding, cell adhesion	0.52
Gata6	GATA binding protein 6	transcription regulator activity, metal ion binding	0.52
Rmrp	RNA component of mitochondrial RNAase P	Molecular function	0.51
Nppb (Bnf)	natriuretic peptide precursor type B	regulation of blood vessel size	0.50
Stk17b	serine/threonine kinase 17b (apoptosis-inducing)	protein amino acid phosphorylation , apoptosis , kinase activity, transferase activity	-0.50
Zfp72	zinc finger protein 72	zinc ion binding, metal ion binding	-0.50
Mrc1	mannose receptor, C type 1	receptor activity, calcium ion binding , integral to membrane	-0.50
Mpdz	multiple PDZ domain protein	protein binding, tight junction , cell adhesion	-0.51
Kras	v-Ki-ras2 Kirsten rat sarcoma viral oncogene homolog	nucleotide binding, GTPase activity , GTPase activity, protein binding, GTP binding	-0.51
Ctsc	cathepsin C	cysteine-type endopeptidase activity, lysosome, proteolysis	-0.51
Mrgprh	MAS-related GPR, member H	signal transducer activity	-0.52

Results

Symbol	Description	Function	log2FC KOvsWT
B3galt2	UDP-Gal:betaGlcNAc beta 1,3-galactosyltransferase, polypeptide 2	protein amino acid glycosylation integral to membrane , manganese ion binding	-0.52
Pkia	protein kinase inhibitor, alpha	negative regulation of transcription from RNA polymerase II promoter , protein kinase inhibitor activity	-0.52
Tm4sf5	transmembrane 4 superfamily member 5	integral to membrane	-0.52
Lrtm1	leucine-rich repeats and transmembrane domains 1	protein binding, membrane, integral to membrane	-0.53
Kcnd2	potassium voltage-gated channel, Shal-related family, member 2	potassium channel activity	-0.54
3110057O12Rik	RIKEN cDNA 3110057O12 gene	extracellular region	-0.54
C7	complement component 7	complement component 7	-0.55
Gpm6a	glycoprotein m6a	membrane, integral to membrane	-0.55
P4ha1	procollagen-proline, 2-oxoglutarate 4-dioxygenase (proline 4-hydroxylase), alpha 1 polypeptide	metal ion binding oxidation reduction	-0.56
Mrpl50	mitochondrial ribosomal protein L50	mitochondrion, ribosome, ribonucleoprotein complex	-0.56
Dcun1d1	DCN1, defective in cullin neddylation 1, domain containing 1 (S. cerevisiae)	unknown	-0.56
Dab2	disabled homolog 2 (Drosophila)	involved in differentiation cell morphogenesis and utero embryonic development	-0.57
Alkbh8	alkB, alkylation repair homolog 8 (E. coli)	oxidoreductase activity, transferase activity	-0.59
ENSMUSG00000049380	predicted gene, ENSMUSG00000049380	unkown	-0.59
Zmpste24	zinc metallopeptidase, STE24 homolog (S. cerevisiae)	metalloendopeptidase activity, proteolysis, nuclear envelope organization, zinc ion binding	-0.59
Scn4a	sodium channel, voltage-gated, type IV, alpha	Sodium ion transport, muscle contraction,	-0.61
Myl1	myosin, light polypeptide 1	motor activity, calcium ion binding, myosin complex	-0.61

Results

Symbol	Description	Function	log2FC KOvsWT
OTTMUSG00000003605	predicted gene, OTTMUSG00000003605	unknown	-0.63
Ptp4a1	protein tyrosine phosphatase 4a1	p protein amino acid dephosphorylation& cell cycle	-0.65
AW061290	expressed sequence AW061290	membrane, integral to membrane	-0.65
Angpt1	angiopoietin 1	angiogenesis, receptor binding, signal transduction, cell differentiation	-0.66
6430514L14Rik	RIKEN cDNA 6430514L14 gene	unknown	-0.66
Tbc1d8b	TBC1 domain family, member 8B	GTPase activator activity & calcium ion binding intracellular	-0.68
Fktn	fukutin	integral to membrane , transferase activity	-0.71
Hcn1	hyperpolarization- activated, cyclic nucleotide-gated K+ 1	potassium channel activity, sodium channel activity, ion transport	-0.71
100039652	predicted gene, 100039652	unknown	-0.72
Upk1b	uropod protein 1B	membrane, integral to membrane	-0.73
EG433229	predicted gene, EG433229	unknown	-0.76
Chordc1	cysteine and histidine- rich domain (CHORD)- containing, zinc-binding protein 1	calcium ion binding	-0.77
EG434373	predicted gene, EG434373	unknown	-0.77
Hsph1	heat shock 105kDa/110kDa protein 1	response to stress, chaperone cofactor-dependent protein folding	-0.77
Mme	membrane metallo endopeptidase	proteolysis, peptidase activity, metallopeptidase activity, zinc ion binding	-0.85
C3	complement component 3	positive regulation of type IIa, hypersensitivity , immune response	-0.94
Lgi1	leucine-rich repeat LGI family, member 1	protein binding , extracellular region	-1.09
Maob	monoamine oxidase B	mitochondrion, amine oxidase activity , oxidoreductase activity	-1.11
EG628276	predicted gene, EG628276	unknown	-1.51
Hspa4	heat shock protein 4		-2.01

Table 3.2 Selected genes which their expression was altered in *Hspa4* mutant hearts.

Symbol	Name	log ₂ FC KOvsWT	Note
A- Hypertrophic markers			
Anf	natriuretic peptide precursor type A	1.79	
Acta1	actin, alpha 1, skeletal muscle	1.01	
Myh7	myosin, heavy polypeptide 7, cardiac muscle, beta	0.58	
Bnf	natriuretic peptide precursor type B	0.5	
B- Hypertrophy related genes			
Fktn	fukutin	-0.71	-Mutation of Fktn cause hypertrophic cardiomyopathy and muscular dystrophy
Gata6	GATA binding protein 6	0.52	-GATA factors are sufficient regulators of cardiomyocyte hypertrophy - Overexpression in transgenic mice induce hypertrophy
Igfbp3	insulin-like growth factor binding protein 3	0.64	Mice overexpressed of hIgfbp3- has organomegaly
C- Ion transport			
Kcne1	potassium voltage-gated channel, Isk-related subfamily, member 1	1.02	- Involved in potassium channel - Overexpression of KCNE1 in transgenic mice resulted in a cardiac phenotype similar to that in the thyroid hormone receptor-alpha1 (TRalpha1)-deficient mice, including a lower heart rate and prolonged QT time
Kcnd2	potassium voltage-gated channel, Shal-related	-0.54	- Involved in potassium channel

	family, member 2		-The down-regulation of kcnd2 expression contributed to the ventricular hypertrophy and pulmonary hypertension
Scn4a	sodium channel, voltage-gated, type IV, alpha	-0.61	Involved in sodium channel
Hcn1	hyperpolarization-activated, cyclic nucleotide-gated K+ 1	-0.7	-It contribute to spontaneous rhythmic activity in both heart and brain
Irx4	Iroquois related homeobox 4 (Drosophila)	0.57	- controls cardiac potassium channel Kv4.2 gene transcription - Adult Irx4 KO mice developed cardiac hypertrophy
D- Oxidative stress			
Maob	monoamine oxidase B	-1.11	-Neutralized oxygen in mitochondria, -deletion of Mao caused hypertrophy
Gnao1	guanine nucleotide binding protein, alpha O	0.75	-Is critical target of oxidative stress
Ptp4a1	protein tyrosine phosphatase 4a1	-0.65	-It stimulates cell growth (stimulates progression from G1 into S phase during mitosis) -It is modulated under oxidative stress
Mme (NEP)	membrane metallo endopeptidase	-0.85	-Hypoxia resulted in a significant decrease mme
E- synaptic junction			
Lgi1	leucine-rich repeat LGI family, member 1	-0.1.09	- Lgi1(-/-) causes abnormal synaptic transmission and epilepsy

The differentially expressed genes include natriuretic peptide precursor type A (*Anf*), natriuretic peptide precursor type B (*Bnf*), actin, alpha 1, skeletal muscle (*Acta1*) and myosin, heavy polypeptide 7, cardiac muscle, beta (*Myh7*) and genes involved in ion channel signaling, potassium voltage-gated channel, Isk-related subfamily, member 1 (*Kcne1*), potassium voltage-gated channel, Shal-related family, member 2 (*Kcnd2*), sodium channel, voltage-gated, type IV, alpha (*Scn4a*), hyperpolarization-activated, cyclic nucleotide-gated K⁺ 1 (*Hcn1*) and Iroquois related homeobox 4 (*Irx4*). In addition, differential expression of genes, which are involved in protection of cells against oxidative stress, were also observed. These genes are guanine nucleotide binding protein, alpha O (*Gnao1*), protein tyrosine phosphatase 4a1 (*Ptp4a1*) and membrane metallo endopeptidase (*Mme*). We have also studied the expression of the monoamine oxidase B (*Maob*), which induces the oxidative stress in cardiomyocyte by oxidation of monoamine to hydrogen peroxide in the mitochondria (Naoi *et al.*, 2006). The *Maob* is downregulated in *Hspa4*^{-/-} heart by microarray analysis.

3.2.6.8 Quantitative real-time PCR analysis

Quantitative real-time PCR analysis was used to confirm the expression levels of selected genes shown to be differentially expressed by microarray analysis. cDNAs of heart were prepared from 25- day- and 3-month-old mice and used to determine the expression of *Kcne1*, *Kcnd2*, *Scn4a*, *Hcn1*, *Irx4*, *Maob*, *Mme*, *Gnao1*, *Ptp4a1*, GATA6, *Fktn*, *Igfbp3*, *Lgi1* by quantitative real time PCR. In 18-day- and 3-month-old *Hspa4*-null heart, expression of *Kcne1* and *Irx4* transcripts that control K⁺ channel was upregulated in *Hspa4*-null ventricle compared with control (Fig.3. 29A, B). Whereas the expression of *Kcnd2*, another gene encoding for Potassium voltage-gated channel subfamily D member 2, was significantly downregulated in mutant heart (Fig.3.29C). The expression of *Hcn1*, encoding pacemaker channel protein, was significantly reduced in *Hspa4*-mice in comparison to wild-type (Fig.3.29D). Expression of *Scna4* was also downregulated in *Hspa4*^{-/-} heart compared with control at both ages (Fig.3. 29E).

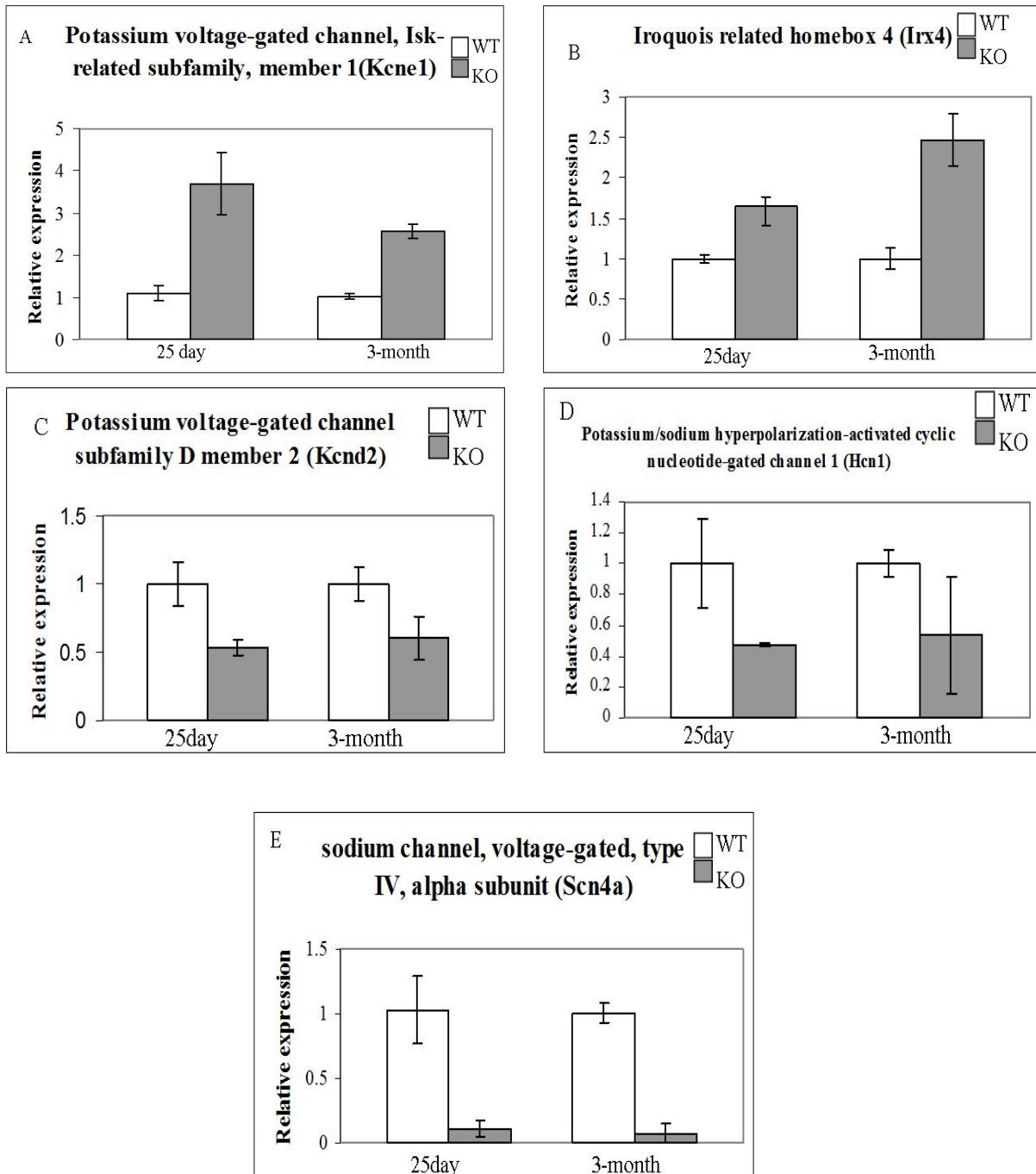


Fig. 3.29. Expression levels of *Kcne1* (A), *Irx4* (B), *Kcnd2* (C), *Hcn1* (D) and *Scn4a* (E) in hearts of wild-type and *Hspa4*^{-/-} mice at age of 25 days and 3 months. Quantitative real time PCRs were carried out in triplicate and in 3 mice per group at different postnatal stages. All values obtained were normalized to *Sdha*.

Maob is involved in the metabolism of serotonin and catecholamines that generates hydrogen peroxide (H_2O_2). Defects in this pathway lead to an increase of serotonin and catecholamines, which leads to an increase of blood pressure, and in consequence to cardiomyopathy. In 25-day- and 3-month-old *Hspa4a*-null heart, the expression level of *Maob* was significantly reduced compared with wild-type at both ages (Fig.3.30A). The downregulation of *maob* may be one of the causes for development of hypertrophy in *Hspa4*-deficiency. Expression of *Gnao1* is known to be induced by reactive oxygen species (Nishida, *et al.*, 2000). Levels of *Gnao1* mRNA were significantly increased in heart of 25-day- and 3-month-old mice mutant compared with wild-type (Fig.3.30B). The *Mme* is a proteolytic enzyme responsible for degradation of *Anf*. Quantitative real time PCR showed that gene expression of *Mme* is significantly reduced in *Hspa4*^{-/-} heart compared with wild type (Fig. 3.30C). The zinc finger-containing transcription factors GATA4 and GATA6 are important regulators of basal and inducible gene expression in cardiac and smooth muscle cell types. Overexpression of either GATA4 or GATA6 is sufficient to induce cardiomyocyte hypertrophy characterized by enhanced sarcomeric organization (Liang, *et al.*, 2001). In *Hspa4*^{-/-} heart, GATA6 was significantly increased in comparison with wild-type (Fig. 3.30D). Treatment of cardiac myocyte cultures with *Igfbp-3* demonstrated an increase in *Anf* expression level (Henson *et al.*, 2000). A significant increase of *Igfbp-3* transcript was observed in heart of *Hspa4*^{-/-} mice at 25 days and 3-months of age compared with wild type (Fig. 3.30E). Mutation of *Fktn* cause hypertrophic cardiomyopathy and muscular dystrophy (Arimura, *et al.*, 2009). Analysis of the expression of *Fktn* showed that expression of this gene is relatively low in 25-day-old wild-type and mutant heart, but its expression level at 3-month-old heart did not significantly differed between WT and KO mice (Fig. 3.30F). Leucine-rich, glioma inactivated 1 (*Lgil*) regulates voltage-gated potassium channels assembly of *Kcna1*, *Kcna4* and *Kcnab1* and positively regulates synaptic transmission mediated by *AMPA*-type glutamate receptors. At day 18 and at 3-months, expression levels of *Lgil* sharply decreased in mutant heart compared with wild type (Fig. 3.30G).

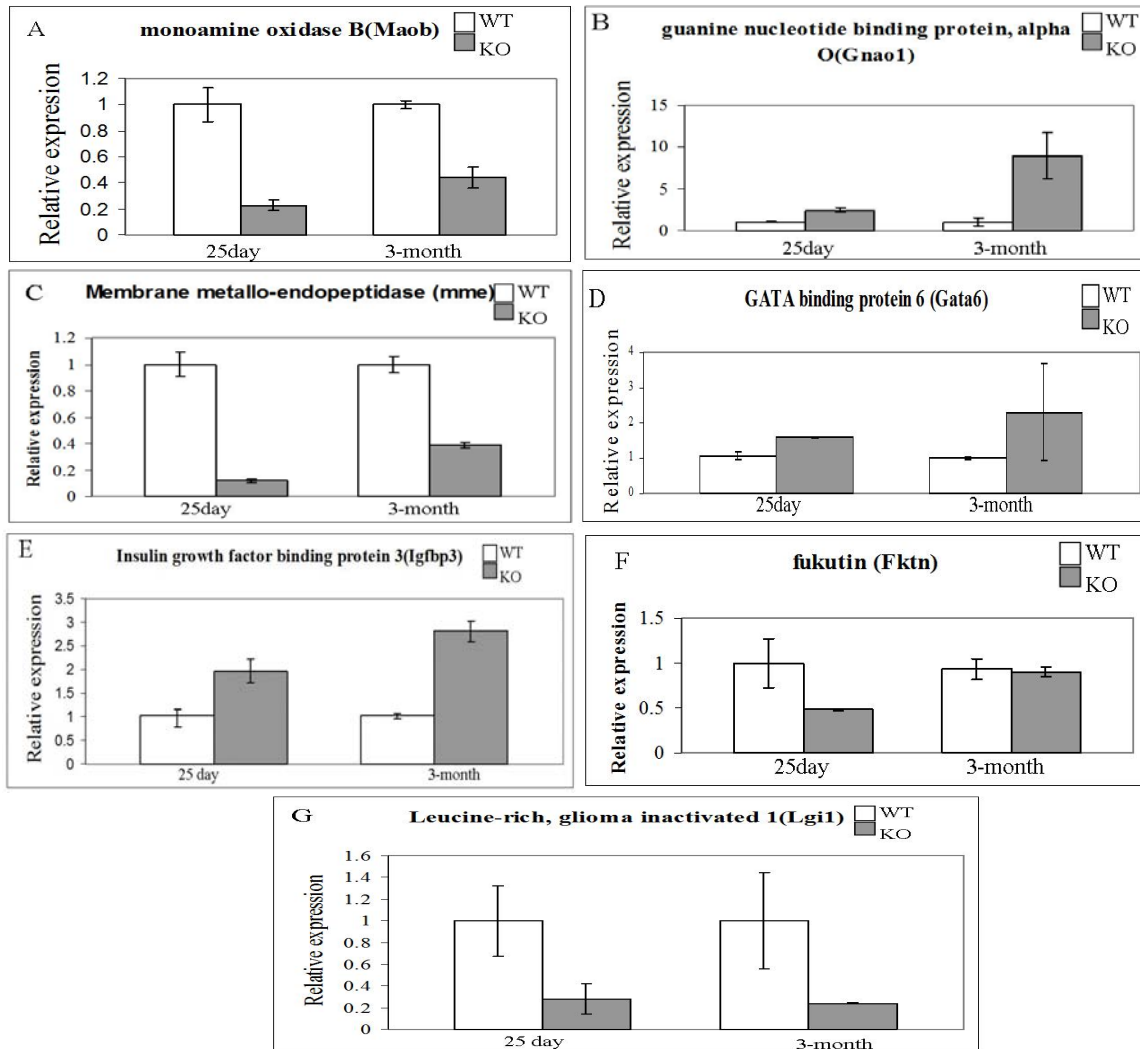


Fig. 3.30 Relative levels of *Maob* (A), *Gnao1* (B) *Mme* (C) *GATA6* (D), *Igfbp3* (E) *Fktn* (F) and *Lgi1* (G) mRNA expression in heart of *Hspa4^{-/-}* mice at age of 25 days and 3 months. Expression levels were normalised to the expression of endogenous control (*Sdha*). The results are representations of 3 independent experiments, each carried out in triplicate

3.2.7 Expression analysis of HSPA4L and HSPH1 in *Hspa4*-deficiency

Two other members of HSP110 family (HSPA4L and HSPH1) have been reported to be localized in cytoplasm as HSPA4. We examined the expression of both genes in *Hspa4*^{-/-} heart at protein level, because *Hspa4*-deficiency may alter the expression levels of both proteins. Total protein extracts were isolated from heart of 3-month-old wild-type and *Hspa4*^{-/-} mice, separated on PAGE-SDS gel and blotted on nitrocellulose filters. Blots were probed with HSPA4, HSPA4L and HSPH1 antibodies. No change in expression levels of HSPA4L and HSPH1 proteins were detected in the heart of *Hspa4*-deficient mice (Fig. 3.31). These results suggest that the loss of *Hspa4* expression in *Hspa4*^{-/-} heart is not compensated for by a detectable increase of the expression of *Hspa4l* and *Hsph1*.

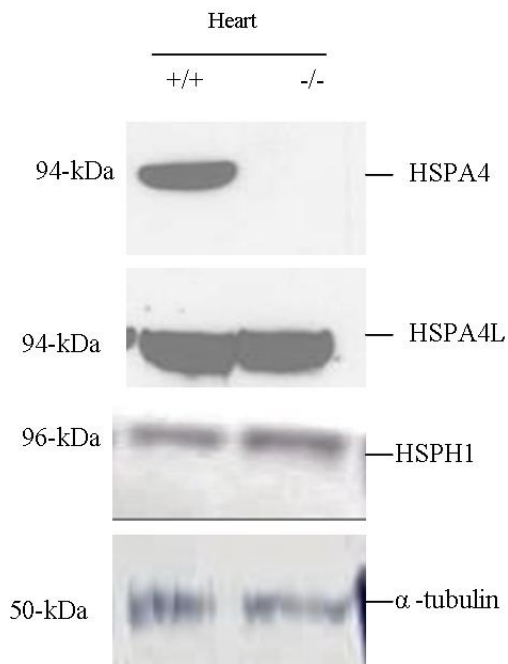


Fig. 3.31. Expression of HSPA4L and HSPH1 in heart of *Hspa4*^{-/-} mice. Western blots with protein extracts from heart of 3-month-old *Hspa4*^{+/+} and *Hspa4*^{-/-} mice were probed with anti-HSPA4, HSPA4L and HSPH1 antibodies. The membranes were stripped and subsequently probed with α -tubulin antibody.

3.2.8 The effect of aging and oxidative stress on expression of HSPA4

At least 11 families of HSPs have been described. Most of them are expressed constitutively or strongly induced by stress conditions such as heat, osmotic or oxidative stress. Expression of other HSPs is induced at certain developmental stages (Bodega *et al.*, 2002). It is also known that biochemical stresses resulting from hypertension, hypoxia and other forms of myocytes injury induce cardiac hypertrophy. Biochemical stresses affect the folding of proteins and cause a progressive loss of cardiomyocytes. Therefore, increased expression of HSP proteins prevents accumulation of misfolded proteins in cells. We have determined whether the expression of HSPA4 is increased in response to different stresses. Firstly, we determined the HSPA4 expression in wild-type heart at different ages. It is known that old hearts are exposed to more stresses than young hearts. Total cellular proteins were isolated from 3-, 6-, 9-, 12-month-old wild-type heart, electrophoresed on SDS-PAGE and transferred onto a nitrocellulose membrane. The Western blot was probed with HSPA4 antibody. Thereafter, the membrane was stripped and subsequently probed with HSP4L antibody. As shown in figure 3.32, the expression of HSPA4 is significantly increased in hearts with advancing age. In contrast, the expression level of HSP4L was not changed with increasing age.

These results lead us to suggest that the upregulation of *Hspa4* in aging heart is linked with accumulation of stress such as oxidative stress. To prove the validity of this hypothesis, the expression of *Hspa4* in heart was studied after paraquat injection, which induces oxidative stress. 3-month-old- wild type mice (n=3) were intraperitoneally injected with paraquat (50 mg/kg body weight). Control mice (n=3) were injected with PBS. Heart tissues were isolated from the mice 7 hrs after injection. Firstly, we checked whether the paraquat treatment induces oxidative stress in heart by analysis of the expression of oxidative stress marker superoxide dismutase [Cu-Zn] (SOD1) and *Gnao1* (G protein binding) by quantitative real time PCR. The results demonstrate that the expression levels of SOD1 and *Gnao1* are increased in heart of paraquat- injected mice compared to untreated mice (Fig. 3.33A, B). This result suggests that paraquat induces the oxidative stress in heart. However, there were no significant differences in the expression levels of *Hspa4* between heart of paraquat-treated and control mice (Fig. 3.33C). These results suggest that *Hspa4* is not induced by oxidative stress.

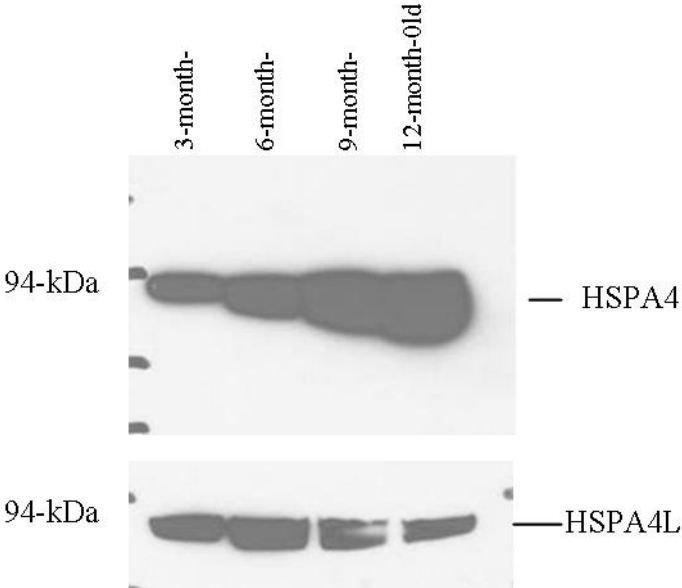


Fig. 3.32. Increased expression of HSPA4 with aging. Western blot of HSPA4 expression in 3-, 6-, 9-, 12 wild-type heart. The membrane was stripped and subsequently probed with anti HSPA4L antibody (B).

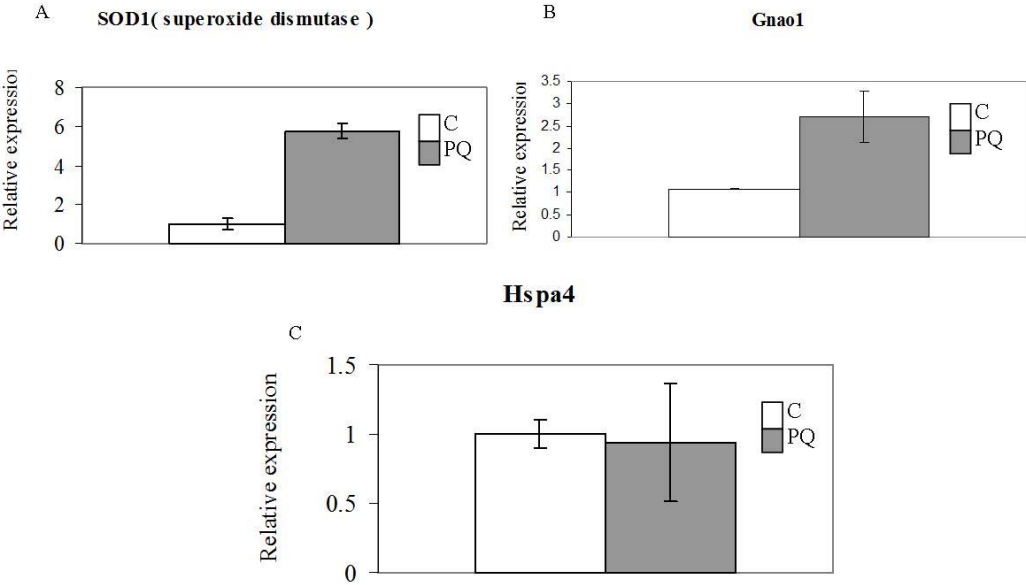


Fig.3.33. Effect of oxidative stress on expression of Hspa4 in heart. Expression of heart SOD1 (A) ,Gnao1 (B), Hspa4(C), genes in 3-month-old wild-type mice after paraquat (PQ) injection measured by real-time PCR . Expression of these genes normalized by Sdha and compared with control (C) without stress.

4. Discussion

4.1 Overview of results of this study

Analysis of *Hspa4* mutant mice in hybrid C57BL/6J x 129/Sv genetic background demonstrated that male infertility is the most apparent phenotype. Number of spermatozoa and their motility in epididymis of infertile *Hspa4*-null mice were found to be drastically reduced, suggesting that spermatogenesis is disrupted (Held, 2008). To identify the spermatogenic stage at which spermatogenesis is affected by *Hspa4* deficiency, testicular sections from different postnatal days were histologically and immunohistologically analysed. The results of these studies revealed that *Hspa4*-deficiency resulted in partial arrest of the first wave of spermatogenesis at the late stage of prophase I. To determine whether the observed loss of germ cells is a result of enhanced apoptosis in *Hspa4*-null mice, Tunnel assay was performed. The results of these analyses indicated that germ cells at meiotic stages appear to be the most affected cells in *Hspa4*-deficient testis. Furthermore, the down-regulation of transcription levels of genes known to be expressed in spermatocytes at late stages of prophase I and post-meiotic spermatids let us suggest to that spermatogenesis is arrested at late stages of meiotic prophase I. These results provide evidence that HSPA4 is required for normal spermatogenesis.

In contrast to *Hspa4* deficiency in the hybrid C57BL/6Jx129/Sv genetic background, most of *Hspa4*-deficient mice with the inbred 129/Sv genetic background display growth retardation and die between the third and fourth week after birth. To identify whether the cause of growth retardation is due to defect in glucose homeostasis, we determined the serum glucose levels during postnatal development. The results showed that a reduction of blood glucose level is only manifested in *Hspa4*^{-/-} animals at age between 22 to 28 days. However, hypoglycemia found in fasted *Hspa4*^{-/-} mice is not due to impaired gluconeogenesis. To address the question whether their growth retardation is a result of malabsorption of lipids in the intestine, expression analyses of apolipoprotein components of chylomicrons (ApoB and ApoAIV) were performed by RNA analysis. The ApoB gene is upregulated in intestine and liver of *Hspa4*^{-/-} mice at postnatal days 20 and 25, while the level of ApoAIV mRNA is higher in intestine of 20- and 25-day-old *Hspa4*^{-/-} mice. The upregulation of both apolipoprotein genes let us to suggest that the proteins in *Hspa4*^{-/-} intestine are unstable. The degradation of both proteins may lead to feedback regulation and upregulation of ApoB and

ApoIV genes. However, Western blot analysis did not show a significant reduction of APOB proteins in *Hspa4*^{-/-} intestine (Held, 2008). These results suggest that the absorption of lipid in *Hspa4*^{-/-} intestine is not affected. We have then determined whether the growth retardation can be due to a defect in growth hormone (GH) signaling. However, normal expression of two GH-responsive genes in liver of *Hspa4*^{-/-} mice excludes the impairment of the GH-signaling in *Hspa4*-deficient mice.

Development of kyphosis in *Hspa4*-deficient mice of advanced age leads us to examine whether these mice suffer from skeletal muscle myopathy. Microscopic examination of different skeletal muscles was carried out on 4-month-old wild-type and *Hspa4*^{-/-} mice. Tibialis anterior, Vastus intermedius and Soleus muscles of *Hspa4*^{-/-} mice were found to display myopathic changes. An abundant pathology was found in paraspinal muscle of 18-month-old mice. These results suggest that myopathy of the paraspinal muscle is a cause of kyphose development in aging *Hspa4*^{-/-} mice. Furthermore, skeletal muscle myopathy was also shown in 13- and 19-day-old Soleus muscle of *Hspa4*^{-/-} mice. This indicates that growth retardation in *Hspa4*^{-/-} mice is a result of skeletal muscle myopathy.

To determine whether skeletal muscle myopathy is also realized in heart as hypertrophic cardiomyopathy, hearts from 12-month-old wild-type and *Hspa4*-deficient mice in the inbred 129/Sv genetic background were subjected to histological analysis. These histological analyses revealed the development of hypertrophic cardiomyopathy and fibrosis in *Hspa4*^{-/-} mice. Further histological analyses revealed that cardiac hypertrophy and fibrosis were first observed in hearts of 2-month-old *Hspa4*^{-/-} mice. Two-dimensional directed M-mode echocardiograms were performed to further confirm the cardiac hypertrophy phenotype. Significant hypertrophy with increase of interventricular septal thickness, left ventricle posterior wall thickness during diastole compared with control littermates was found. Furthermore, the calculated ratio of wall thickness to heart radius at diastole (H/R) was significantly increased in mutant mice, suggesting a concentric pattern of enlargement. Echocardiographic measurement in *Hspa4*-null mice at 17-days of age showed a lower degree of hypertrophy but with a significant increase in septal wall thickness compared with wild-type controls. Ultrastructure analysis revealed myofibrillar disarray and disassembly, abnormal nuclei and increased collagen accumulation (fibrosis) in heart of *Hspa4*^{-/-} mice. To identify when the development of cardiac hypertrophy and fibrosis starts in *Hspa4*^{-/-} heart, we studied expression of marker genes for hypertrophy and fibrosis in hearts from different

postnatal stages by Northern blot and real time PCR analyses. These results indicated that the development of cardiac hypertrophy and fibrosis in *Hspa4*-null mice starts in early postnatal life. We suggest that the early postnatal lethality in *Hspa4*^{-/-} mice in inbred 129/Sv genetic background could be due to the progression of skeletal and cardiac muscle myopathy.

In order to identify the signal pathways that mediate cardiac hypertrophy in *Hspa4*^{-/-} mice, we determined the expression of some genes and proteins, which are involved in Gp130/STAT3, MAPK and calcineurin-NFAT signaling pathways, in heart of wild-type and *Hspa4*^{-/-} mice. The results of these analyses suggest that STAT3 and MAPK signaling pathways are not responsible for the development of cardiac hypertrophy in *Hspa4*-null mice. However, the increased activity of calcineurin/NFAT in *Hspa4*^{-/-} heart can be responsible for modulation of the cardiac hypertrophy.

Microarray analysis was used as a screening tool to identify altered expression in the *Hspa4*-deficient hearts at 25 days compared with that of wild-type mice. 98 genes were identified as differentially expressed. Several genes were selected and classified according to their function in the development of cardiac hypertrophy (Table 3.2). To confirm the results of microarray analysis, quantitative real-time PCR was performed. We confirmed that genes involved in ion channel signaling (*Kcne1*, *Kcnd2*, *Scn4a*, *Hcn1* and *Irx4*), in protection of cells against oxidative stress (*Gnao1*, *Ptp4a1* and *Mme1*) and in inducing oxidative stress (*Maob*) are differentially expressed in heart of *Hspa4*^{-/-} mice as compared to wild-type mice.

Expression analysis of HSPA4L and HSPH1 proteins in *Hspa4*^{-/-} heart was done in order to show whether the expression of these members of HSP110 family are altered in *Hspa4* deficiency. The loss of expression of *Hspa4* in *Hspa4*^{-/-} heart is not compensated for by a detectable increase in the expression of *Hspa4l* and *Hsph1*. It is known that older hearts are exposed to more stress than young hearts. To investigate whether the expression of HSPA4 protein increases with aging, we determined the HSPA4 expression in wild-type heart at different ages. The data showed that the expression level of HSPA4 is significantly increased in hearts with advanced age. This result leads us to examine the expression of *Hspa4* under condition of oxidative stress. Results of this experiment suggest that expression level of *Hspa4* is not induced by oxidative stress.

4.2 The role of HSPA4 for germ cell development

Expression of HSPA4 is widespread in different tissues (Yasuda *et al.*, 1995; Kaneko *et al.*, 1997; Xue *et al.*, 1998). However, the HSPA4 expression is highly enriched in male and female germ cells of prenatal gonads. Expression of HSPA4 in male gonocytes is gradually decreased after their migration to basement layers of seminiferous tubules and differentiation to spermatogonia (Held, 2008). The preferential expression leads us to study the specific role of HSPA4 in germ cell development. Analyses of *Hspa4*-deficient mice revealed that all *Hspa4*-null mice of the hybrid 129Sv X C57Bl/6J background were born at Mendelian ratio and were apparently normal, although expression of HSPA4 can be detected in all tissues of wild-type mice. Male infertility was the most apparent phenotype for *Hspa4*-deficient mice. Male infertility is histologically characterised by a decreased number of postmeiotic germ cells, and an increased number of meiotic and postmeiotic cells undergoing apoptosis. *Hspa4* mutants display an arrest of the first wave of spermatogenesis in juvenile testes by postnatal day 15 when the most advanced germ cells in the testes remain at the late pachytene spermatocyte stage. These results indicate that *Hspa4* deficiency impair the development of most germ cells in late prophase I.

Numerous proteins that are required for the development of male germ cells through meiotic and post-meiotic stages are mostly translated in pachytene spermatocytes (Mons *et al.*, 1999). Failure of molecular chaperones to direct correct folding of newly synthesized proteins in pachytene spermatocytes might lead to accumulation of misfolded and damaged proteins, which would trigger spermatocytes to release meiotic division and initiate apoptosis. Based on the high similarity of HSP110 family members, we expected that the molecular chaperones, which also include the NEF members of HSP110 family, would be abnormal or partially affected in *Hspa4*^{-/-} mice.

The relatively leaky phenotype of *Hspa4*-deficient mice led us to suggest that other members of HSP110 family can partially compensate for the loss of HSPA4 function. HSPA4L and HSPH1 were possible candidates, since both proteins are widely expressed and localized in the cytoplasm like HSPA4. Therefore, compensation for the absence of HSPA4 by HSPA4L and HSPH1 would be the cause that *Hspa4*^{-/-} mice are viable and display normal development except for disruption of spermatogenesis. We tested this possibility by Western blot analysis. However, we did not detect a significant up-regulation of HSPA4L or HSPH1 expression in *Hspa4*^{-/-} testes.

Impaired male fertility was also reported for *Hspa4l*-deficient mice (Held *et al.*, 2006). Thus, approximately 42% of *Hspa4l*^{-/-} male mice suffered from fertility defects. Whereas the

seminiferous tubules of *Hspa4l^{-/-}* testes contained all stages of germ cells, the number of mature sperm in the epididymis and sperm motility was drastically reduced. The reduction of the sperm count was due to the elimination of a significant number of developing germ cells via apoptosis. Partial penetrance and similarity of male infertility phenotype in both *Hspa4* and *Hspa4l* knockout mice prompted us to generate HSPA4 and HSPA4L double knockout mice. Analyses of double knockout mice revealed that the *Hspa4^{-/-}/Hspa4l^{-/-}* mice are dying immediately after birth (Held, 2008). Immunohistological analysis demonstrated that the number of gonocytes in *Hspa4^{-/-}/Hspa4l^{-/-}* testes of E18.5 was not significantly reduced compared to wild-type littermates (data not shown).

The expression of some HSP proteins is inducible by environmental stress, but expression of others can be either constitutive or developmentally regulated (Dix, 1997). The HSPA4L is highly expressed in spermatogenic cells, from late pachytene spermatocytes to postmeiotic spermatids. No HSPA4L could be detected in germ cells of prenatal testis and ovary (Held *et al.*, 2006; unpublished results). In contrast, HSPA4 and HSPH1 are ubiquitously expressed proteins and become relatively enriched in gonocytes after colonization of gonads by primordial germ cells (Held, 2008). The enrichment of both proteins in germ stem cells suggests their significant role for male and female germ cells. The results showed that gonocytes are not affected in *Hspa4*-deficient mice suggesting a redundant function of both proteins in germ cell development. To our knowledge, there is no report describing abnormal spermatogenesis in *Hsph1*-deficient mice. In one study, *Hsph1*-null mice were described as normally fertile (Nakamura *et al.*, 2008). The generation of HSPA4 and HSPH1 double knockout mice will help us to study the role of both proteins in development of germ stem cells in male and female gonads.

Several reports which used microarray analysis to identify preferentially expressed genes in different stem cells revealed that the *Hspa4* is highly expressed in embryonic and different tissue-specific stem cells and its expression is down-regulated in their differentiated counterparts (Ramalho-Santos *et al.*, 2002; Bhattacharya *et al.*, 2004). *Hspa4* was one of 216 enriched genes, which were found to be expressed at high levels in embryonic, neural and hematopoietic stem cells. Our results demonstrating high expression of HSPA4 in gonocytes further confirm the requirement of HSPA4 function for development of germ stem cells. Although the physiological role of molecular chaperones for self-renewal of stem cells is not known, it is believed that molecular chaperones may protect stem cells from aging due to oxidative stress (Ramalho-Santos *et al.*, 2002). *Caenorhabditis elegans* that have an extended life-span have elevated levels of

molecular chaperones and enzymes that process oxidative free radicals and appear to be resistant to environmental stress (Finkel and Holbrook, 2000).

A high incidence of male infertility was found among *Hspa4*-null mice in F2 generation, which contains a high level of inter-individual genetic variability. The decline in incidence of infertility phenotype in subsequent generations would point to a selection bias against that genotype. Therefore, partial penetrance of male infertility among *Hspa4*-null mice may be due to segregation of genetic modifier on the mixed genetic background. Analyses of different mice models revealed the consequence of background-related differences in male infertility phenotypes. Mice deficient for *Tnp2*, mitochondria solute carrier protein (*MSCP*), POU domain class 5 transcription factor 2 (*Sperm-1*), *Hspa4l* and insulin-like 6 (*Insl6*) showed the highest incidence of male infertility in F2 generation and in inbred genetic background (Bitgood *et al.*, 1996; Pearse *et al.*, 1997; Yu *et al.*, 2000; Adham *et al.*, 2001; Nayernia *et al.*, 2002; Burnicka-Turek *et al.*, 2009).

Several reports demonstrated the essential role of other heat shock proteins in the progress of spermatogenesis. Male *Hsp70-2* knockout mice are infertile, whereas females are fertile. Like spermatogenic arrest in *Hspa4*-deficient mice, spermatogenesis of *Hsp70-2*^{-/-} is arrested in prophase I of meiotic division. The number of apoptotic spermatocytes was slightly increased in *Hsp70-2*-mutant mice on postnatal day 15 and increased significantly at P17 (Dix *et al.*, 1997; Mori *et al.*, 1997). According to phenotype similarity between *Hspa4*- and *Hsp70-2*-deficient mice, we suggest that HSPA4 might be a cochaperone of HSP70-2 and the chaperone containing HSP70-2 and HSPA4 has an essential role in repair and clearance of misfolded proteins during meiotic phase of spermatogenesis. To prove this hypothesis, we have to check in the future whether HSPA4 interacts with HSP70-2.

BAT3 is a member of the Bag family that acts as a cochaperone for the heat shock protein HSP70 and is involved in various developmental processes, cellular stress and viability (Corduan *et al.*, 2009). Most *Bat3*-deficient male germ cells die at meiotic prophase I and *Bat3*^{-/-} testes contain increased number of apoptotic germ cells. Interestingly, the testis specific *Hsp70-2* protein was undetectable in *Bat3*-deficient germ cells even though *Hsp70-2* transcript levels were normal. Further experiments revealed that *Bat3* interacts with *Hsp70-2* and this interaction protects *Hsp70-2* from degradation (Sasaki *et al.*, 2008). In yeast, HSP110 proteins are a nucleotide exchange factor for HSP70 proteins. On the basis of the similarity in phenotype

between knockout mice for *Hspa4*, *Hsp70-2* and *Bat3*, we suggest that HSPA4, BAT3 and HSP70-2 cooperate to regulate diverse chaperone-assisted processes in male germ cells at pachytene stage. A depletion of one of these proteins could be a cause for accumulation of damaged proteins and a signal to induce cell death.

In a current study immunostaining with an antibody against synaptonemal complex protein 3 (SYCP3) showed that the formation of synaptonemal complexes in the *Hspa4*^{-/-} meiotic cells was indistinguishable from that in wild-type. In contrast, a higher number of unsynapsed or partially synapsed chromosomes was observed in pachytene spermatocytes of *Bat3*-deficient testis. Immunostaining with anti-phosphorylated histone H2AX antibody, which recognizes DNA double strand breaks, revealed that multiple γ -H2AX-positive foci were observed on paired and unpaired *Bat3*^{-/-} chromosomes (Sasaki *et al.*, 2008). These data indicate that multiple synaptic abnormalities occur in *Bat3*-deficient pachytene spermatocytes. HSP70-2 has been found to associate with the lateral element of the synaptonemal complex (SC) (Allen *et al.*, 1996). Although SC assembled in early pachytene stage of *Hsp70-2*^{-/-} mice, later studies showed that SC was fragmented at late pachytene stage. Immunostaining of wild-type pachytene spermatocytes with anti-HSPA4 antibody revealed that HSPA4 protein is not associated with SC. These data suggest that HSPA4 is not involved in the regulation of chromosome dynamics during meiosis.

The expression of heat shock *Hsc70t* gene is restricted to post-meiotic spermatids (Zakeri and Wolgemuth, 1987; Maekawa *et al.*, 1989; Matsumoto and Fujimoto, 1990). *Hsc70t*^{-/-} male mice have normal fertility and histological studies indicated that germ cell development during the late postmeiotic phase was not affected. However, ATP levels are low in the sperm of *Hsc70t*-deficient testis and their ability to produce ATP appears to be compromised. This suggests that HSC70t possesses unique chaperone capabilities that are required by postmeiotic germ cells for the assembly and function of protein complexes involved in energy production (Eddy, 2002).

4.3 Potential role of *Hspa4* in regulation of cell cycle

Arrest of spermatogenesis during meiosis lead us to suggest that *Hspa4* has a role in control of cell cycle during meiotic division. Among the most well established heat shock effects on cell cycle kinetics are the transient arrests of cells at the G1/S or G2/M border (Kühl and Rensing, 2000). During cell cycle, chaperones play an important stabilizing role. They associate with cell cycle or signal proteins in order to translocate them to their targets, to keep them in a required conformational state, or to eliminate degraded or mutated forms (Sato and Torigoe,

1998). It has been reported that HSPA4 regulates cell cycle by competing the transcription factor ZONAB for binding to the SH3 domain of ZO-1. As a result of a dissociation of ZONAB/ZO-1, ZONAB is translocated to the nucleus where it regulates G1/S phase progression (Fig. 4.1).

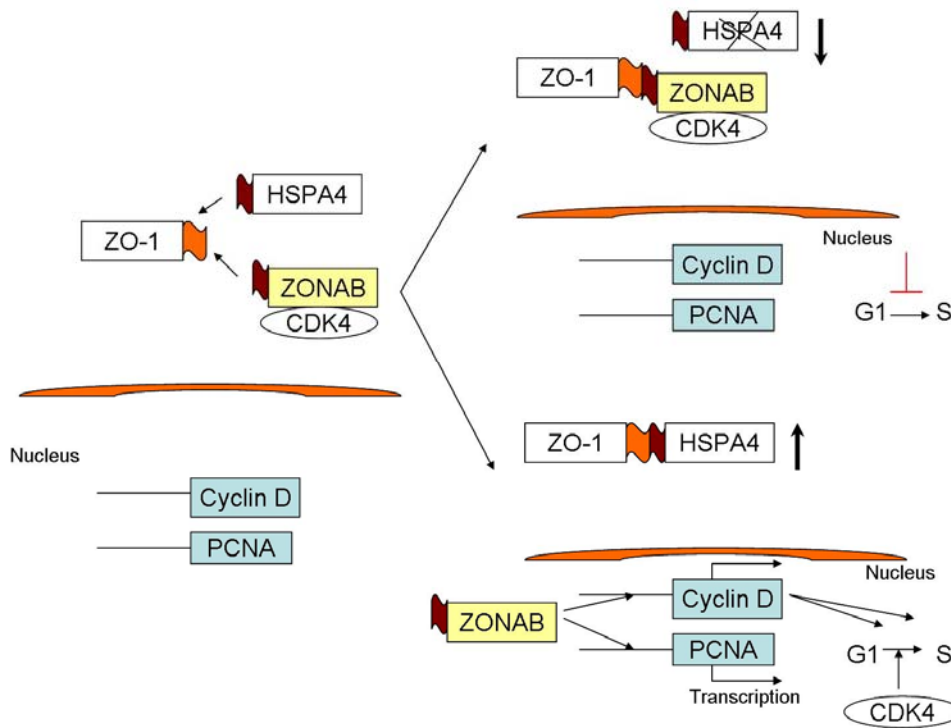


Fig. 4.1. Potential function of HSPA4 as a regulator of cell cycle. HSPA4 compete with ZONAB for binding to the SH3 domain of ZO-1. At low level of HSPA4 or during binding of HSPA4 with HSP70 chaperone, ZO-1 binds to ZONAB. This interaction accumulates ZONAB in cytoplasm and arrest the cell cycle at G1 phase. At high level of HSPA4 or when the process of folding and correct the misfolded protein successfully completed during the G1 phase, HSPA4 releases the HSP70 chaperone and then binds to ZO-1 resulting in dissociation of ZONAB from ZO-1. Subsequently, ZONAB interacts then with CDK4 and ZONAB-CDK4 translocates from cytoplasm to nucleus. In nucleus, ZONAB-CDK4 regulates G1/S phase transition by transcriptional regulation of cyclin D1 and the initiation of DNA replication by transcriptional regulation of replication factors, such as PCNA (modified from Sourisseau et al., 2006; Tsapara et al., 2006).

ZONAB affects cell cycle progression by two distinct mechanisms. Firstly, it regulates the nuclear accumulation of the cell division kinase CDK4 via a direct interaction. Second, it regulates expression of genes encoding cell cycle regulators such as PCNA and cyclin D1 (Balda *et al.*, 2003; Sourisseau *et al.*, 2006). These data lead us to suggest that during binding of HSPA4 with HSP70 chaperone and their function to correct the misfolding proteins and folding of new synthesized proteins. ZO-1 binds to and keeps ZONAB inactive in the cytosol. Thus, inhibition of nuclear accumulation of ZONAB by its binding with ZO-1 reduces the nuclear pool of CDK4. A consequence of that is the inhibition of G1/S phase progression. When the process of folding and correction of misfolded proteins is successfully completed, HSPA4 translocates to plasma membrane and binds to ZO-1. Then, ZONAB interacts with CDK4 and this complex ZONAB - CDK4 codistributed to the nucleus, where they promoted G1/S phase transition. We expected that percentage of cells in S phase would be decreased in *Hspa4*-mutant testis as a result of cytosol accumulation of ZONAB and missfolded proteins. The arrest of cell cycle at G1 phase might be triggered the spermatocytes to initiate apoptosis.

4.4 The cause of growth retardation in *Hspa4*-deficient mice

In several mouse models, growth retardation in early postnatal development has been shown to be a result of defect in growth hormone signaling. Growth hormone (GH), acting through its receptor (GHR), is essential for somatic growth, development and maintaining metabolic homeostasis. Growth hormone receptor-deficient ($GHR^{-/-}$) mice exhibit proportional growth retardation and drastically diminished insulin-like growth factor- (IGF-1) levels (Robertson *et al.*, 2006). Insulin-like growth factor-I (*Igf-1*)-deficient animals have severe growth deficiency, organ hypoplasia and diminished survival (Baker *et al.*, 1993; Liu *et al.*, 1993; Powell-Braxton *et al.*, 1993; Liu *et al.*, 1998; Wang *et al.*, 1999). In addition, hepatocyte nuclear factor 1 α (HNF-1 α) is required for postnatal growth and development in mice. Growth retardation in *Hnf-1* α null mice was found to be due to downregulation of growth hormone -responsive genes that are crucial for growth and development (Lee *et al.*, 1998). Therefore, HNF-1 α -related growth retardation results from a defect in the GH signaling (Lin *et al.*, 2008). To determine whether the growth retardation of *Hspa4*^{-/-} mice is due to defect in GH-signaling, we analyzed the expression of two GH- responsive genes, Amyloid P component (APCS) and solute carrier organic anion transporter family, member 1b2 (SLCO1B2), in liver of wild-type and *Hspa4*^{-/-} animals. The results suggested that GH-signaling is not altered in *Hspa4*^{-/-} mice.

Other mouse models reveal that growth retardation is due to malabsorption of lipids in the intestine. Fat malabsorption is one of several causes, which are contributing to growth retardation in glial cell line–derived neurotrophic factor family receptor $\alpha 2$ (*Gfra2*)-null mice (Rossi *et al.*, 2003). During fat absorption in the intestine, luminal digestion products of dietary fats are absorbed across the microvillus border of the enterocyte. Apolipoprotein B (apoB) and apo AIV are known to have a particularly critical role in the assembly of the triglyceride-rich lipoproteins. (Young, 1990; Havel and Kane, 1995; Kane and Havel, 1995). ApoA-IV may physically interact with ApoB in the secretory pathway to modulate the process of triglyceride-rich lipoprotein assembly and secretion (Gallagher *et al.*, 2004). The chylomicron-deficient mice lack all apoB expression in the intestine, which prevents the assembly and secretion of TG-rich lipoproteins from the intestine. These mice accumulate massive amounts of cytosolic fat droplets within the absorptive enterocytes of the intestine and manifest severe intestinal fat malabsorption and -retarded growth (Young *et al.*, 1995). To address the question whether growth retardation in *Hspa4*-deficient mice is due to lipid malabsorption, we determined the expression levels of ApoB and ApoAIV in liver and intestine of *Hspa4*^{-/-} and wild-type. This expression analysis indicated that ApoB mRNA level is upregulated in intestine and liver of *Hspa4*^{-/-} mice, while ApoAIV is higher in intestine of *Hspa4*^{-/-} mice compared with wild-type animals. However, Held (2008) found in Western-blot analysis that the ApoB levels markedly reduced in *Hspa4*^{-/-} intestine. It has been reported that yeast HSP110, SSE1p, associates with and stabilizes ApoB (Hrizo *et al.*, 2007). These results suggest that HSPA4 might stabilize ApoB and overexpression of ApoB gene in *Hspa4*^{-/-} mice is due to feedback regulation of ApoB gene in a consequence of ApoB degradation.

4.5 Role of *Hspa4* in skeletal muscle development

Mammalian skeletal muscle consists of multinucleated myofibers which are formed during development by fusion of mononucleated muscle progenitors, some of which remain associated to adult myofibers as satellite cells, which is a specific type of stem cells (Ciciliot and Schiaffino, 2010). Adult skeletal muscle fibers are terminally differentiated. Muscle growth and regeneration are accomplished by proliferation of satellite cells. In the unperturbed state, satellite cells remain in a nonproliferative, quiescent state. However, in response to stimuli such as myotrauma, satellite cells present around the damaged muscle become activated, proliferate, and

resulting myoblasts express myogenic markers (Fig. 4.2). Ultimately, these myoblasts fuse to existing muscle fibers or fuse together to form new myofibers during regeneration of damaged skeletal muscle (Bischoff *et al.*, 1994; Schultz, 1996).

Several knockout mouse models display growth retardation, which is a result of skeletal muscle myopathy. Analysis of these mouse models revealed that the skeletal muscle myopathy is either due to severe muscle degradation, impaired muscle regeneration or both. Severe muscle degradation was the main cause for the postnatal growth retardation of knockout mice for *Bag3*, serum response factor (SRF) and mammalian target of rapamycin (mTOR), respectively. Similar to skeletal muscle myopathy observed in *Hspa4*-deficient mice, *Bag3*^{-/-} mice cease to gain weight after postnatal day 12 and die. Skeletal muscle of *Bag3*^{-/-} animals showed a marked variation in myofiber size, with evidence of atrophic fibers characterized by non inflammatory myofibrillar degradation with apoptotic features (Homma *et al.*, 2006). Few centrally located nuclei were found in *Bag3*^{-/-} myofibers, suggesting absence of a regenerative response. In contrast, myofibers with centrally located nuclei can be detected in *Hspa4*^{-/-} mice suggesting a regenerative response in *Hspa4*^{-/-} mice following muscle degradation. However, we have not determined in this work whether the growth retardation of the *Hspa4*^{-/-} is due to severe muscle degradation or impairment in the process of muscle regeneration. The mTOR knockout mouse displays severe skeletal muscle myopathy, displaying features of muscle dystrophy and metabolic myopathy leading to decreased growth rate, which starts at 4 weeks of age. By the age 13 week, mutant mTOR mice start to develop spinal deformity (kyphosis), a sign of muscle weakness, and most mutants eventually die between 22 and 28 weeks of age (Risson *et al.*, 2009).

Impaired regeneration capacity is the cause for growth retardation in a number of gene knockout mouse models such for melanoma antigen, family D, 1 (*Maged1*), tetradecanoyl phorbol acetate-induced sequence 7 gene (*Tis7*) and for forkhead/winged helix transcription factor (*Foxk1/Mnf*). *Maged1* deficiency results in defective cell cycle exit and impaired myotube maturation (Nguyen *et al.*, 2010). While disruption of the *Tis7* gene delayed muscle regeneration (Vadivelu *et al.*, 2004). *Foxk1*^{-/-} mice display growth retardation and a severe impairment in skeletal muscle regeneration following injury. Such impairment in muscle regeneration in *Foxk1*^{-/-} skeletal muscle is due to a reduction in number of satellite cells and arrest cell cycle progression at G0/G1 phase (Hawke *et al.*, 2003). It is possible according to the hypothesis (Fig 4.1) that the competition between the HSPA4 and ZONAB to bind with ZO-1 may be regulated

the transition of cell cycle at G1/S phase of proliferated satellite cells and the HSPA4 depletion results in a G1/S arrest in significant number of proliferated satellite cells. Other possibility that the *Hspa4*-deficiency delays the withdrawal of myoblasts from the cell cycle to differentiation. ZO-1 is a tight junction adaptor protein that regulates gene expression and junction assembly. Aijaz *et al.* (2007) have reported that the interaction of HSP4A with ZO-1 is also important for junction formation and epithelial morphogenesis. Thus, depletion of HSPA4 in Madin-Darby canine kidney epithelial cells (MDCK) retards junction assembly and inhibits epithelial morphogenesis. On the basis on these data, we propose that *Hspa4* deficiency may impair the fusion of myogenic cells during skeletal muscle regeneration and formation of new myofibers.

4.6 Development of cardiac hypertrophy in *Hspa4*-deficient mice.

Cardiomyocytes are terminally differentiated cells and lose their ability to proliferate soon after birth. Thereafter, cardiomyocytes grow in cell size without cell division to adapt to a demand for an increased workload. In a number of pathological conditions (eg, hypertension, valvular disease, myocardial infarction, and cardiomyopathy) that impose overwork on the heart, postnatal cardiomyocytes undergo cardiac hypertrophy. Although cardiac hypertrophy is initially compensatory for an increased workload, prolongation of this process leads to congestive heart failure, arrhythmia, and sudden death (Levy *et al.*, 1990; Lorell and Carabello, 2000). Cardiac myocyte hypertrophy is associated with changes in gene expression including increased expression of immediate early genes (e.g. *c-jun*, *c-fos* and *egr1*), heat shock protein genes (such as *Hsp70* and *CryAB*) and re-expression of fetal genes for atrial natriuretic factor (*Anf*), brain natriuretic peptide (*Bnf*), β -myosin heavy chain 7 (*Myh7*) and skeletal α actin 1 (*Acta1*). High expression of these fetal genes in heart has been used as indices of hypertrophy (Hoshijima and Chien, 2002; Dorn *et al.*, 2003; Kumarapeli *et al.*, 2008). Our RNA analysis revealed that expression levels of hypertrophic markers *Anf*, *Myh7* and *Acta1* are increased in *Hspa4*-null heart at postnatal day 15 compared with control littermates. Thereafter, a significant increase in expression levels of hypertrophic markers was observed through the postnatal developmental stage of *Hspa4*-deficient hearts. These results revealed that cardiac hypertrophy develops in the heart of young *Hspa4*-deficient mice.

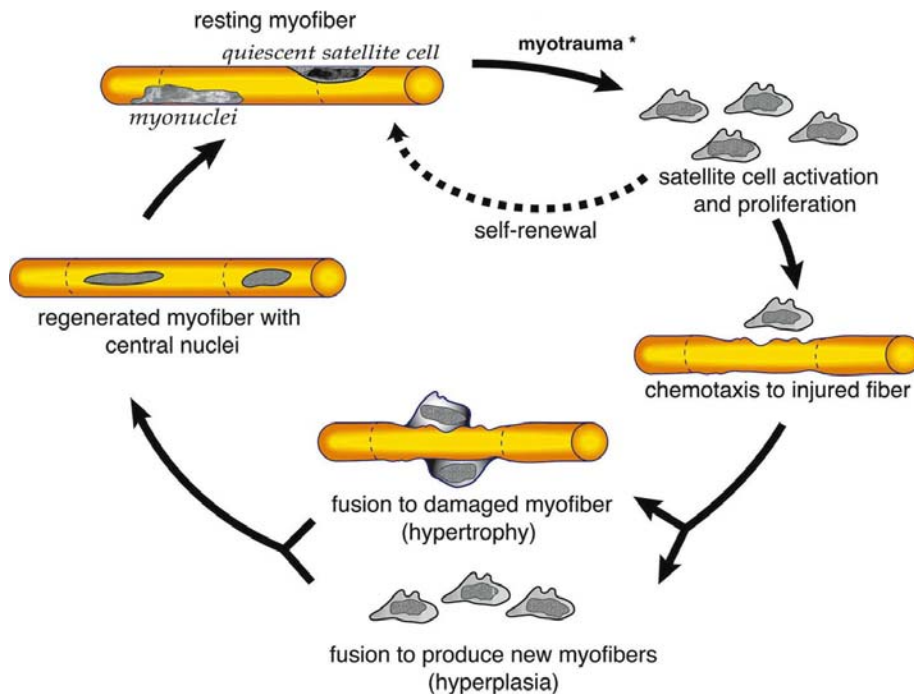


Fig. 4.2 Satellite cell response to myotrauma. Skeletal muscle trauma or injury may be minor - (e.g., resistance training) or may be more extensive (e.g., toxin injection, Duchenne muscular dystrophy). In response to an injury, satellite cells become activated and proliferate. Some of the satellite cells will reestablish a quiescent satellite cell pool through a process of self-renewal. Satellite cells will migrate to the damaged region and, depending on the severity of the injury, fuse to the existing myofiber or align and fuse to produce a new myofiber. In the regenerated myofiber, the newly fused satellite cell nuclei will initially be centralized but will later migrate to assume a more peripheral location (Hawke and Garry, 2001).

There are different stress pathways that modulate cardiac hypertrophy, such as P13k/GSK-3, dependent MAPK/ERK, IL6/gp130/STAT3 and calcineurin/NFAT signaling pathway (Ruwhof and van der Laarse, 2000; Frey and Olsen, 2003; Baines and Molkentin, 2005; Hill and Olson., 2008). To determine the molecular pathway which is responsible for the development of cardiac hypertrophy in *Hspa4*-null mice, we determined the activities of signaling pathways in heart of *Hspa4*-deficient mice.

4.6.1 MAPK/ERK signaling pathway

Mitogen-activated protein kinase (MAPK) signaling pathways consist of a sequence of successively acting kinases that ultimately result in the dual phosphorylation and activation of terminal kinases such as p38, c-Jun N-terminal kinases (JNKs), and extracellular signal-regulated kinases (ERKs) (Widmann *et al.* 1999). MAPK pathways provide an important link between external stimuli and the nucleus via phosphorylation and regulation of multiple transcription factors. The MAPK signaling cascade is initiated in cardiac myocytes by G protein-coupled receptors (angiotensin II, endothelin-1, and adrenergic receptors) and cardiotrophin-1 (gp130 receptor), and by stress stimuli (Sugden and Clerk 1998). Once activated, p38, JNKs and ERKs each phosphorylate of a wide array of intracellular targets that includes numerous transcription factors resulting in the reprogramming of cardiac gene expression as part of the hypertrophic program (Bueno and Molkentin., 2002) (Fig. 4.3). The ERK family members, ERK1 (p42) and ERK2 (p44), are directly phosphorylated by two MAPK kinases, MEK1 and MEK2 (Garrington and Johnson 1999). Transgenic overexpression of MEK1, that activates ERK1/2, results in considerable cardiac hypertrophy (Bueno *et al.*, 2000). Glennon *et al.*, (1996) demonstrated that antisense oligodeoxynucleotides against the ERK isoforms p42 and p44 inhibited the morphological changes of hypertrophy in cardiomyocytes exposed to phenylephrine. MAPK/ERK signaling was found to mediate cardiac hypertrophy in several mouse models (Table 4.1). Deletion of *Smad4*, which is the central intracellular mediator of TGF β signaling, resulted in cardiac hypertrophy and fibrosis. Phosphorylated extracellular signal-regulated kinase (ERK) 1/2 and mitogen-activated protein kinase-ERK (MEK) 1 were increased in the *Smad4* mutants (Wang *et al.*, 2005). To investigate whether the activation of MAPK signaling is responsible for development of cardiac hypertrophy in *Hspa4*-null mice, we analyzed the expression of ERK 1/2 and phospho-ERK1/2. Our study showed that MAPK/ERK signaling is not activated in heart of

Hspa4^{-/-} mice.

Table 4.1. Activated signal pathway in different mouse models for cardiac hypertrophy

<i>Knockout mice</i>	<i>Activated signaling pathways</i>
Natriuretic peptides receptor1 (<i>Npr1</i> ^{-/-})	calcineurin–NFAT (Ellmers <i>et al.</i> , 2007)
α B-crystallin (CryAB) /Hspb2 <i>CryAB</i> ^{-/-} / <i>Hspb2</i> ^{-/-}	calcineurin-NFAT pathway (Kumarapeli <i>et al.</i> , 2008)
cardiac myosin binding protein C (<i>cMyBP-C</i> ^{-/-})	MAPK pathway including JNK, p38-MAPK but not ERK pathway (Eijssen <i>et al.</i> , 2008)
Heat shock protein 70 (<i>Hsp70</i> ^{-/-})	JNK, p38-MAPK, and Raf-1/ERK. (Kim <i>et al.</i> , 2006)
Forkhead box transcription factor, O3 (<i>Foxo3</i> ^{-/-})	Calcineurin/NFAT signaling (Ni <i>et al.</i> , 2006)
Neurofibromatosis type 1 (<i>Nf1</i> ^{-/-})	Ras-Erk pathway (Xu <i>et al.</i> , 2009)
Mitogen-activated protein kinase kinase (<i>Mkk4</i> ^{-/-})	JAK-calcineurin-NFAT signaling pathway (Liu <i>et al.</i> , 2009)
Ras associated with diabetes GTPase (<i>rad</i> ^{-/-})	CaMKII pathway (Chang <i>et al.</i> , 2007)
Profilin 1 (<i>Pfn1</i> -TG)	JNK and ERK pathways (Moustafa-Bayoumi <i>et al.</i> , 2007)
Adiponectin (<i>Adipoq</i> ^{-/-})	ERK signaling pathway (Shibata <i>et al.</i> , 2004)
The Insulin-like Growth Factor 1 Receptor (IGF1R-TG)	PI3K pathway and the mitogen-activated protein kinase (MAPK) pathway (McMullen <i>et al.</i> , 2004)
mothers against decapentaplegic homolog 4 (<i>Smad4</i> ^{-/-})	MEK1–ERK1/2 signaling (Wang <i>et al.</i> , 2005)

angiotensin converting enzyme 2 (<i>Ace2</i> ^{-/-})	AT1-ERK1/2, JNK1/2 and p38 pathways (Oudit <i>et al.</i> , 2007)
--	--

4.6.2 IL-6-gp130-STAT3 signalling pathway

Activation of the JANK/STAT pathway by overload was found to be mediated by glycoprotein 130 receptor (gp130), and at least cadiotrophin-1(CT-1) and IL-6 were involved in activation of this pathway (Pan *et al.*, 1997). Binding of ligands (i.e. member of interleukin (IL)-6 family such as IL-6 and CT-1) to gp130 receptor, leads to formation of dimers of gp130 and activated JAKs (Kishimoto *et al.*, 1994). As presented in figure 4.4, STAT factors bind to certain phosphotyrosines of gp130, leading to phosphorylation by JAK. Phosphorylated STAT factors form homo- and hetero- dimers, and translocate to the nucleus, where they induce gene expression (Kamimura *et al.*, 2003). It has been found that induction of gp130-dependent signaling leads to activation of both MAPK and JAK/STAT pathways (Hoshijima and Chien., 2002). Specifically, STAT3 is translocated to the nucleus in response to gp130 activation, which results in the induction of genes involved in hypertrophy and survival pathways (Yamauchi-Takahara and Kishimoto, 2000). Overexpression of STAT3 in transgenic mice is sufficient to induce cardiomyocyte hypertrophy in vitro (Kunisada *et al.*, 1998) and in vivo (Kunisada *et al.*, 2000). Eijssen *et al.* (2008) reported that the lack of the cMyBP-C protein resulted in cardiac hypertrophy, which is mediated by activation of the gp130/STAT3 and MAPK signaling pathways. We examined whether STAT3 activation is involved in cardiac hypertrophy in *Hspa4*-mutant mice. Protein analysis revealed that the levels of phosphorylated STAT3 in *Hspa4*^{-/-} hearts are not significantly different from that in wild-type. This data suggest that gp130/STAT3 pathway is not involved in development of cardiac hypertrophy of *Hspa4*^{-/-} mice.

4.6.3 Calcineurin/NFAT signaling pathway

Neuroendocrine factors such as angiotensin II (Ang II) and endothelin-1 (ET-1) can stimulate G protein-coupled receptors (GPCRs). GPRCRs are typically coupled to G proteins, which lead to elevation of interacellular Ca²⁺. An increase in cytoplasmic Ca²⁺ binds to calmodulin and activates calcineurin, which can dephosphorylate NFATs (nuclear factors of activated T-cells) (Fig. 4.5). Dephosphorylated NFATs migrate into the nucleus and promotes gene expression.

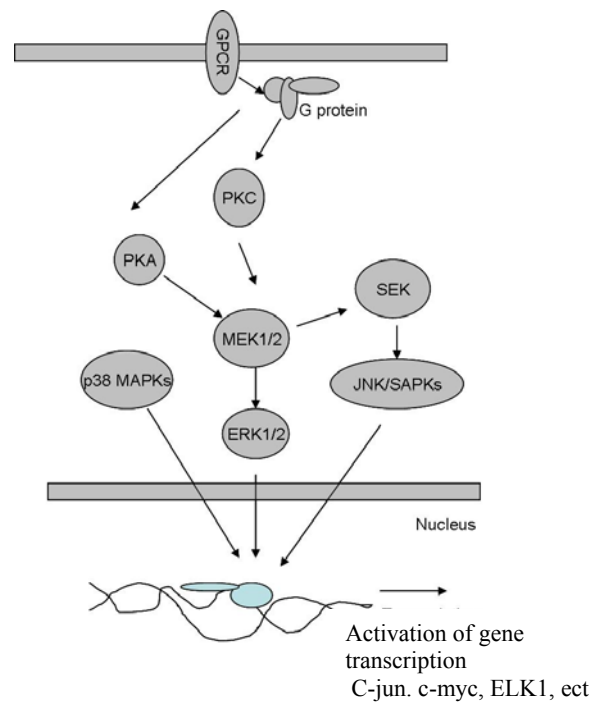


Fig. 4.3 Schematic representation of the activation of MAPK pathway. Activation of specific MAPKs involves highly regulated and modulated cascades of phosphorylation events mediated by sequential and concerted activation of upstream kinases. ERKs are phosphorylated by members of the MEK family; JNK/SAPKs and p38 MAPKs are phosphorylated by SEKs and MKKs.

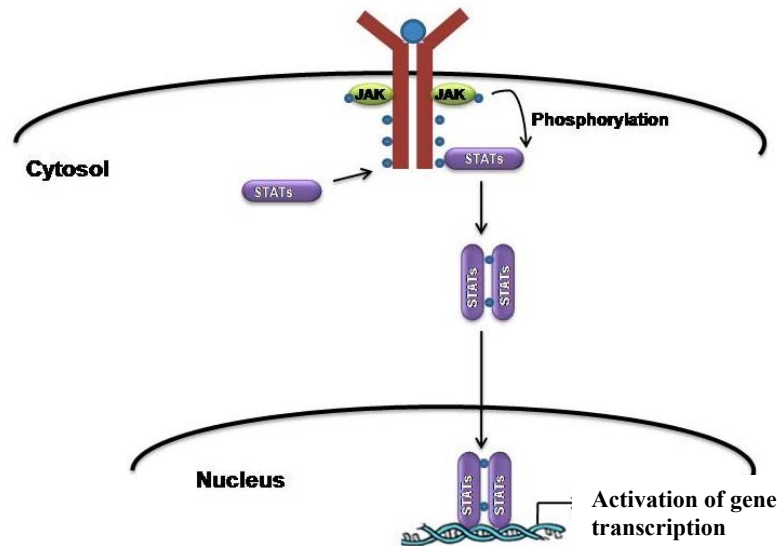


Fig. 4.4. Binding of ligands to their cytokine receptors, such as cardiotrophin-1 (CT-1) leads to phosphorylation and activation of receptor-JAK complex with subsequent recruitment of STATs. Activated STATs migrate into the nucleus, and bind to promoters of targeted genes and stimulate gene transcription (Ruwhof and van der Laarse, 2000).

Genetic manipulation of signaling pathways in mice and biochemical analyses have shown that calcium/calmodulin (Ca^{2+} /Calm)-dependent signaling plays a pivotal role in pathological cardiac hypertrophy (Wilkins *et al.*, 2004). NFAT and GATA4 cooperatively activate transcription of hypertrophic gene program, including *Anf* and *Bnf* genes. *Anf* and *Bnf* may create negative-feedback loop that suppress calcineurin activity (Tokudome *et al.*, 2005). Deletion of several genes such as *Npr1*, *CryAB/HspB2*, *Foxo3* and *Mkk* in mice leads to activate calcineurin/NFAT signaling and induces hypertrophic responses (summarized in table 4.1) (Ni *et al.*, 2006; Ellmers *et al.*, 2007; Kumarapeli *et al.*, 2008; Liu *et al.*, 2009). In our current study we have determined whether the inactivation of the *Hspa4* gene stimulates the activity of calcineurin-NFAT signaling pathway. Expression analysis revealed that calcineurin/NFAT pathway is significantly activated in *Hspa4*^{-/-} heart.

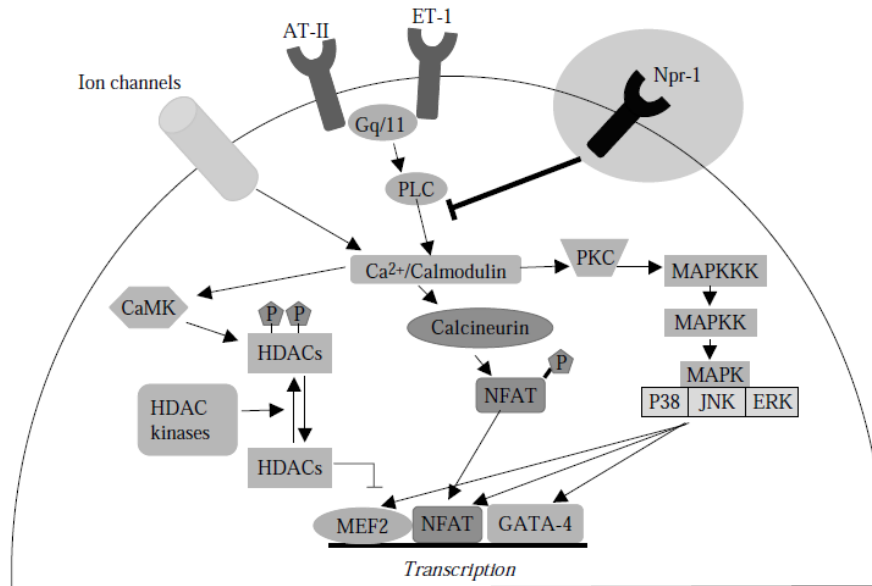


Fig 4.5 Calcineurin/NFAT signaling pathway. Activation of G protein-coupled or mechanical stretch receptors leads to an elevation of intracellular Ca²⁺ and activation of the calmodulin-regulated phosphatase, calcineurin. Calcineurin activation causes nuclear localization of NFAT transcription factors by direct dephosphorylation. Calcineurin also directly activates nuclear MEF2 factors. These factors, along with GATA-4 and other partners cooperatively activate transcription of the hypertrophic gene programme (Wilkins and Molkenin, 2002).

Endothelin 1 (ET-1), a potent vasoconstrictor peptide expressed by endothelium, is also upregulated in the heart in response to a variety of stresses (Shohet *et al.*, 2004). ET-1 activates two G-protein-coupled receptors, endothelin A (ET_A) and endothelin B (ET_B), with approximately equal affinity (Arai *et al.*, 1990, Sakurai *et al.*, 1990). The binding of ET-1 to both ET_A and ET_B receptors in cardiomyocytes results in activation of G protein signaling and increased intracellular calcium (Beyer, *et al.*, 1995). ET-1 and its receptors mediate stress-induced remodeling in the mammalian heart. In vitro experiments show that ET-1-mediated activation of either ET_A or ET_B receptors on cardiomyocytes results in cellular hypertrophy (Ito *et al.*, 1993a; Cullen *et al.*, 2001). ET-1 acts as a local factor involved in cardiac and craniofacial development, as well as in the regulation of cardiac contractility and hypertrophy (Kedzierski and Yanagisawa 2001). It has been reported that ET-1 stimulates the accumulation of *Hsp 27* (Kawamura *et al.* 1999) and *Hsp70* (Pan *et al.*, 2004). In our present study, ET-1, ET_A and ET_B

expression levels were markedly increased in heart of *Hspa4*-null mice at 3 months. We suggest that HSPA4 protect cells against deleterious stimuli after induction of ET-1 in response to stress.

Calmodulin1 (CALM) is a small cytoplasmic Ca^{2+} binding protein that regulates numerous cellular activities. CALM may exert its action through a direct interaction with its target proteins or indirectly by regulating the activity of Ca^{2+} /CALM-dependent protein kinase and CALM stimulated protein phosphatase (calcineurin) (Maier and Bers, 2002; Saimi and Kung, 2002). *Calm* transgenic (*Calm*-TG) mice develop marked cardiac hypertrophy and exhibit up-regulation of calcineurin, atrial natriuretic factor (ANF) and β -myosin heavy chain gene expression in the heart during the first 2 weeks after birth (Obata *et al.*, 2005). In the present study calmodulin 1 expression level was found to be upregulated in heart of 3-month-old *Hspa4*^{-/-} mice. We suggest that calmodulin, which is a central mediator of several hypertrophic-signalling pathways, mediates the cardiac hypertrophy that occurs in response to the lack of *Hspa4*.

The activity of calcineurin is influenced by cofactors known as modulatory calcineurin-interacting proteins (MCIPs) or calcipressins (Rothermel *et al.*, 2003). MCIP1 is upregulated by calcineurin signaling and has been proposed to function in a negative feedback loop to modulate calcineurin activity (Vega *et al.*, 2003). The MCIP1.4 isoform has been shown to be tightly controlled by an alternative promoter containing 15 cis-acting elements of transcription factor NFAT cis-acting elements in the intron located upstream of MCIP1 exon 4 (Yang *et al.*, 2000). MCIP1.4 expression can serve as a functional surrogate for calcineurin activity (van Rooij *et al.*, 2004). Because MCIP1.4 is a target gene for activated NFAT transcription, MCIP1.4 expression is a better marker for calcineurin activity than calcineurin protein level (Ni *et al.*, 2006). Calsarcin-1 overexpression in transgenic mice prevents AngII-induced cardiomyocyte hypertrophy via inhibition of calcineurin signaling, which results in downregulation level of MCIP1.4 (Frank *et al.*, 2007). In addition, mice lacking calsarcin-1 are sensitized to calcineurin signaling and show accelerated cardiomyopathy in response to pathological biomechanical stress (Frey *et al.*, 2004). Foxo proteins decrease calcineurin phosphatase activity and repress both basal and hypertrophic agonist-induced expression of MCIP1.4. Furthermore, hearts from Foxo3-null mice exhibit increased MCIP1.4 abundance and a hypertrophic phenotype (Ni *et al.*, 2006). We have found that expression levels of MCIP1.4 is increased 15-fold in heart of 3-month-old *Hspa4*^{-/-} mice compared to wild type mice. These results indicate that activation of calcineurin-NEFAT signaling is responsible for development of cardiac hypertrophy in *Hspa4*-deficient

mice.

Activated NFAT transcription factor induces in collaboration with transcription factor *Mef* and GATA4 the expression of hypertrophic genes such *Anf*, *Bnf* and *Myh7* (Akazawa and Komuro, 2003). In current study, RNA analysis revealed the significant increase in expression of *Mef2* and GATA4 in the heart of *Hspa4*^{-/-} mice

Histone deacetylases (HDACs) regulate chromatin remodeling. Phosphorylation of class II HDACs are regulated by various signal-transduction pathways. For example prohypertrophic signals modify HDAC kinases such as protein kinase D (PKD), PKC and Calm Kinase, which phosphorylate HDACs, resulting in their subsequent nuclear export. Histone deacetylases (HDACs) have been shown to associate with and repress MEF2 activation (Miska *et al.*, 1999; Lu *et al.*, 2000a, b; Youn *et al.*, 2000). In hypertrophic heart of Calm kinase IV transgenic mice, MEF2 activation was suggested to occur through phosphorylation and dissociation of class II HDACs from MEF2 (Passier *et al.*, 2000; Zhang *et al.*, 2007). Ellmers *et al.* (2007) showed that *Hdac 7a* expression was increased in hypertrophic heart of *Npr1*^{-/-} males. Here the Expression level of *Hdac 7a* was increased in RNA of *Hspa4*-null hearts at 18 days and 3 months. This finding let us suggest that calmodulin and its kinase contribute to cardiac hypertrophy in *Hspa4*-null hearts through nuclear export of HDAC7 by phosphorylation and MEF2 transcription factors activation. Finally figure 4.6 gives our proposal for a pathway that modulates the cardiac hypertrophy of *Hspa4*^{-/-} mice.

4.6.4 Cardiac fibrosis in *Hspa4*^{-/-} mice

Cardiac fibrosis is a classical feature of hypertrophy and is characterized by the expansion of the extracellular matrix due to the accumulation of collagen, particularly collagen types I and III (Manabe *et al.* 2002). TGF- β stimulates fibroblast growth, enhances collagen synthesis, and suppresses collagen degradation (Mehta and Attramadal, 2007). TGF- β is an important mediator of cardiac hypertrophy induced by Ang II (Williams, 2001; Schultz *et al.*, 2002). It plays an important role in myofibroblast differentiation during wound healing and fibrocontractive diseases by regulating the expression of alpha-SM actin in these cells (Desmoulière *et al.*, 1993). In our study, collagen 1, collagen II and TGF- β expression levels were markedly increased in 3-month *Hspa4*^{-/-} animals, but were not apparent in the heart of 18 day-old mice.

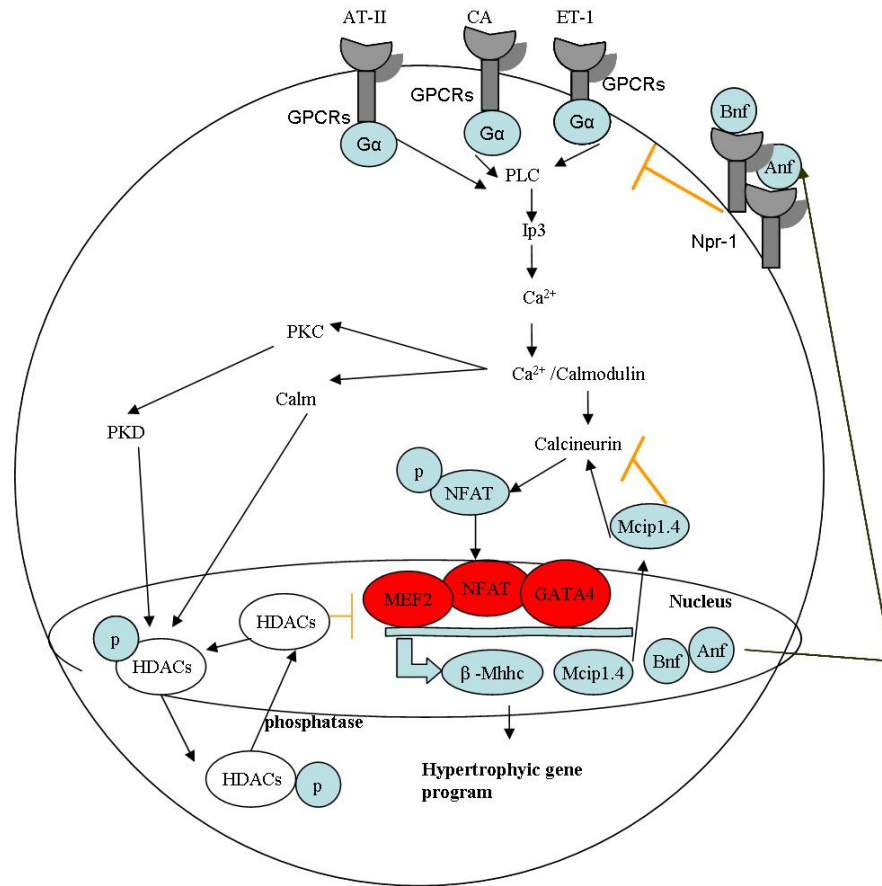


Fig. 4.6 Schematic representation of our proposal signaling pathways contributing to cardiac hypertrophy in *Hspa4*-null mice. Hypertrophic stimuli acting via the α subunit of guanine nucleotide-binding proteins after binding of G protein-coupled receptors (GPCRs), recruit PLC β to the membrane, where it hydrolyses phosphatidylinositol 4,5 bisphosphate (PIP₂), releasing inositol 1,4,5-triphosphate (IP₃) and diacylglycerol (DAG). IP₃ binds to receptors in the sarcoplasmic reticulum (SR), releasing calcium. The increase in cytosolic [Ca²⁺] together with calmodulin activates the protein phosphatase calcineurin. Calcineurin dephosphorylates several residues in the amino-terminal region of the transcription factor NFAT, allowing it to translocate to the nucleus and activate transcription of hypertrophic response genes. Calm regulates myogenesis and prevents formation of MEF2/HDAC complexes by inducing phosphorylation and nuclear export of HDACs. MCIP1.4 proteins actually facilitate Calcineurin activity for specific target proteins by serving as targeting subunits.

The late increase in the expression of collagen 1, collagen III and TGF- β in 3-month-old *Hspa4*^{-/-} mice indicates that in this mouse model of cardiac disease, hypertrophy occurs in early postnatal life, whilst the fibrotic response occurs later .

4.6.5 Role of heat shock in heart protection

Hypertrophic growth of cardiomyocytes is a result of different physiological and pathological stresses. Heat shock proteins were originally discovered as proteins, whose expression is induced by heat shock. Subsequent experiments have revealed that HSPs expression is also induced by different cellular stresses, including mechanical ischemia/hypoxia and neural/hormonal. Therefore, this generic stress response molecule such HSP may also have a highly specific role in regulating cardiac hypertrophy under pathological stimulation (Vondriska and Wang, 2008). A number of studies have shown that HSPs in the heart have a protective effect against severe stress such as mechanical stress or pressure overloaded (Morimoto, 1993). These results have been obtained by analysing the effects of overexpression of an individual HSP in cultured cardiac cells and in the heart of transgenic animals. Kumarapeli, *et al.* (2008) showed that *Cryab/Hspb2* deficiency activates the NFAT/calcineurin signaling and induces cardiac hypertrophic responses at the unstressed or minimal stress conditions and exacerbates cardiac malfunction on pressure overload. In contrast, *Cryab* overexpression significantly attenuates pressure-overloaded. Overexpression of NFAT-targeted gene MCIP1.4 was observed in *Cryab/Hspb2*- deficient heart. Kim *et al.* (2006) studied the role of *Hsp70* in maintaining cardiac contractility and calcium handling by investigation of *Hsp70*-knockout mice. We have shown that the depletion of HSPA4 causes cardiac hypertrophy, which suggests that HSPA4 confers cardioprotection against stimulated or metabolic stress. To confirm the cardioprotective effect of HSPA4, we have to determine which stress induces the expression of HSPA4 in heart. Generation of *Hspa4* transgenic mice, in which HSPA4 is specifically overexpressed in cardiomyocytes, will help us to determine the protective effect of *Hspa4* against different stresses that induces cardiac hypertrophy.

4.6.6 Expression profiles of *Hspa4*^{-/-} heart

With the emergence of the DNA microarray technique, it is possible to have a more comprehensive characterization of the hypertrophic response at the global gene expression than in traditional single-gene studies (Liew and Dzau 2004, Liew 2005). Microarray analysis was

performed to identify gene expression profiles and expand the knowledge of pathways regulating the development of cardiac hypertrophy in *Hspa4*-null mice. Results of DNA microarray analysis identified 98 differentially expressed genes that were upregulated or downregulated in *Hspa4*-null heart at least 1.5 fold with P values of < 0.05. Differentially expressed genes related to oxidative stress, ion channel signaling and synaptic junction were selected for further study (Table 3.2). Result of DNA microarray showed a wide spectrum of changes in gene expression, which may be responsible for development of cardiac fibrosis and hypertrophy of *Hspa4*-null mice. A key finding of the microarray analysis was that expression of hypertrophic genes *Anf*, *Bnf*, *Acta1* and *Myh7* was upregulated. These results confirm our hypothesis suggesting that pathologic hypertrophy of *Hspa4*^{-/-} heart is accompanied by reactivation of fetal gene programs. DNA microarray studies of other genetic animal models of hypertrophy revealed that activation of *Anf* and/or *Bnf* seems to be the most predominant change at the gene expression level (Aronow *et al.* 2001; Fischer, *et al.*, 2005; Mirotsoou *et al.* 2006).

Monoamine oxidases (MAOs) are mitochondrial flavoenzymes, which catalyze oxidative deamination of catecholamines (CAs) and biogenic amine such as serotonin. During this process, they generate hydrogen peroxide (H₂O₂), which can potentially source of oxidative stress in the heart. MAOs exist in two forms, MAOA and MAOB (Shih *et al.*, 1999). Both enzymes catalyze the oxidative deamination of monoamine neurotransmitters such as serotonin, norepinephrine and phenylethylamine (Youdim and Bakhle, 2006; Bortolato *et al.*, 2008). *Maoa*-knockout mice have elevated brain levels of serotonin, norepinephrine and to a lesser extent, dopamine (Cases *et al.*, 1995), whereas only 2-phenylethylamine levels are increased in *Maob*-Knouckout mice (Youdim *et al.*, 2006). *Maoa*-KO mice displayed exaggerated ventricular hypertrophy which is due to increase serotonin levels (Lairez *et al.*, 2009). Cardiomyocyte receptor that couples to Gq stimulates cardiomyocyte hypertrophy, the most important receptor of which are the 1-adrenergic receptors for norepinephrine and phenylephrine (Molkentin and Dorn 2001). Mice that are unable to synthesize norepinephrine, because of targeted disruption of the dopamine β-hydroxylase gene, exhibit less cardiac hypertrophy and preserved ventricular function after surgical constriction of the transverse aorta (Esposito *et al.*, 2002). In contrast, depletion of MAOA was associated with an increase in whole blood serotonin and exacerbates left ventricle thickening and fibrosis (Lairez *et al.*, 2009). The present results showing reduced *Maob* expression in heart of 25-day and 3-month-old *Hspa4*-null mice suggest that the reduction of

Maob in *Hspa4*-mutant mice increases the catecholamine stress and blood pressure. Such increase of catecholamine stress and blood stress induces cardiac hypertrophy via receptor 1-adrenergic receptors that initiate G- protein signaling cascade.

The main receptors involved in the regulation of heart muscle contraction are prototypical G protein-coupled receptors in response to neurohumoral induction (Rockman *et al.*, 2002). They activate heterotrimeric G proteins that are comprised of α -, β -, and γ -subunits (Offermanns, 2003). The activation of a G protein is accomplished by the dissociation of its α subunit from the $\gamma\beta$ dimer, both of which in turn modulate target effectors (Zhu and Birnbaumer, 1996). Guanine nucleotide binding protein also known as alpha O (*Gnao1/G α_o*) protein belongs to the G-alpha family. Targeted deletion of both isoforms of *G α_o* in mice lead to altered potassium and calcium channel regulation in neuronal cells and neurological abnormalities (Valenzuela *et al.*, 1997; Tanaka *et al.*, 1999; Greif *et al.*, 2000; Kamp and Hell, 2000). Nishida *et al.* (2000) demonstrated that hydrogen peroxide (H_2O_2) induced *Gnao1* expression in rat neonatal cardiomyocytes. The α -Adrenoceptors mediate the contractile response in rat aorta by coupling to both binding of Gq protein and the GNAO1 protein (Gurdal *et al.*, 1997). A constitutively active form of GNAO* (*G α_o **) exerts positive effect on cardiac Ca^{2+} -cycling and contractile function in ventricular myocytes of *Gnao** transgenic mice (Zhu *et al.*, 2008). The present results show a significant increase of *Gnao1* expression in heart of 25-day- and 3-month-old *Hspa4*-null mice. We suggest that increase of GNAO1 activates phospholipase C, resulting in production of inositol trisphosphate and release of intracellular calcium after binding of norepinephrine to α -adrenoceptor (AR) in *Hspa4*-knockout. This results support the involvement of this pathway in the development of cardiac hypertrophy.

Insulin-like growth factor-binding protein3 (*Igfbp3*) is one of six members of protein family that bind with insulin-like growth factor1 (IGF1). These IGFBPs are capable to increase the half-life of IGF1 in the circulation and are able to either potentiate the cell specific effects of IGF1 or act as inhibitors to block its action by preventing delivery to responding cell types (Ito *et al.*, 1993b). Murphy *et al.* (1995) reported that expression of human IGFBP3 in transgenic mice causes organomegaly (heart, liver and spleen). Henson *et al.* (2000) demonstrated that *Igfbp3* expression was significantly increased in heart of rodent models for heart hypertrophy. Increased IGFBP-3 protein was shown to induce transcription of atrial natriuretic factor (*Anf*) and β -myosin heavy chain (*β -Mhc/Myh7*). Moreover, the hypertrophy in these rodent models is independent of

ANGII, cardiotrophin-1 and IGF-1. In this study, Igfbp-3 transcript was markedly increased in heart of *Hspa4*^{-/-} mice at 25 days and 3-months of age.

Prolongation of the repolarization time has often been observed before fibrosis or clinical signs of heart failure in animal model become evident. Cardiac hypertrophy is characterized by electrical remodeling with increased risk of arrhythmogenicity. This electrical remodeling process is at least partially determined by a reprogramming of cardiac gene expression and the reactivation of ‘fetal’ cardiac genes. Among the differentially expressed genes in the *Hspa4*-null heart are genes encoding ion channel proteins. The hyperpolarization-activated cyclic nucleotide-gated channel (HCN) gene family, Ca²⁺, K⁺ and Na⁺ channels playing an important role in the electrical remodeling process (Boixel *et al.*, 2006). Four genes that encode HCN channels have been identified: *Hcn1*, *Hcn2*, *Hcn3*, and *Hcn4*. HCN channels carry an inward current, the depolarizing Na/K current I_f, that underlies cardiac pacemaker activity (Jongbloed *et al.*, 2008). *KCNE1* encodes the potassium ion channel β subunit that co-assembles with KCNQ1 to produce a channel that mediates the slowly activating delayed rectifier potassium current, IKs (Barhanin *et al.*, 1996; Sanguinetti *et al.*, 1996). Loss of *Kcne1* function prolongs ventricular action potentials in humans and in *Kcne1*^{-/-} mice and display unexpectedly shortened atrial action potentials and prolonged electrocardiographic QT intervals (Temple *et al.*, 2005). Leucine-rich glioma inactivated gene 1 (*Lgil*) regulates voltage-gated potassium channels assembly of *Kcna1*, *Kcna4* and *Kcnab1* and positively regulates synaptic transmission mediated by AMPA-type glutamate receptors (Schulte *et al.*, 2006; Diani *et al.*, 2008; Sagane, 2008). The expression of the *Hcn2*, *Hcn4*, as well as *Kcne1* and *Kcne2* genes in cultured ventricular cell, which are isolated from acute myocardial infarction rat hearts, underwent dynamic expression changes, reaching peak levels at 1 or 2 weeks post-acute myocardial infarction. The increased expression may be related to ventricular arrhythmogenesis after acute myocardial infarction (Xia *et al.*, 2010). In current study, we showed that expression of *Kcne1* transcripts in heart of *Hspa4a*-null mutant is upregulated. In contrast, the expression levels of *Kcnd2*, *Hcn1* and *Lgil* are significantly decreased in *Hspa4*-mutant heart compared with wild type. We propose that electrical remodeling is associated with ventricular hypertrophy in *Hspa4*-null.

5. Summary

The aims of this study were to determine the underlying causes of male infertility, growth retardation and cardiac hypertrophy in *Hspa4*^{-/-} mice.

In order to identify the spermatogenic stage, at which spermatogenesis is affected by *Hspa4* deficiency in mice with hybrid C57BL/6J x 129/Sv genetic background, we performed histological and immunological analysis. Analysis of germ cell development during juvenile life of *Hspa4*^{-/-} mice showed an arrest of first wave of spermatogenesis in late stage of prophase I. RNA analysis showed a marked reduction in expression of late meiotic and postmeiotic-specific marker genes, whereas expression of early meiotic-specific genes was unaffected in the *Hspa4*^{-/-} testes. These results suggest that HSPA4 is required for the regulation of diverse chaperone processes and cell cycle during germ cell progression.

The second aim of this study was concentrated to study the cause of growth retardation in *Hspa4*^{-/-} mice with inbred 129/Sv genetic background. To investigate whether growth retardation is due to skeletal muscle myopathy, histological analyses of different skeletal muscles were carried out. Histological analyses revealed that Tibialis anterior, Vastus intermedius, Soleus and paraspinal muscles of *Hspa4*^{-/-} adult mice displayed myopathic changes. Moreover, myopathic change was already present at an early postnatal stage of *Hspa4*^{-/-} mice development. This suggested that skeletal muscle myopathy is the cause of growth retardation. Furthermore, these results suggest that HSPA4 has protective effect that confers the protection of skeletal muscle against mechanical or metabolic stress, which induce skeletal muscle degradation.

To determine whether skeletal muscle myopathy is also realized in heart as hypertrophic cardiomyopathy, histological molecular analyses and two-dimensional directed M-mode echocardiograms were performed. Histological analyses revealed the development of cardiac hypertrophy and fibrosis in heart of *Hspa4*-deficient mice. Ultrastructure analysis revealed myofibrillar disarray and disassembly in cardiomyocytes and increased collagen accumulation (fibrosis) in heart of *Hspa4*-deficient mice. Echocardiographic measurements further confirm the cardiac hypertrophy phenotype in *Hspa4*-null mice. To identify when the development of cardiac hypertrophy and fibrosis starts in *Hspa4*^{-/-} hearts, we studied expression of hypertrophic and fibrotic marker genes in heart from different postnatal stages by Northern blot and real time PCR

analyses. These results indicate that the development of cardiac hypertrophy and fibrosis in *Hspa4*-null mice starts in early postnatal life and let us to suggest that the early postnatal lethality in *Hspa4*^{-/-} mice in an inbred 129/SV genetic background can be contributed to the progression of skeletal muscle myopathy and hypertrophic cardiomyopathy. In contrast to skeletal muscle and heart phenotype in *Hspa4*^{-/-} mice with inbred background, histological analysis and expression analysis of hypertrophic genes showed that cardiac hypertrophy is not developed in *Hspa4*^{-/-} mice with hybrid 129/Sv x C57BL genetic background.

In order to identify the signal pathways that mediate cardiac hypertrophy in *Hspa4*^{-/-} mice, we determined the expression of some genes and proteins, which are involved in Gp130/STAT3, MAPK and calcineurin-NFAT signalings, in heart of wild-type and *Hspa4*^{-/-} mice. Results of these analyses suggest that STAT3 and MAPK signaling pathways are not responsible for the development of cardiac hypertrophy in *Hspa4*-null mice. On the contrary, increased activity of calcineurin/NFAT in *Hspa4*^{-/-} heart seems to modulate the cardiac hypertrophy.

Microarray analysis was used as a screening tool to identify altered gene expression in *Hspa4*-deficient heart at 25 days compared with that of wild-type mice. 98 genes were identified as differentially expressed. Several genes were selected and classified according to their function in the development of cardiac hypertrophy. To confirm the results of microarray analysis, quantitative real-time PCR was performed. We confirmed that genes involved in ion channel signaling (*Kcne1*, *Kcnd2*, *Scn4a*, *Hcn1* and *Irx4*), in protection of cells against oxidative stress (*Gnao1*, *Ptp4a1* and *Mme1*) and those inducing oxidative stress (*Maob*), are differentially expressed in heart of *Hspa4*^{-/-} mice. The altered expression of these genes may be involved in the development of cardiac hypertrophy in *Hspa4*^{-/-} mice.

6. References

- Abbasi S., Lee J.D., Su B., Chen X., Alcon J.L., Yang J., Kellems, R.E, Xia Y. (2006) Protein kinase-mediated regulation of calcineurin through the phosphorylation of modulatory calcineurin-interacting protein 1. *J. Biol. Chem.* 281 (12): 7717-26.
- Adham P.M., Nayernia K., Burkhardt-Gottges E., Topaloglu O., Dixkens C., Holstein A.F., Engel W. (2001) Teratozoospermia in mice lacking the transition protein 2 (Tnp2). *Mol. Hum. Reprod.* 7: 513 – 520.
- Aijaz S., Sanchez-Heras E., Balda M. S., Matter K. (2007). Regulation of tight junction assembly and epithelial morphogenesis by the heat shock protein Apg-2. *BMC Cell Biol.* 8: 49.
- Akazawa H., Komuro I (2003) Roles of Cardiac Transcription Factors in Cardiac Hypertrophy. *Circ Res.* 92:1079.
- Allen, J. W., Dix, D. J., Collins, B. W., Merrick, B. A., He, C., Selkirk, J. K., Poorman-Allen, P., Dresser, M. E. and Eddy, E. M. (1996). HSP70-2 is part of the synaptonemal complex in mouse and hamster spermatocytes. *Chromosoma* 104: 414-21.
- Arai H., Hori S., Aramori I., Ohkubo H., Nakanishi S. (1990) Cloning and expression of a cDNA encoding an endothelin receptor. *Nature.* 348 (6303):730–732.
- Arimura T., Hayashi Y. K., Murakami T., Oya Y., Funabe S., Arikawa-Hirasawa E., Hattori N., Nishino I., Kimura A. (2009) Mutational analysis of fukutin gene in dilated cardiomyopathy and hypertrophic cardiomyopathy. *Circ J* 73:158-61.
- Aronow B. J., Toyokawa T., Canning A., Haghighi K., Delling U., Kranias E., Molkentin J.D., Dorn, G.W. II. (2001). Divergent transcriptional responses to independent genetic causes of cardiac hypertrophy. *Physiol. Genomics* 6:19–28.

References

- Ausubel F. M., Brent R., Kingston R. E., Moore D. D., Seidman J. G., Smith J. A., Struhl K., (1994) "Current protocols in molecular biology." John Wiley & Sons Inc., USA.
- Baines C. P., Molkenstin J. D. (2005) Stress signaling pathways that modulate cardiac myocyte apoptosis. *J Mol Cell Cardiol.* 38:47–62.
- Baker J., Liu J. P., Robertson E. J. , Efstratiadis A. (1993) Role of insulin-like growth factors in embryonic and postnatal growth. *Cell.* 75(1):73-82.
- Balda M. S., Garrett M. D., Matter K. (2003) The ZO-1-associated Y-box factor ZONAB regulates epithelial cell proliferation and cell density. *J Cell Biol.* 160(3): 423–432.
- Barhanin J., Lesage F., Guillemare E., Fink M., Lazdunski M., Romey G. (1996) KvLQT1 and Isk (minK) proteins associate to form the IKs cardiac potassium current. *Nature* 384:78–80.
- Beyer, M. E., Slesak G., Hoffmeister H. M. (1995) In vivo hemodynamic and inotropic effects of the endothelinB agonist IRL 1620. *J Cardiovasc. Physiol.* 26S3:S190–S192.
- Bhattacharya B., Miura T., Brandenberger R., Mejido J., Luo Y., Yang A. X., Joshi B. H., Ginis I., Thies R. S., Amit M., Lyons I., Condie B. G., Itskovitz-Eldor J., Rao M. S., Puri R. K. (2004) Gene expression in human embryonic stem cell lines: unique molecular signature. *Blood.* 103: 2956-2964.
- Birnboim H. C., Doly J. (1979) A rapid alkaline extraction procedure for screening recombinant plasmid DNA. *Nucleic Acids Res.* 7(6):1513–1523.
- Bischoff R. (1994) The satellite cell and muscle regeneration. In: Myology. 2nd ed. Engel AG, Franzini-Armstrong C, Eds. New York: McGraw-Hill, pp. 97-118.
- Bitgood M.J., Shen L., McMahon A.P. (1996) Sertoli cell signaling by Desert hedgehog regulates the male germline. *Curr Biol.* 6: 298–304.

References

- Black D. D. (2007) Development and physiological regulation of intestinal lipid absorption. I. Development of intestinal lipid absorption: cellular events in chylomicron assembly and secretion. *Am J Physiol Gastrointest Liver Physiol.* 293(3):G519-24.
- Bodega G., Hernández C., Suárez I., Martín M. , Fernández B. (2002) HSP70 Constitutive Expression in Rat Central Nervous System from Postnatal Development to Maturity. *J. Histochem. and Cytochem.* 50: 1161-1168.
- Boixel C., Gavillet B., Rougier J. S., Abriel H. (2006). Aldosterone increases voltage-gated sodium current in ventricular myocytes. *Am J Physiol Heart Circ Physiol* 290: H2257–H2266.
- Bortolato M., Chen K., Shih J. C. (2008) Monoamine oxidase inactivation: from pathophysiology to therapeutics. *Adv Drug Deliv Rev.* 60(13-14): 1527–1533.
- Bradford M. M., (1976) “A rapid and sensitive method for the quantitation of microgram quantities of protein utilizing the principle of protein-dye binding. *Anal Biochem.*72:248-54.
- Bueno O. F., Molkentin J. D. (2002) Involvement of Extracellular Signal-Regulated Kinases 1/2 in Cardiac Hypertrophy and Cell Death. *Circ Res.* 91:776.
- Bueno, O.F., De Windt L. J., Tymitz K. M., Witt S. A., Kimball T. R., Klevitsky R., Hewett T. E., Jones S. P., Lefer D. J., Peng C. F., Kitsis R. N., Molkentin J. D.(2000). The MEK1-ERK1/2 signaling pathway promotes compensated cardiac hypertrophy in transgenic mice. *Cancer Res.* 60: 5887–5894.
- Buj-Bello A., Fougereousse F., Schwab Y., Messaddeq N., Spehner D., Pierson C. R., Durand M., Kretz C., Danos O., Douar A. M., *et al.* (2008). AAV-mediated intramuscular delivery of myotubularin corrects the myotubular myopathy phenotype in targeted murine muscle and suggests a function in plasma membrane homeostasis. *Hum. Mol. Genet* 17:2132–2143.

References

- Burnicka-Turek O., Shirneshan K., Paprotta I., Grzmil P., Meinhardt A., Engel W. Adham I. M. (2009) Inactivation of Insulin-Like Factor 6 Disrupts the Progression of Spermatogenesis at Late Meiotic Prophase. *Endocrinology*. 150(9): 4348-4357.
- Cases O., Seif I., Grimsby J., Gaspar P., Chen K., Pournin S., Muller U., Aguet M., Babinet C., Shih J.C., et al. (1995) Aggressive behavior and altered amounts of brain serotonin and norepinephrine in mice lacking MAOA. *Science*. 268:1763–1766.
- Chang L., Zhang J., Tseng Y. H. , Xie C. Q. , Ilany J. , Brüning J. C. , Sun Z. , Zhu X. , Cui T., Youker K. A., Yang Q., Day S. M., Kahn C. R., Chen Y. E. (2007) Rad GTPase deficiency leads to cardiac hypertrophy. *Circ*. 116(25): 2976-83.
- Chien K. R., Knowlton K. U., Zhu H., Chien S. (1991) Regulation of cardiac gene expression during myocardial growth and hypertrophy: molecular studies of an adaptive physiologic response. *FASEB J*. 5, 3037–3046.
- Chomczynski P., Sacchi N. (1987) Single-step method of RNA isolation by acid guanidinium thiocyanate-phenol-chloroform extraction. *Anal Biochem*. 162: 156-159.
- Ciciliot S., Schiaffino S. (2010) Regeneration of Mammalian Skeletal Muscle: Basic Mechanisms and Clinical Implications. *Current Pharmaceutical Design*. 16: 906-914.
- Connell P., Ballinger C. A., Jiang J., Wu Y., Thompson L. J., Hohfeld J., Patterson C. (2001) The co-chaperone CHIP regulates protein triage decisions mediated by heat-shock proteins. *Nat Cell Biol*. 3: 93–96.
- Corduan A., Lecomte S., Martin C., Michel D., Desmots F. (2009) Sequential interplay between BAG6 and HSP70 upon heat shock. *Cell Mol Life Sci*. 66 (11-12): 1998-2004.
- Cullen, J. P., Bell D., Kelso E. J., McDermott B. J. (2001). Use of A-192621 to provide evidence for involvement of endothelin ETB receptors in endothelin- 1-mediated cardiomyocyte hypertrophy. *Eur. J. Pharmacol*. 417:157–168.

References

- Dehne T., Schenk R., Perka C., Morawietz L., Pruss A., Sittinger M., Kaps C., Ringe J. (2010) Gene expression profiling of primary human articular chondrocytes in high-density micromasses reveals patterns of recovery, maintenance, re- and dedifferentiation. *Gene*. 462 (1-2):8-17.
- Denhardt D.T. (1966) A membrane-filter technique for the detection of complementary DNA. *Biochem Biophys Res Commun*. 23: 641-646.
- Desmoulière A., Geinoz A., Gabbiani F., Gabbiani, G. (1993). Transforming growth factor-beta 1 induces alpha-smooth muscle actin expression in granulation tissue myofibroblasts and in quiescent and growing cultured fibroblasts. *J Cell Biol*. 122, 103-111.
- Diani E., Di Bonaventura C., Mecarelli O., Gambardella A., Elia M., Bovo G., Bisulli F., Pinardi F., Binelli S., Egeo G., Castellotti B., Striano P., Striano S., Bianchi A., Ferlazzo E., Vianello V., Coppola G., Aguglia U., Tinuper P., Giallonardo A.T., Michelucci R., Nobile C. (2008) Autosomal dominant lateral temporal epilepsy: absence of mutations in ADAM22 and Kv1 channel genes encoding LGI1-associated proteins. *Epilepsy Res*. 80(1):1-8.
- Dix D. J. (1997) Hsp70 expression and function during gametogenesis. *Cell Stress Chap*. 2:73–77.
- Dorn GWII, Robbins J., Sugden P. H. (2003). Phenotyping hypertrophy. Eschew obfuscation. *Circ Res*. 92:1171–1175.
- Dragovic Z., Broadley S. A., Shomura Y., Bracher A., Hartl F. U. (2006) Molecular chaperones of the Hsp110 family act as nucleotide exchange factors of Hsp70s. *EMBO J*. 25; 2519–2528.
- Eddy E. M. (2002) Male germ cell gene expression. *Recent Prog. Horm. Res*. 57:103-128.
- Eijssen L. M., van den Bosch B. J., Vignier N., Lindsey P. J., van den Burg C. M., Carrier L., Doevendans P. A., van der Vusse G. J., Smeets H. J. (2008) Altered myocardial gene

References

- expression reveals possible maladaptive processes in heterozygous and homozygous cardiac myosin-binding protein C knockout mice. *Genomics*. 91(1):52-60.
- Ellmers L. J. , Scott N. J. A., Piuhola J., Maeda N., Smithies O., Frampton C. M., Richards A., M. Cameron V. A. (2007) Npr1-regulated gene pathways contributing to cardiac hypertrophy and fibrosis. *J Molecular Endocrinology*. 38: 245-257.
- Enders G.C., May J. J., 2nd. (1994) Developmentally regulated expression of a mouse germ cell nuclear antigen examined from embryonic day 11 to adult in male and female mice. *Dev Biol*. 163: 331–340.
- Engblom, D., Kornfeld, J.W., Schwake, L., Tronche, F., Reimann, A., Beug, H., Hennighausen, L., Moriggl, R., Schutz, G.(2007) Direct glucocorticoid receptor–Stat5 interaction in hepatocytes controls body size and maturation-related gene expression. *Genes & Dev*. 21:1157–1162.
- Esposito G., Rapacciuolo A., Naga Prasad S. V, Takaoka H., Thomas S. A, Koch W. J., Rockman H. A. (2002) Genetic alterations that inhibit in vivo pressure-overload hypertrophy prevent cardiac dysfunction despite increased wall stress. *Circ*. 105: 85–92.
- Feinberg AP and Vogelstein B, 1989. “A technique for radiolabeling DNA restriction endonuclease fragments to high specific activity.” *Anal Biochem*. 123:6-13.
- Finkel T., Holbrook N. J. (2000) Oxidants, oxidative stress and the biology of ageing. *Nature*. 408(6809):239-47.
- Fischer A., Klattig J., Kneitz B., Diez H., Maier M., Holtmann B., Englert C., Gessler M. (2005) Hey Basic Helix-Loop-Helix Transcription Factors Are Repressors of GATA4 and GATA6 and Restrict Expression of the GATA Target Gene ANF in Fetal Hearts. *Mol Cell Biol*. 25(20):8960-70.
- Frank D., Kuhn C., van Eickels M., Gehring D., Hanselmann C., Lippl S., Will R., Katus H. A., Frey N. (2007) Calsarcin-1 protects against Angiotensin-II-induced cardiac hypertrophy. *Circ*. 116: 2587–2596.

- Frey N., Olson E. N. (2003) Cardiac hypertrophy: the good, the bad, and the ugly. *Annu Rev Physiol* 65: 45–79.
- Frey N., Barrientos T., Shelton J. M., Frank D., Rütten H., Gehring D., Kuhn C., Lutz M., Rothermel B., Bassel-Duby R., Richardson J. A., Katus H. A., Hill J. A., Olson E. N. (2004) Mice lacking calstabin-1 are sensitized to calcineurin signaling and show accelerated cardiomyopathy in response to pathological biomechanical stress. *Nat Med*. 10(12):1336-43.
- Frydman J. (2001) Folding of newly translated proteins in vivo: the role of molecular chaperones. *Annu. Rev. Biochem.* 70: 603–647.
- Gallagher J. W., Weinberg R. B., Shelness G. S. (2004) ApoA-IV tagged with the ER retention signal KDEL perturbs the intracellular trafficking and secretion of apoB. *J Lipid Res.* 45: 1826-1834.
- Garrington T.P., Johnson G.L. (1999) Organization and regulation of mitogen-activated protein kinase signaling pathways. *Curr. Opin. Cell Biol.* 11: 211–218.
- Gershoni J. M., Palade G.E. (1982) Electrophoretic transfer of proteins from sodium dodecyl sulfate-polyacrylamide gels to a positively charged membrane filter. *Anal Biochem.* 124: 396-405.
- Glennon PE, Kaddoura S, Sale EM, Sale GJ, Fuller SJ, Sugden PH (1996) Depletion of mitogen-activated protein kinase using an antisense oligodeoxynucleotide approach downregulates the phenylephrine-induced hypertrophic response in rat cardiac myocytes. *Circ Res* 78:954-961.
- Gotoh K., Nonoguchi K., Higashitsuji H., Kaneko Y., Sakurai T., Sumitomo Y., Itoh K., Subject J. R., Fujita, J (2004).). Apg-2 has a chaperone-like activity similar to Hsp110 and is overexpressed in hepatocellular carcinomas. *FEBS Lett.* 560: 19–24.

References

- Greif G. J., Sodickson D. L., Bean B. P., Neer E. J., Mende U. (2000) Altered regulation of potassium and calcium channels by GABAB and adenosine receptors in hippocampal neurons from mice lacking $G_{\alpha o}$. *J Neurophysiol.* 83: 1010–1018.
- Guo W., Jung W. E., Marionneau C., Aimond F., Xu H., Yamada K. A., Schwarz T. L., Demolombe S., Nerbonne J. M. (2005) Targeted deletion of Kv4.2 eliminates Ito,f and results in electrical and molecular remodeling, with no evidence of ventricular hypertrophy or myocardial dysfunction. *Circ Res* 97: 1342–13.
- Guo C., Willem M., Werner A., Raivich G., Emerson M., Neyses. L, Mayer U. (2006). Absence of alpha 7 integrin in dystrophin-deficient mice causes a myopathy similar to Duchenne muscular dystrophy. *Hum Mol Genet.* 15(6):989-98.
- Gurdal H., Seacholtz T. M., Wang H.-Y., Brown R. D., Johnson M. D., Friedman E. (1997). Role of G alpha q or G alpha o proteins in alpha 1-adrenoceptor subtype-mediated responses in Fischer 344 rat aorta. *Mol. Pharmacol.* 52: 1064-1070.
- Havel, R. J., Kane J. P. (1995) Introduction: Structure and metabolism of plasma lipoproteins. In *The Metabolic and Molecular Bases of Inherited Disease*. 7th edition. Vol. 2. Scriver C. R., Beaudet A. L., Sly W. S., Valle D., editors. McGraw-Hill, New York, pp. 1841–1851.
- Hawke T. J, Garry D. J. (2001) Myogenic satellite cells: physiology to molecular biology *J. Appl. Physiol.* 91: 534-551.
- Hawke T. J., Jiang N., Garry D. J. (2003) Absence of p21CIP rescues myogenic progenitor cell proliferative and regenerative capacity in Foxk1 null mice. *J Biol Chem.* 278(6):4015-20.
- Hayashi J., Kajino K., Umeda T., Takano S., Arakawa Y., Kudo M. and Hino O. (2002). Somatic mutation and SNP in the promoter of dbpA and human hepatocarcinogenesis. *Int. J Oncol.* 21:847-850.

References

- Held T., Paprotta I., Khulan J., Hemmerlein B., Binder L., Wolf S., Schubert S., Meinhardt A., Engel W., Adham I. M. (2006) Hspa41-deficient mice display increased incidence of male infertility and hydronephrosis development. *Mol Cell Biol.* 26:8099–8108.
- Held T. (2008) PhD thesis. The university of Göttingen. Structural and functional analysis of murine genes of the Hsp110 family.
- Henson M., Damm D., Lam A., Garrard L. J., White T., Abraham J. A., Schreiner G. F., Stanton L.W., Joly A. H. (2000) Insulin-like growth factor-binding protein-3 induces fetalization in neonatal rat cardiomyocytes. *DNA Cell Biol.* 19 (12):757-63.
- Hill J. A., Olson E. N. (2008) Cardiac plasticity. *N Engl J Med.* 358(13):1370-80.
- Hodge R. (1994). Preparation of RNA Gel Blots. *Methods. Mol. Biol.* 28: 49-5.
- Homma S., Iwasaki M., Shelton G. D., Engvall E., Reed J. C., Takayama S. (2006) BAG3 deficiency results in fulminant myopathy and early lethality. *Am J Pathol.* 169: 761–773.
- Hoshijima M., Chien K. R. (2002) Mixed signals in heart failure: cancer rules. *J Clin Invest.* 109: 849–55.
- Hzizo S. L., Gusarova V., Habielski D. M., Goekeler J. L., Fisher E.A., Brodsky J. L. (2007). The Hsp110 molecular chaperone stabilizes apolipoprotein B from endoplasmic reticulum-associated degradation (ERAD). *J Biol Chem* 282: 32665-32675.
- Irimia J. M., Meyer, C. M., Peper C. L., Zhai L., Bock C. B., Previs S. F. McGuinness O. P., DePaoli-Roach A., Roach P. (2010) Impaired Glucose Tolerance a Predisposition to the Fasted State in Liver Glycogen Synthase Knock-out Mice. *J Biol Chem.*, 285: 12851-12861.

References

- Ishikawa T., Yanagisawa M., Kimura S., Goto K., and Masaki T. (1988) Positive chronotropic effects of endothelin, a novel endothelium-derived vasoconstrictor peptide. *Pfluegers Arch.* 413:108–110.
- Ito H., Hirata Y., Adachi S., Tanaka M., Tsujino M., Koike A., Nogami A., Murumo F., Hiroe M. (1993a) Endothelin-1 is an autocrine/paracrine factor in the mechanism of angiotensin II-induced hypertrophy in cultured rat cardiomyocytes. *J Clin. Investig.* 92:398–403.
- Ito H., Hiroe M., Hirata Y., Tsujino M., Adachi S., Shichiri M., Koike A., Nogami A., Marumo F. (1993b) Insulin-like growth factor-I induces hypertrophy with enhanced expression of muscle specific genes in cultured rat cardiomyocytes. *Circ.* 87(5):1715-21.
- Jongbloed M. R., Mahtab E. A., Blom N. A., Schalij M. J., Gittenberger-de Groot A. C. (2008) Development of the cardiac conduction system and the possible relation to predilection sites of arrhythmogenesis. *ScientificWorldJournal.* 8:239-69.
- Joya J. E., Kee A. J., Nair-Shalliker V., Ghodduzi M., Nguyen M.-A. T., Luther P., Hardeman E. C. (2004) Muscle weakness in a mouse model of nemaline myopathy can be reversed with exercise and reveals a novel myofiber repair mechanism *Hum. Mol Genet.* 13 (21): 2633-2645.
- Kamimura D, Ishihara K, Hirano T. (2003) IL-6 signal transduction and its physiological roles: the signal orchestration model. *Rev Physiol Biochem Pharmacol* 149: 1–38.
- Kamp T. J., Hell J. W. (2000) Regulation of cardiac L-type calcium channels by protein kinase A and protein kinase C. *Circ Res.* 87: 1095–1102.
- Kane J. P., Havel R. J. (1995) Disorders of the biogenesis and secretion of lipoproteins containing the B apolipoproteins. In *The Metabolic Bases of Inherited Disease*. 7th edition. Vol. 2. Scriver C. R., Beaudet A. L., Sly W. S., Valle D., editors. McGraw-Hill, New York, pp. 1853-1885.

References

- Kaneko, Y., Nishiyama, H., Nonoguchi, K., Higashitsuji, H., Kishishita, M. and Fujita, J. (1997) A novel hsp110-related gene, *apg-1*, that is abundantly expressed in the testis responds to a low temperature heat shock rather than the traditional elevated temperatures. *J Biol Chem.* 272: 2640-2645.
- Kawamura H., Otsuka T., Matsuno H., Niwa M., Nobuo Matsui N., Kato K., Uematsu T., Kozawa O. (1999) Endothelin-1 stimulates heat shock protein 27 induction in osteoblasts: involvement of p38 MAP kinase. *Am J Physiol Endocrinol Metab.* 277(6): E1046-E1054.
- Kedzierski, R. M., Yanagisawa M. (2001). Endothelin system: the doubleedged sword in health and disease. *Annu. Rev. Pharmacol. Toxicol.* 41:851–876.
- Kim Y.-K., Suarez J., Hu Y., McDonough P. M., Boer C., Dix D. J., Dillmann W. H. (2006) Deletion of the Inducible 70-kDa Heat Shock Protein Genes in Mice Impairs Cardiac Contractile Function and Calcium Handling Associated With Hypertrophy. *Circ.* 113: 2589-259.
- Kishimoto T, Taga T and Akira S. (1994) Cytokine signal transduction. *Cell.* 76: 253-262.
- Kojima R., Randall J. D., Ito E., Manshio H., Suzuki Y., Gullans S. R. (2004) Regulation of expression of the stress response gene, *Osp94*: identification of the tonicity response element and intracellular signalling pathways. *Biochem. J.* 380:783–794.
- Kojima R., Randall J., Brenner B. M., Gullans S. R. (1996) Osmotic stress protein 94 (*Osp94*). A new member of the *Hsp110/SSE* gene subfamily. *J Biol. Chem.* 271:12327–12332.
- Komuro I., Yazaki Y. Control of cardiac gene expression by mechanical stress. *Annu Rev Physiol.* 1993; 55: 55–75.
- Kühl N. M., Rensing L. (2000) Heat shock effects on cell cycle progression. *Cell Mol. Life Sci.* 57(3):450-63.

References

- Kumarapeli A. R. K., Su H., Huang W., Tang M., Zheng H., Horak K. M., Li M., Wang X. (2008) B-Crystallin Suppresses Pressure Overload Cardiac Hypertrophy. *Circ Res.* 103:1473-1482.
- Kunisada K., Hirota H., Fujio Y., Matsui H., Tani Y., Yamauchi-Takahara K., Kishimoto T. (1996) Activation of JAK-STAT and MAP kinases by leukemia inhibitory factor through gp130 in cardiac myocytes. *Circ* 94:2626-2632.
- Kunisada K, Tone E, Fujio Y, Matsui H, Yamauchi-Takahara K, Kishimoto T (1998) Activation of gp130 transduces hypertrophic signals via STAT3 in cardiac myocytes. *Circ* 98(4):346-52.
- Kunisada K., Negoro S., Tone E., Funamoto M., Osugi T., Yamada S., Okabe M., Kishimoto T., Yamauchi-Takahara K. (2000) Signal transducer and activator of transcription 3 in the heart transduces not only a hypertrophic signal but a protective signal against doxorubicin-induced cardiomyopathy. *Proc Natl Acad Sci U S A.* 97(1):315-9.
- Laemmli U. K. (1970) "Cleavage of structural proteins during the assembly of the head of the bacteriophage T4." *Nature.* 227:680-685.
- Laird P. W, Zijderveld A, Linders K, Rudnicki M. A, Jaenisch R, Berns A. (1991). Simplified Mammalian DNA Isolation Procedure. *Nucleic. Acids. Res.* 19: 4293.
- Lairez O., Calise D., Bianchi P., Ordener C., Spreux-Varoquaux O., Guilbeau-Frugier C., Escourrou G., Seif I., Roncalli J., Pizzinat N., Galinier M., Parini A., Mialet-Perez J. (2009) Genetic deletion of MAO-A promotes serotonin-dependent ventricular hypertrophy by pressure overload. *J Mol Cell Cardiol.* 46(4):587-95.
- Lee, Y.-H., Sauer, B., Gonzalez, F.J. (1998) Laron dwarfism and noninsulin-dependent diabetes mellitus in the Hnf-1a knock out mouse. *Mol. Cell. Biol.*, 18, 3059-3068.

References

- Levy D., Garrison R. J., Savage D. D., Kannel W. B., Castelli W. P. (1990). Prognostic implications of echocardiographically determined left ventricular mass in the Framingham Heart Study. *N. Engl. J. Med.* 322: 1561–6.
- Li C., Liu D., Yuan Y., Huang S., Shi M., Tao K., Feng W. (2010) Overexpression of Apg-2 increases cell proliferation and protects from oxidative damage in BaF3-BCR/ABL cells. *Int. J. Oncol.* 36(4):899-90.
- Liang, Q., De Windt, L. J., Witt, S. A., Kimball, T. R., Markham, B. E., Molkenin, J. D. (2001) The transcription factors GATA4 and GATA6 regulate cardiomyocyte hypertrophy in vitro and in vivo. *J Biol Chem.* 276, 30 245–30 253.
- Liew C. C., Dzau V. J. (2004) Molecular genetics and genomics of heart failure.. *Nature.* 5: 811-25.
- Liew C. C. (2005) Expressed genome molecular signatures of heart failure. *Clin Chem Lab Med.* 43(5):462-9.
- Lin W. Y., Hu Y. J., Lee Y. H. (2008) Hepatocyte nuclear factor-1alpha regulates glucocorticoid receptor expression to control postnatal body growth. *Am J Physiol. Gastrointest. Liver Physiol.* 295(3):G542-51.
- Lindquist S. and Craig EA (1988). The heat shock proteins. *Annu. Rev. Genet.* 22: 631–677.
- Liu, J. P., Baker, J., Perkins, A. S., Roberson, E. J. and Efstratiadis, A. (1993) Mice carrying null mutations of the gene encoding insulin-like growth factor-1 (IGF-1) and type 1 IGF receptor (IGF-1R). *Cell* 75: 59-72.
- Liu J. L., Grinberg A., Westphal H., Sauer B., Accili D., Karas M., LeRoith D. (1998) Insulin-like growth factor-I affects perinatal lethality and postnatal development in a gene dosage-dependent manner: manipulation using the Cre/loxP system in transgenic mice. *Mol. Endocrinol* 12:1452-1462.

References

- Liu Q. and Hendrickson W. A. (2007) Insights into Hsp70 chaperone activity from a crystal structure of the yeast Hsp110 Sse1. *Cell*. 131(1): 106-120.
- Liu W., Zi M., Jin J. Prehar S., Oceandy D., Kimura T. E., Lei M., Neyses L., Weston A. H., Cartwright E. J., Wang X. (2009) Cardiac-Specific Deletion of Mkk4 Reveals Its Role in Pathological Hypertrophic Remodeling but Not in Physiological Cardiac Growth. *Circ Res*. 104:905.
- Lorell B. H., Carabello B. A. (2000) Left ventricular hypertrophy: pathogenesis, detection, and prognosis. *Circ*. 102(4):470-9.
- Lu J., McKinsey T.A., Nicol R.L., Olson E.N. (2000a) Signal-dependent activation of the MEF2 transcription factor by dissociation from histone deacetylases. *Proc. Natl. Acad. Sci. USA*. 97: 4070–4075.
- Lu, J., McKinsey, T.A., Zhang, C.L. and Olson, E.N. (2000b) Regulation of skeletal myogenesis by association of the MEF2 transcription factor with class II histone deacetylases. *Mol. Cell*. 6: 233–244.
- Maekawa M., O'Brien D. A., Allen R. L., Eddy E. M. (1989) Heat-shock cognate protein (hsc71) and related proteins in mouse spermatogenic cells. *Biol Reprod*. 40: 843–852.
- Maier L. S., Bers D. M. (2002) Calcium, calmodulin, and calcium-calmodulin kinase II: heartbeat to heartbeat and beyond. *J Mol Cell Cardiol*. 34:919-39.
- Manabe I., Shindo T., Nagai R. (2002) Gene expression in fibroblasts and fibrosis: involvement in cardiac hypertrophy. *Circ Res*. 91: 1103-1113.
- Matsumoto, M., Fujimoto, H. (1990). Cloning of a hsp70-related gene expressed in mouse spermatids. *Biochem. Biophys. Res. Commun*. 166: 43-49.
- Mayer M.P. and Bukau B. (2005) Hsp70 chaperones: cellular functions and molecular mechanism. *Cell. Mol Life Sci*. 62(6):670-84.

- McDonough H., Patterson C. (2003) CHIP: a link between the chaperone and proteasome systems. *Cell Stress Chaperones* . 8(4):303-8.
- McMullen J. R. , Shioi T. , Huang W. Y. , Zhang L. , Tarnavski O. , Bisping E. , Schinke M. , Kong S. , Sherwood M. C., Brown J., Riggi L., Kang P. M., Izumo S. (2004) The insulin-like growth factor 1 receptor induces physiological heart growth via the phosphoinositide 3-kinase (p110alpha) pathway. *J Biol Chem*. 279(6):4782-93.
- Mehta, J. L., Attramadal, H. (2007) The TGF β superfamily in cardiovascular biology. *Cardiovasc. Res*. 74: 181–183.
- Mirotsov M., Dzau V. J. , Pratt R. E. , Weinberg E. O. (2006) Physiological genomics of cardiac disease: quantitative relationships between gene expression and left ventricular hypertrophy. *Physiol Genomics*. 27(1):86-94.
- Miska, E.A., Karlsson, C., Langley, E., Nielsen, S.J., Pines, J. and Kouzarides, T. (1999) HDAC4 deacetylase associates with and represses the MEF2 transcription factor. *EMBO J.*, 18: 5099–5107.
- Molkentin J. D, Dorn GW., II (2001) Cytoplasmic signaling pathways that regulate cardiac hypertrophy. *Annu. Rev. Physiol*. 63:391–426.
- Mons, N. J. L. Guillou, R. Jaffard. 1999. The role of Ca²⁺/calmodulin-stimulable adenylyl cyclases as molecular coincidence detectors in memory formation. *Cell. Mol. Life Sci*. 55:525-533.
- Mori C., Nakamura N., Dix D.J., Fujioka M., Nakagawa S., Shiota K., Eddy E.M. (1997). Morphological analysis of germ cell apoptosis during postnatal testis development in normal and Hsp 70-2 knockout mice. *Dev. Dyn*. 208(1):125-36.
- Morimoto R. (1993) Cells in stress: transcriptional activation of heat shock genes. *Science* 259:1409–1410.

References

- Morozov A., Subject J., Raychaudhuri P. (1995) HPV16 E7 oncoprotein induces expression of a 110 kDa heat shock protein. *FEBS Lett.* 371:214–218.
- Moustafa-Bayoumi M., Alhaj M. A., El-Sayed O., Wisel S., Chotani M. A., Abouelnaga Z. A., Hassona M. D. H., Rigatto K., Morris M., Nuovo G., *et al.* (2007) Vascular Hypertrophy and Hypertension Caused by Transgenic Overexpression of Profilin 1. *J Biol. Chem.* 282(52): 37632 - 37639.
- Mukai H., Kuno T., Tanaka H., Hirata D., Miyakawa T., Tanaka C. (1993) Isolation and characterization of SSE1 and SSE2, new members of the yeast HSP70 multigene family. *Gene.* 132: 57–66.
- Murphy L. J., Molnar P., Lu X., Huang H. (1995) Expression of human insulin-like growth factor-binding protein-3 in transgenic mice. *J Mol Endocrinol.* 15(3):293-303.
- Nakamura J., Fujimoto M., Yasuda K., Takeda K., Akira S., Hatayama T., Takagi Y., Nozaki K., Hosokawa N., Nagata K.(2008) Targeted disruption of Hsp110/105 gene protects against ischemic stress. *Stroke.* 39(10):2853-9.
- Nakatsura T., Senju S., Yamada K., Jotsuka T., Ogawa M. Nishimura, Y. (2001). Gene cloning of immunogenic antigens overexpressed in pancreatic cancer. *Biochem. Biophys. Res Commun.* 281: 936-944.
- Naoi M., Maruyama W., Akao Y., Yi H. and Yamaoka Y. (2006) Involvement of type A monoamine oxidase in neurodegeneration: regulation of mitochondrial signaling leading to cell death or neuroprotection. *J Neural Transm. Suppl.* 71, 67–77.
- Nayernia K., Adham, I. M., Burkhardt-Gottges E., Neesen J., Rieche M., Wolf S., Sancken U., Kleene K., Engel, W. (2002) Asthenozoospermia in mice with targeted deletion of the sperm mitochondrion-associated cysteine-rich protein (Smcp) gene. *Mol Cell Biol.* 22: 3046-3052.

References

- Nguyen T. H., Bertrand M. J., Sterpin C., Achouri Y., De Backer O. R. (2010) Maged1, a new regulator of skeletal myogenic differentiation and muscle regeneration. *BMC Cell Biol.* 11:57.
- Ni Y. G., Berenji K., Wang N., Oh M., Sachan N., Dey A., Cheng J, Lu G., Morris D. J., Castrillon D. H., Gerard R. D., Rothermel B. A., Hill Y. A. (2006) Foxo Transcription Factors Blunt Cardiac Hypertrophy by Inhibiting Calcineurin Signaling. *Circ.* 114:1159-1168.
- Nishida M., Maruyama Y., Tanaka R., Kontani K., Nagao T., Kurose H. (2000) G alpha(i) and G alpha(o) are target proteins of reactive oxygen species. *Nature.* 408(6811):492-5.
- Nonoguchi, K., Itoh, K., Xue, J. H., Tokuchi, H., Nishiyama, H., Kaneko, Y., Tatsumi, K., Okuno, H., Tomiwa, K., and Fujita, J. (1999) Cloning of human cDNAs for Apg-1 and Apg-2, members of the Hsp110 family, and chromosomal assignment of their genes. *Gene.* 237: 21–28.
- Obata K., Nagata K., Iwase M., Odashima M., Nagasaka T., Izawa H., Murohara T., Yamada Y., Yokota M. (2005) Overexpression of calmodulin induces cardiac hypertrophy by a calcineurin-dependent pathway. *Biochem Biophys Res Commun.* 338(2):1299-305.
- Offermanns, S. (2003). G-proteins as transducers in transmembrane signalling. *Prog. Biophys. Mol Biol.* 83: 101–130.
- Ogita K., Takagi R. , Oyama N., Okuda H., Ito F., Okui M., Shimizu N. Yoneda Y. (2001) Decrease in level of APG-2, a member of the heat shock protein 110 family, in murine brain following systemic administration of kainic acid . *Neuropharmacology.* 41(3): 285-293.
- Okui M., Ito F., Ogita K., Kuramoto N., Kudoh J., Shimizu N. , Ide T (2000) Expression of APG-2 protein, a member of the heat shock protein 110 family, in developing rat brain. *Neurochem. Int.* 36: 35–43.
- Oudit G. Y., Kassiri Z., Patel M. P., Chappell M., Butany J., Backx P. H., Tsushima R. G., Scholey J. W., Khokha R., Penninger J. M. (2007) Angiotensin II-mediated oxidative

References

- stress and inflammation mediate the age-dependent cardiomyopathy in ACE2 null mice. *Cardiovasc Res.* 75(1):29-39.
- Pan J., Fukuda. K., Kodama H., Makino S., Takahashi T., Sano M., Hori S., Ogawa S. (1997) Role of angiotensin II in activation of the JAK/STAT pathway induced by acute pressure overload in the rat heart. *Circ Res.* 81(4):611-7.
- Pan Y. X., Lin L., Ren A. J., Pan X. J., Chen H., Tang C. S., Yuan W. J. (2004) HSP70 and GRP78 Induced by Endothelin-1 Pretreatment Enhance Tolerance to Hypoxia in Cultured Neonatal Rat cardiomyocytes. *J Cardiovasc Pharmacol.* 44 Suppl 1:S117-20.
- Passier R., Zeng H., Frey N., Naya F. J., Nicol R. L., McKinsey T. A., Overbeek P., Richardson J. A., Grant S. R., Olson E. N. (2000). CaM kinase signaling induces cardiac hypertrophy and activates the MEF2 transcription factor in vivo. *J. Clin. Invest.* 105:1395-1406.
- Pearse, R.V., Drolet, D.W., Kalla, K.A. Hooshmand F., Bermingham J. R. Jr, Rosenfeld M. G. (1997) Reduced fertility in mice deficient for the POU protein sperm-1. *Proc. Natl. Acad. Sci. USA.* 94: 7555–7560.
- Polier S., Dragovic Z., Hartl F. U., Bracher A. (2008). Structural basis for the cooperation of Hsp70 and Hsp110 chaperones in protein folding. *Cell.* 133(6):1068-79.
- Powell-Braxton L., Hollingshead P., Warburton C., Dowd M., Pitts-Meek S., Dalton D., Gillett N., Stewart T. A. (1993) IGF-I is required for normal embryonic growth in mice. *Genes and Development.* 7: 2609–2617.
- Rajas F, Croset M, Zitoun C, Montano S & Mithieux G (2000). Induction of PEPCK gene expression in insulinopenia in rat small intestine. *Diabetes* 49, 1165–1168.
- Ramalho-Santos M., Yoon S., Matsuzaki Y., Mulligan R. C., Melton D. A. (2002) "Stemness": Transcriptional Profiling of Embryonic and Adult Stem Cells Originally. *Science.* 298 (5593): 597 – 600.

References

- Raviol H., Sadlish H., F Rodriguez F., Mayer M. P. and Bukau B. (2006) Chaperone network in the yeast cytosol: Hsp110 is revealed as an Hsp70 nucleotide exchange factor. *EMBO J.* 25:2510 – 2518.
- Risson V., Mazelin L., Roceri M., Sanchez H., Moncollin V.,Corneloup C., Richard-Bulteau H., Vignaud H., Baas D., *et al.* (2009) Muscle inactivation of mTOR causes metabolic and dystrophin defects leading to severe myopathy. *J Cell Biol.* 187(6): 859–874.
- Robertson K., Kopchick J. J., Liu J. (2006) Growth hormone receptor gene deficiency causes delayed insulin responsiveness in skeletal muscles without affecting compensatory islet cell overgrowth in obese mice. *Am J Physiol. Endocrinol. Metab.* 291: E491–E498.
- Rockman H. A, Koch W. J, Lefkowitz R. J. (2002) Seven-transmembrane-spanning receptors and heart function. *Nature.*415: 206–212.
- Romrell, L. J., Brillve, A. R. & Fawcett, D. W. (1976). Separation of mouse spermatogenic cells by sedimentation velocity. A morphological characterization. *Devi Biol.* 49, 119-131.
- Rossi J., Herzig K. H., Võikar V., Hiltunen P. H., Segerstråle M., Airaksinen M.S. (2003) Alimentary tract innervation deficits and dysfunction in mice lacking GDNF family receptor alpha2. *J Clin Invest.* 112(5):707-16.
- Rothermel B. A., Vega R. B., Williams R. S. (2003) The role of modulatory calcineurin-interacting proteins in calcineurin signaling. *Trends Cardiovasc Med.* 13(1):15-21.
- Ruwhof C., van der Laarse A. (2000) Mechanical stress-induced cardiac hypertrophy: mechanisms and signal transduction pathways. *Cardiovasc. Res.* 47(1):23–37.
- Sagane K., Ishihama Y., Sugimoto H. (2008) LGI1 and LGI4 bind to ADAM22, ADAM23 and ADAM11. *Int J Biol Sci.* 4(6):387-96.
- Saimi Y., Kung C. 2002. Calmodulin as an ion channel subunit. *Ann Rev Physiol.* 64: 289–311.

References

- Sakurai T., Yanagisawa M., Takawa Y., Miyazaki H., Kimura S., Goto K., Masaki T. (1990) Cloning of a cDNA encoding a non-isopeptide-selective subtype of the endothelin receptor. *Nature*. 348(6303):732–735.
- Sambrook, P. N, Cohen, M. L, Eisman, J. A, Pocock, N. A, Champion, G. D, Yeates M. G. (1989). Effects of Low Dose Corticosteroids on Bone Mass in Rheumatoid Arthritis: a Longitudinal Study. *Ann. Rheum. Dis.* 48: 535-8.
- Sanger F., Nicklen S., Coulson A.R. (1977) DNA sequencing with the chain terminating inhibitors. *Proc Natl Acad Sci U S A.* 74: 5463-5467.
- Sanguinetti M. C., Curran M. E., Zou A., Shen J., Spector P. S., Atkinson D. L., Keating M. T. (1996) Coassembly of KvLQT1 and minK (IsK) proteins to form cardiac I(Ks) potassium channel. *Nature* 384:80–83.
- Sasaki M., Abe R., Fujita Y., Ando S., Inokuma D., Shimizu H. (2008). Mesenchymal stem cells are recruited into wounded skin and contribute to wound repair by transdifferentiation into multiple skin cell type. *J. Immunol.* 180(4): 2581–2587.
- Sato N., Torigoe T. (1998) The molecular chaperones in cell cycle control. *Ann N Y Acad. Sci.* 851: 61–66.
- Schulte U., Thumfart J. O., Klöcker N., Sailer C. A., Bildl W., Biniossek M., Dehn D., Deller T., Eble S., Abbass K., Wangler T., Knaus H. G., Fakler B.(2006)The epilepsy-linked Lgi1 protein assembles into presynaptic Kv1 channels and inhibits inactivation by Kvbeta1. *Neuron.* 49(5):697-706.
- Schultz E. (1996) Satellite cell proliferative compartments in growing skeletal muscles. *Dev Biol.* 175:84–94.
- Schultz J. J., Witt S. A., Glascock B. J., Nieman M. L., Reiser P. J., Nix S. L., Kimball T. R., Doetschman T. (2002) TGF-beta1 mediates the hypertrophic cardiomyocyte growth induced by angiotensin II. *J. Clin. Invest.* 109: 787-796.

References

- Shaner L. , Trott A., Goeckeler J. L., Brodsky J. L., Morano K. A. 2004. The function of the yeast molecular chaperone Sse1 is mechanistically distinct from the closely related Hsp70 family. *J Biol Chem* 279: 21992–22001.
- Shaner, L., and Morano, K. A. (2007) All in the family: atypical Hsp70 chaperones are conserved modulators of Hsp70 activity. *Cell Stress Chaperones*. 12: 1–8.
- Shibata R., Ouchi N., Ito M., Kihara S., Shiojima I., Pimentel D. R., Kumada M., Sato K., Schiekofer S., Ohashi K. *et al.* (2004) Adiponectin-mediated modulation of hypertrophic signals in the heart. *Nature Medicine*. 10 :1384–1389.
- Shih J. C., Chen K., Ridd M. J. (1999) Monoamine oxidase: from genes to behavior. *Annu Rev Neurosci* 22:197–217.
- Shohet R. V., Kisanuki Y. Y., Zhao X.-S., Siddiquee Z., Franco F., Yanagisawa M. (2004) Mice with cardiomyocyte-specific disruption of the endothelin-1 gene are resistant to hyperthyroid cardiac hypertrophy. *Proc Natl Acad Sci U S A*. 101(7): 2088–2093.
- Sourisseau T., Georgiadis A., Tsapara A., Ali R. R., Pestell R., Matter K., Balda M. S. (2006) Regulation of PCNA and cyclin D1 expression and epithelial morphogenesis by the ZO-1 regulated transcription factor ZONAB/DbpA. *Mol. Cell. Biol.* 26: 2387-2398.
- Steel G. J., Fullerton D. M., Tyson J. R., Stirling C. J. (2004) Coordinated activation of Hsp70 chaperones. *Science* 303: 98–101.
- Sugden P.H., Clerk A. (1998) ‘Stress-responsive’ mitogen-activated protein kinases (c-Jun N-terminal kinases and p38 mitogen-activated protein kinases) in the myocardium. *Circ. Res.* 24: 345–352.
- Tanaka M., Treloar H., Kalb R. G., Greer C. A., Strittmatter SM (1999). Go protein-dependent survival of primary accessory olfactory neurons. *Proc Natl Acad Sci USA*. 96: 14106–14111.

- Temple J., Frias ., Rottman J., Yang T., Wu Y., Verheijck E. E., Zhang W., Siprachanh C., Kanki H., Atkinson J. B, King P., Anderson M. E, Kupershmidt S., Roden D. M. (2005) Atrial fibrillation in KCNE1-null mice. *Circ Res.* 97(1):62-9.
- Tokudome T., Horio T., Kishimoto I., Soeki T., Mori K., Kawano Y., Kohno M., Garbers D. L., Nakao K., Kangawa K. (2005) Calcineurin-nuclear factor of activated T cells pathway-dependent cardiac remodeling in mice deficient in guanylyl cyclase A, a receptor for atrial and brain natriuretic peptides. *Circ.* 111(23):3095-104.
- Tronche, F., Opherk, C., Moriggl, R., Kellendonk, C., Reimann, A. Schwake, L., Reichardt, H.M., Stangl, K., Gau, D., Hoeflich, A., *et al.* (2004) Glucocorticoid receptor function in hepatocytes is essential to promote postnatal body growth. *Genes & Dev.* 18:492–497.
- Tsapara A., Matter K. and Balda M. S. (2006) The heat shock protein Apg-2 binds to the tight junction protein ZO-1 and regulates transcriptional activity of ZONAB. *Mol. Biol. Cell* 17, 1322-1330.
- Vadivelu S. K., Kurzbauer R., Dieplinger B., Zweyer M., Schafer R, Wernig A., Victor I., Huber L. K. (2004) Muscle Regeneration and Myogenic Differentiation Defects in Mice Lacking TIS7. *Mol Cell Biol.* 24(8): 3514-3525.
- Valenzuela D., Han X., Mende U., Fankhauser C., Mashimo H., Huang P., Pfeffer J., Neer E. J., Fishman M. C.(1997) $G_{\alpha o}$ is necessary for muscarinic regulation of Ca^{2+} channels in mouse heart. *Proc Natl Acad Sci USA.* 94: 1727–1732.
- van Rooij E., Doevendans P. A. , Crijns H. J., Heeneman S., Lips D. J., van Bilsen M., Williams R. S., Olson E. N., Bassel-Duby R., Rothmel B. A., De Windt L. J. (2004) MCIP1 overexpression suppresses left ventricular remodeling and sustains cardiac function after myocardial infarction. *Circ Res.* 94: e18–e26.

References

- Vega R.B., Rothermel, B.A., Weinheimer, C.J., Kovacs, A., Naseem, R.H., Bassel-Duby, R., Williams, R.S., and Olson, E.N. 2003. Dual roles of modulatory calcineurin-interacting protein 1 in cardiac hypertrophy. *Proc. Natl. Acad. Sci.* 100: 669–674.
- Vondriska T. M., Wang Y. A (2008) New (Heat) Shocking Player in Cardiac Hypertrophy. *Circ Res.* 103:1194.
- Vos M. J., Hageman J., Carra S, Kampinga H. H. (2008) Structural and functional diversities between members of the human HSPB, HSPH, HSPA, and DNAJ chaperone families. *Biochem.* 47:7001–7011.
- Wang J., Xu N., Feng X., Hou N., Zhang J., Cheng X., Chen Y., Zhang Y., Yang X. (2005). Targeted disruption of Smad4 in cardiomyocytes results in cardiac hypertrophy and heart failure. *Circ Res.* 97(8):821-8.
- Wang J., Zhou J., Bondy C. A. (1999) IGF-I promotes longitudinal bone growth by insulin-like actions augmenting chondrocyte hypertrophy. *FASEB J.* 13:1985–1990.
- Welch W. J. (1992) Mammalian stress response: Cell physiology, structure/function of stress proteins, and implications for medicine and disease. *Physiol. Rev.* 72: 1063–1081.
- Widmann C., Gibson S., Jarpe M. B., Johnson G. L. (1999). Mitogen-activated protein kinase: conservation of a three-kinase module from yeast to human. *Physiol. Rev.* 79: 143-180.
- Wilkins B. J., Molkenin J. D. (2002) Calcineurin and cardiac hypertrophy: Where have we been? Where are we going? *J Physiol.* 541: 1-8.
- Wilkins B. J., Dai, Y. S., Bueno O. F., Parsons S. A., Xu J., Plank, D. M., Jones F., Kimball T. R., Molkenin, J. D. (2004). Calcineurin/NFAT coupling participates in pathological, but not physiological, cardiac hypertrophy. *Circ Res.* 94: 110–118.
- Williams, B. (2001) Angiotensin II and the pathophysiology of cardiovascular remodeling. *Am J Cardiol.* 87: 10C-17C.

References

- Wurst W. and Joyner A. L. (1993) Production of targeted embryonic stem cell clones, p. 33–61. In A. L. Joyner (ed.), *Gene targeting: a practical approach*. IRL Press, Oxford, England.
- Xia S., Wang Y., Zhang Y., Deng S. B., Du J. L., Wang X. C., She Q. (2010) Dynamic changes in HCN2, HCN4, KCNE1, and KCNE2 expression in ventricular cells from acute myocardial infarction rat hearts. *Biochem Biophys Res Commun.* 395(3):330-5.
- Xue J. H., Fukuyama H., Nonoguchi K., Kaneko Y., Kido T., Fukumoto M., Fujibayashi Y., Itoh K., Fujita J. (1998) Induction of apg-1, a member of the heat shock protein 110 family, following transient forebrain ischemia in the rat brain. *Biochem. Biophys. Res. Commun.* 247: 796–801.
- Xu J., Ismat F. A., Wang T., Lu M. M., Antonucci N., Epstein J. A. (2009) Cardiomyocyte-specific loss of neurofibromin promotes cardiac hypertrophy and dysfunction. *Circ Res.* 105(3):304-11.
- Yamauchi-Takahara K, Kishimoto (2000) A novel role for STAT3 in cardiac remodeling. *Trends Cardiovasc Med.* 10(7):298-303.
- Yang J., Rothermel, B., Vega, R.B., Frey, N., McKinsey, T.A., Olson, E.N., Bassel-Duby, R., and Williams, R.S. 2000. Independent signals control expression of the calcineurin inhibitory proteins MCIP1 and MCIP2 in striated muscles. *Circ. Res.* 87: E61–E68.
- Yasuda K., Nakai, A., Hatayama T. and Nagata K. (1995) Cloning and expression of murine high molecular mass heat shock proteins, HSP105. *J. Biol. Chem.* 270: 29718-29723.
- Youdim M. B. H., Bakhle Y. S. (2006) Monoamine oxidase: isoforms and inhibitors in Parkinson's disease and depressive illness. *Br. J. Pharmacol.* 147(S1): S287–S296.
- Youdim M. B., Edmondson D., Tipton K. F. (2006) The therapeutic potential of monoamine oxidase inhibitors. *Nat. Rev. Neurosci.* 7(4):295-309.

References

- Youn H. D., Chatila T.A., Liu J.O. (2000). Integration of calcineurin and MEF2 signals by the coactivator p300 during T-cell apoptosis. *EMBO J.* 19(16):4323-31.
- Young S. G. (1990) Recent progress in understanding apolipoprotein B. *Circ.* 82:1574-1594.
- Young S. G. ,Cham C. M., Pitas R. E. , Burri B. J., Connolly A., Flynn L., Pappu A. S., Wong J. S., Hamilton R. L., Farese, Jr. R. V. (1995) A genetic model for absent chylomicron formation: mice producing apolipoprotein B in the liver, but not in the intestine. *J Clin Invest.* 96(6): 2932–2946.
- Yu Y.E., Zhang Y., Unni E., Shirley C. R., Deng J. M., Russell L.D., Weil M.M., Behringer R.R., Meistrich M. L. (2000) Abnormal spermatogenesis and reduced fertility in transition nuclear protein 1-deficient mice. *Proc Natl Acad Sci. USA.* 97:4683–4688.
- Zakeri Z. F. , Wolgemuth D. J. (1987) Developmental-stage-specific expression of the hsp70 gene family during differentiation of the mammalian male germ line. *Mol. Cell. Biol.* 7: 1791–1796.
- Zhang T., Kohlhaas M., Backs J., Mishra S., Phillips W., Dybkova N., Chang S., Ling H., Bers D. M., Maier L. S., Olson N., Brown J. H. (2007). CaMKII δ isoforms differentially affect calcium handling but similarly regulate HDAC/MEF2 transcriptional responses. *J Biol. Chem.* 282:35078-35087.
- Zhu M., Gach A. A., Liu G., Xu X., Lim C. C., Zhang J. X., Mao L., Chuprun M., Koch W. J., Liao R., Koren G, Blaxall B. C., Mende U. (2008). Enhanced calcium cycling and contractile function in transgenic hearts expressing constitutively active G α^* protein Am *J Physiol Heart Circ Physiol.* 294: H1335-H1347.
- Zhu X. , Birnbaumer L. (1996) G protein subunits and the stimulation of phospholipase C by Gs- and Gi-coupled receptors: Lack of receptor selectivity of G α_{16} and evidence for a synergic interaction between G $\beta\gamma$ and the α subunit of a receptor activated G protein. *Proc Natl Acad Sci U S A.* 93(7):2827-31.

Acknowledgements

There are many people to whom I wish to thank and who helped me, taught and encouraged me along the way.

I would like to express my gratitude to Prof. Dr. med. Dr. W. Engel for the chance he gave me, to make PhD study in the Institute of Human Genetics. I would like to warmly thank for his support, encouragement, excellent scientific supervision, valuable scientific discussions, and supervision and for always being ready to lend a helping hand in all situation. It has been a pleasure working in such an inspiring and friendly atmosphere as he has created at the Institute of Human Genetics.

I would like to express my gratitude and my sincere to Prof. Dr. I. M. Adham, for his valuable efforts, kind assistance, and encouragement through the course of this work and for all valuable things learned from him. Thank you for provided me with excellent scientific guidance, instructive ideas and theoretical discussion over the period of my PhD study. Thank you for the long hours at your office for learning, for your patience with my language mistakes and for all the corrections and revisions.

I sincerely thank PD Dr. S. Hoyer-Fender for being my co-referee. I also extend my sincere thank you to Prof Dr. J. Wienands, Prof Dr. E. A. Wimmer, Prof Dr. W. Wuttke and Prof. Dr. A. Mansouri for being my dissertation examiners.

I would like to thank all my institute colleagues and co-worker for helpful during my stay. I would like to appreciate the current and former members of our group: Maiada , Ola , Ilona , Lili , Belal, Shuai, Karina, Ozii, Oggie, Gonjee, Chimgee, Chiranjeevi, Katy, Krishna, Sandra, Sandra, Saskia , Janine, Thanks for spending so much time with me in and outside the lab. I really enjoyed it!

I would like also thank S. Meyer and S. Lührig for kindness, support for excellent assistance.

I am grateful to secretaries Mrs. P. Albers and Mrs. A Winkles at the Institute of Human Genetics for excellent administrative assistance and for kind.

Most especially , thank my friends Maiada for her kindness, support, care friendship, thank you for all things (support, helping inside and outside the lab). I would also thank my friends Heba, Basma for support and helping while I was ill

I would like to thank Krishna (for friendship, support and discussion), Grzmil. Dr. Pawel and Zibat, Dr. Arne (for helping and support)

Finally I would like to thank my husband for his support, making me smile, help and love.

Curriculum vitae

Personal details:

Name: Amal Z. A.-Z. Barakat
Address: Am Vogelsang 1, 37075 Göttingen
Telephone: 017663066808
E-mail: amalbarakat2001@yahoo.co.uk
Date of Birth: 30.05.1975
Place of Birth: Cairo, Egypt
Nationality: Egypt
Sex: Female
Marital Status: Married

Educational background:

Since November 2006: PhD study, Institute of Human Genetics, Georg-August University, Goettingen
Title of M. SC. thesis: "Functional analysis of heat shock protein HSPA4"
1999-2002 *Scholarships for master's degree* student in National Research Center, Egypt
2001- 2004: Master thesis, Biochemistry Department, Faculty of Science, Ain Shams University, Egypt
Title of thesis: "Purification and characterization of lipase from Cucurbitaceae"
1994- 1997: Study of Biology at the Ain Shams, University, Cairo, Egypt
1986- 1994: Primary and Secondary School (Cairo, Egypt)

Work Experience:

1998-1999 work in the lab of the *hospital in Egypt*
2002-2004 Research Assistant in National Research Center, Egypt
Since 2004 Assistant Researcher in National Research Center, Egypt

Publications:

Fahmy, A. S., Amal Z. Abo-Zeid, A. Z., Mohamed T. M., Mohamed, S. A., Borai, I. H., Rafat, H. (2008). Characterization of esterases from Cucurbita pepo cv. "Eskandrani". Bioresource Technol. 437-443.